Developing the Molecular Pharmacology of LRRC8-containing Volume-Regulated Anion Channels

By

Eric Emmanuel Figueroa

Dissertation

Submitted to the Faculty of the

Graduate School of Vanderbilt University

in partial fulfillment of the requirements

for the degree of

DOCTOR OF PHILOSOPHY

in

Pharmacology

December 12, 2020

Nashville, Tennessee

Approved:

Jerod S. Denton, Ph.D.

C. David Weaver, Ph.D.

Richard M. Breyer, Ph.D.

David A. Jacobson, Ph.D.

Fred S. Lamb, M.D., Ph.D.

Craig W. Lindsley, Ph.D.

TABLE OF CONTENTS

To my Mom and Dad,

who emigrated from their country,

so that my brothers and I can live better lives.

ACKNOWLEDGEMENTS

First, I would like to thank my mentor, Dr. Jerod Denton. His mentorship, support, and friendship has provided a great environment for me to grow as a scientist. I must also thank members of the Denton lab, past and present, for listening to my questions, providing me with feedback, and for offering their sage advice as I endured my growing pains in graduate school. I would like to especially thank Sujay and Toshiki who were invaluable to me as I learned patch clamp electrophysiology. I would also like to acknowledge my committee members, Dave Weaver, Rich Breyer, David Jacobson, Fred Lamb, and Craig Lindsley, who through their insightful questions and suggestions have encouraged me to think about my project critically and shaped the best possible outcome for my work.

I also must thank Eric Delpire, Joey Barnett, Ege Kavalali, Karen Gieg, and the Pharmacology and IMSD leadership who have been mentors to me not only for my research but for my career. I would like to acknowledge my financial support from grants to Jerod, my NIH F31 fellowship, training grants, and travel awards that allowed me to conduct research as well as travel and share it with my peers. And I must also thank the high-throughput screening center for all the support and, in particular, the Panoptic 2, who has been with me from the beginning.

I must also thank all my friends back home in Arizona, around the country, and in Nashville. Thank you to Chris, Justin, and Lucy, who have lived in the Shanty with me. Thank you to Cody, Brittany, Miaca, Lauren, Mabel and all those who have gone to shows with me, ate at all the restaurants, explored various parts of the city, and who have honestly helped make Nashville my second home. I also would like to thank all my friends I made through my time in the Pharmacology department, Pharmacology graduate student association, including Aparna, Mark, Sheryl, Jamal, Kayla, Bre, Kristin, and James. And I must also thank my best friend and fiancé, Nicole Fisher. Your love, patience and support for me has enabled me to be the best scientist and person I could ever be. I am forever grateful that you have come into my life.

Lastly, I would like to thank my immediate and extended family back home for their support throughout my time in graduate school, especially to Paty, Mason, Alyce, Jackie, and the Tinoco family. I also thank my family in Mexico, whom although I do not get the chance to see often, support and love me just the same. I would like to thank my parents, Maximino and Alejandra, for instilling in me a strong work ethic, dedication to learning, and kindness to others that has prepared me to succeed in my endeavors. I also thank my parents along with my brothers, Max and Adrian, for their love, encouragement, and support whenever I needed them. I share this accomplishment with all of you.

LIST OF TABLES

LIST OF FIGURES

CHAPTER 1. INTRODUCTION

PREFACE

Chloride channels in health and disease

Ion channels in their simplest sense allow charged particles known as ions (i.e. sodium (Na^+), calcium (Ca^{2+}), potassium (K^+) and chloride (Cl^-)) to cross biological membranes down their electrochemical gradient [1]. Ion channels are broadly classified by the main permeant ion(s) (e.g. chloride channels allow Cl^- ions to traverse a biological membrane), the mechanism of gating and/or the channel's response to a stimulus (e.g. intracellular Ca^{2+} and membrane potential activate calcium-activated chloride channels), the subcellular localization, and so on [1]. For the purpose of this dissertation, I will be focusing on the chloride channel superfamily, a class of ion channels that has lagged in the ion channel field compared to the sodium, calcium, and potassium superfamilies. Nevertheless, the role of chloride channels in human health and disease has established these molecules important for investigation.

Chloride is the most abundant anion found in the human body [2]. Therefore, ion channels that facilitate the movement of Cl^- across biological membranes are referred to as chloride channels. In addition to Cl^-, chloride channels are also permeable to other inorganic anionic species (i.e. Br^-, I^-, NO_3^-, HCO_3^-, and SCN^-), as well as organic anions (i.e. glutamate, taurine, ATP) [1]. Hence, sometimes chloride channels are referred to as anion channels. In this dissertation, chloride channels and anion channels will be used interchangeably.

Chloride channels can be subclassified into six major classes by their mode of gating (Figure 1). The ligand-gated chloride channel class consists of $GABA_A$ receptors and glycine receptors [1]. Voltage-gated chloride channels are comprised of members of the CLC protein family: CLC1, CLC2, CLC-K_a, and CLC-K_b (note the remaining five members of the CLC family are in fact Cl^-/H^+ exchangers and not ion channels) [3]. The cAMP-activated chloride channels refer to the cystic fibrosis transmembrane conductance regulator or better known as CFTR [3].

Calcium-activated chloride channels refer to TMEM16A/ANO1 and TMEM16B/ANO2 channels [4]. While the TMEM16 family member, TMEM16F, has been reported to be an anion channel, there are also reports that claim it may be a cation- or a nonselective- channel [5]. Volume-activated chloride channels refer to the volume-regulated anion channel (VRAC, also known as VSOR, VSOAC, VAAC, $I_{Cl,swell}$) [6-8] and the large conductance chloride channel, Maxi-Cl [9]. Acid-activated chloride channels refer to the newly cloned proton-activated chloride channel (PAC) [10], also called proton-activated outwardly rectifying chloride channel (PAORAC) [11], and acid-sensitive outwardly rectifying chloride channel (ASOR) [11].

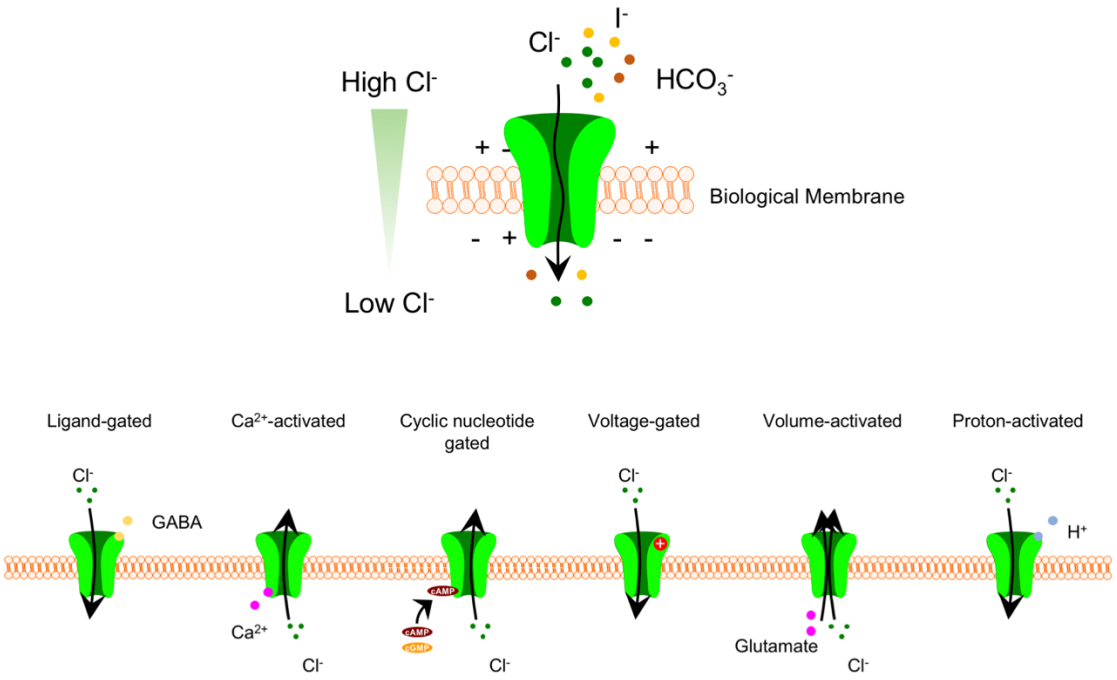

Figure 1. Six classes of chloride channels and their mode of activation

Chloride was historically thought to exist in electrochemical equilibrium across cell membranes, garnering less interest in comparison to sodium, calcium, potassium and the channels they permeate [12]. Studies in the 1950s found that GABA in the central nervous system (via $GABA_A$ receptors) were responsible for chloride-mediated inhibitory postsynaptic currents (IPSCs) [12]. However, since IPSCs had a reversal potential near the cell membrane potential, it was concluded that chloride is normally passively distributed across the cell membrane [13].

Studies in the 1960s and 1970s on skeletal muscle from hereditary myotonic goats and humans showed that chloride was important for regulating the cell membrane potential, preventing muscle fiber hyperexcitability [14-16]. Cystic Fibrosis (CF) is another human disease where early descriptions pointed towards an electrolyte dysfunction, and ultimately a chloride transport deficiency. As early as the 1950s, the sweat of CF patients was described as abnormally salty [17], however, it was not until the 1980s when it was shown that sweat ducts and airways of CF patients had decreased chloride permeability [18]. Despite accumulating evidence for chloride channels as important physiological macromolecules, it was not until the late 1980s and early 1990s when CFTR and CLC-1 were cloned, respectively, that the chloride field began to take off [19-22].

The cloning of chloride channels led to the identification of chloride channel mutations as causes of human disease. CFTR was cloned in 1989 by positional cloning and five years later it was shown to be a *bona fide* chloride channel when heterologously expressed in artificial lipid bilayers [23]. The hesitancy to establish CFTR as a chloride channel was in part due to CFTR belonging to the ABC transporter family [24]. Since its initial cloning, over 1,700 mutations have been identified in the CFTR gene that cause CF [25]. Shortly after CFTR was cloned, Thomas Jentsch, using expression cloning, identified CLC-1 as the chloride channel expressed in human skeletal muscle [26]. Furthermore, Thomas Jentsch and colleagues showed that human myotonia congenita was caused by mutations in CLC-1. These mutations in CLC-1 caused changes in the voltage-sensitivity, as well as changes in the relative anion/cation permeability of the channel [27, 28]. Since these discoveries, chloride channels have been implicated in a myriad of different human physiologies as well as in disease, including, but not limited to: epithelial fluid secretion, acidification of intracellular organelles, insulin release, cell proliferation and cell volume regulation [6, 29, 30].

Chloride channel pharmacology

With the exception of $GABA_A$ receptors and CFTR, chloride channel pharmacology is relatively underdeveloped when compared to cation channels (sodium-, calcium-, and potassium channels). The dearth of specific and potent modulators for chloride channels has slowed progress in understanding their physiology as well as their potential as therapeutic targets. Initial pharmacological characterization of chloride channels relied heavily on organic molecules such as anthracene-9-caboxylic acid (9-AC), 4,4'-diisothiocyanostilbene-2,2'-disulfonic acid (DIDS), tamoxifen, phloretin and 5-nitro-2-(3-phenylpropylamino) benzoic acid (NPPB) [1]. While these compounds are useful in determining if a chloride conductance is responsible for a physiological or pathophysiological event, the lack of specificity for one chloride channel over another makes them poor tool compounds to study individual channels.

The growing importance of chloride channels in human health and disease has led to recent advances in this area. Drug discovery campaigns against emerging therapeutic targets such as CFTR and CaCCs has led to the discovery of high-affinity modulators of these channels that have served useful in establishing proof-of-concept for targeting chloride channels for therapeutic intervention in academia, as well as FDA-approved therapies in industry [31]. In the CF field, Vertex Pharmaceuticals, Inc., has successfully developed four FDA-approved medicines for patients with certain mutations in the gene encoding CFTR. The small molecules that make up the medicines fall under two categories, potentiators and correctors, and are used singly or in combination. The potentiators (ivacaftor), treat Class III CFTR defects, in which the CFTR protein reaches the cell membrane, but have impaired channel activity due to gating a mutation [32]. The correctors (lumacaftor, tezacaftor, elexacaftor), treat Class II CFTR defects, in which the CFTR protein is misfolded in the Golgi apparatus, resulting in decreased expression of CFTR at the cell membrane [33, 34]. In 2019, the FDA approved the latest Vertex medicine, TRIFAKTA®, a triple combination therapy of one potentiator and two correctors (ivacaftor/tezacafor/elexacaftor) [35-37]. A study published in 2017 highlighted that 18 percent of FDA-approved drugs targeted ion

channels, and approximately 25 percent of those drugs targeted anion channels [38]. While a majority of drugs targeted $GABA_A$ receptors, other FDA-approved drugs, in addition to CFTR, targeted glycine receptors and CaCCs channels, underscoring that chloride channels not only play a role in health and disease but may also serve as therapeutic targets [38].

Tools for studying chloride channel pharmacology

The gold standard technique for studying ion channel activity is patch clamp electrophysiology. Originally developed by Erwin Neher and Bert Sakmann in 1976, their patch clamp technique transformed the way we study ion channels to this day [39]. Building off the work from giants in the field such as Cole [40], Hodgkin and Huxley [41], Meech and Standen [42] and Wilson and Goldner [43], Neher and Sakmann were able to develop a technique that allowed for the measurement of single ion channels, definitively showing that ion channels do in fact exist. Using this technique, several parameters can be determined such as a channel's unitary conductance, open probability, channel gating kinetics, and gating mechanism. Moreover, different configurations may be achieved, such as inside-out patch, outside-out patch, cell-attached and whole-cell, allowing control of solution content across both sides of the cell membrane. In the whole-cell configuration, macroscopic currents may be recorded in response to test voltages, and a current(I)-voltage(V) relationship can be determined. The I-V relationship can be ohmic (linear), outwardly rectifying (current is larger at positive voltages), or inwardly rectifying (current is larger at negative voltages) [1, 44].

Furthermore, patch clamp electrophysiology can also be used to study the pharmacology of ion channels [1]. Comparing ion channel currents before and after compound addition can allow for quick analysis of the compound's effect on ion channel activity. In the whole-cell configuration, voltage ramp and voltage step protocols can be utilized to characterize these effects. In a voltage ramp protocol, the voltage is gradually ramped over time (i.e. -100 mV to +100 mV over 200 ms), allowing for the continuous measurement of current over a range of voltages. A voltage step protocol measures currents at steady voltages over a discrete time window (i.e. +100 mV over 1

s) and can be repeated while incrementally changing the voltage, illuminating any time-dependent effects in channel activity at a given voltage. These protocols are useful in determining a compounds effect on overall ion channel activation/inhibition, voltage-dependent properties, as well as effects on time-dependent processes [45]. While patch clamp electrophysiology is a powerful tool for studying ion channels, it is a slow and laborious technique allowing for the analysis of one compound at a time, making it a poor approach for studying a multitude of compounds such as in drug discovery. High throughput-screening (HTS), the process of quickly testing upwards of millions of compounds for activity against a target of interest is the preferred method for identifying novel ion channel modulators [46]. HTS is amendable to automation that can be accomplished not only in biotech/pharmaceutical companies, but also in academic laboratories and institutional research cores. The advent of automatic patch clamp technology in 2003 has provided the first steps in addressing the low-throughput of conventional patch clamp electrophysiology; however, due to the prohibitive cost of instruments and consumables, it has primarily been used in biotech and pharmaceutical companies [46]. Therefore, HTS campaigns for ion channel modulators have been primarily carried out using indirect measurements of ion channel activity, as with ion-sensitive and voltage-sensitive dyes, radiotracer flux, and direct-binding studies [46].

A notable class of ion-sensitive dyes extensively used in studying chloride channel activity and drug discovery are the halide-sensitive green-fluorescent protein (GFP) mutants. A red-shifted GFP mutant, termed yellow-fluorescent protein (YFP) was initially engineered by mutating residues identified from x-ray crystallographic structural data [47]. Further mutations in YFP generated a molecule conferring halide (and nitrate) sensitivity where halide binding near YFP's chromophore led to fluorescence quenching in a halide concentration-dependent manner. Mutating YFP to YFP-H148Q led to 50% fluorescence quenching by 100 mM chloride or 21 mM iodide [48]. Further mutating YFP-H148Q to YFP-H148Q/I152L created a YFP with higher sensitive towards iodide than chloride and adding a third mutation, YFP-F46L/H148Q/I152L,

conferred even brighter fluorescence at 37°C [49, 50]. These genetically encoded fluorescent proteins can be stably expressed in cells where they are brightly fluorescent and strongly-halide sensitive. It is important to note that these proteins are also sensitive to pH [47].

In developing a cell-based assay for high-throughput screening, cell lines that stably express YFP and the chloride channel of interest are necessary. Furthermore, cell lines that show rapid growth, strong adherence to plastic multi-well plates during solution additions/exchanges, and low halide-permeability outside of the chloride channel of interest are preferred [31]. In order to increase assay sensitivity and to circumvent background halide-permeability, overexpression of the channel of interest may be a possible solution, as well as measuring iodide-flux rather than chloride-flux since YFP mutants like YFP-F46L/H148Q/I152L are more sensitive to iodide than chloride and most chloride channels are permeable to iodide [1].

Figure 2 illustrates an iodide-flux based assay for identifying novel modulators of chloride channels. Briefly, cells are plated in a multi-well plate (e.g. 384-well plate) 24-48 hours prior to the experiment. On the day of the experiment, cells are washed and culture media is replaced with an assay buffer. Compounds (and activation stimulus, if needed) are then added and incubated with cells for a brief period (~5-10 mins). Finally, iodide is added to cells, and changes in YFP-fluorescence are determined. Throughout this experiment, YFP fluorescence is measured using a fluorescence kinetic plate reader. Assays such as this have proven fruitful in identifying novel modulators for chloride channels such as $GABA_A$, CFTR, CaCCs, and VRAC [31, 45]. Furthermore, iodide-flux assays coupled with siRNA screening have led to the discovery of the genes that encode VRAC and PAC, again, highlighting the utility of these powerful ion-sensitive dyes [51, 52].

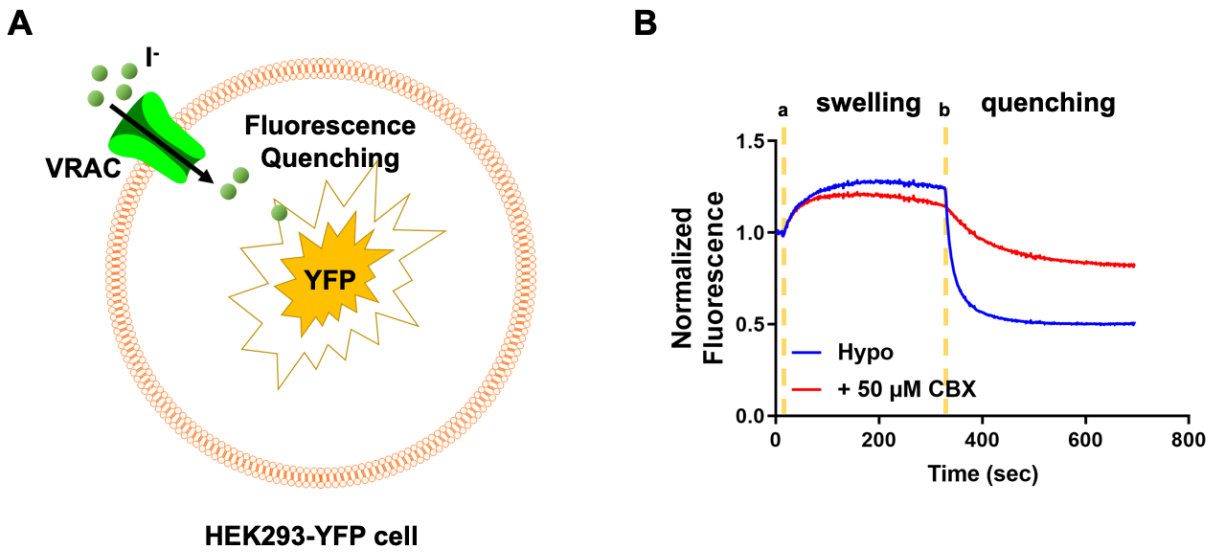

Figure 2. Representative schematic of a YFP-quenching assay for chloride channels

A) Conceptual model of YFP-quenching assay B) Representative traces of YFP-quenching assay using with DMSO or the VRAC inhibitor carbenoxolone. Hypotonic solutions added at time **a** and NaI added at time **b**.

LRRC8-CONTAINING VOLUME-REGULATED ANION CHANNELS

Overview

The ability of a cell to regulate its volume in response to osmotic pressure is an early evolutionary adaptation that allowed complex organisms to escape the primordial ocean and invade the land [53-57]. Perturbations in the osmolality of extracellular or intracellular milieu can lead to cell swelling or cell shrinkage. In the case of cell swelling, either decreases in osmolality of the extracellular solution or increases in osmolality of the intracellular solution lead to an influx of water, and ultimately, cell swelling. If cell swelling continues unperturbed, the cell may eventually rupture [53-57]. In order to counteract this swelling, the cell activates a process known as regulatory volume decrease, or RVD, where certain ion channels and transporters mediate K^+, Cl^-, and organic osmolyte efflux, forcing osmotically obliged water to leave the cell and returning the cell volume back to normal [58]. A major player in this process it the volume-regulated anion channel (VRAC), which can conduct chloride, as well as organic osmolytes (e.g., taurine, glutamate) [6].

Whole cell patch clamp electrophysiology studies in 1988 on T lymphocytes and human intestinal epithelial cells first identified VRAC currents ($I_{Cl,swell}/I_{Cl,vol}$) [59, 60]. Since the initial discovery of these currents, many groups have extensively studied VRAC's biophysics, cell physiology and regulation [7, 61]. VRACs were found to be ubiquitously expressed with varying degrees of pharmacological properties, inactivation kinetics, rates of activation, and osmolyte permeabilities [6]. The heterogeneity of VRAC subtypes in different cells led to several groups referring to VRAC by various terms, such as volume-sensitive outwardly rectifying anion channel (VSOR), volume-sensitive organic osmolyte-anion channel (VSOAC), and the volume-activated anion channel (VAAC) [6]. Several genes were proposed to encode VRAC during this period; however, all were eventually disproven [62-64]. In 2014, after nearly 30 years without a molecular counterpart, two independent groups, Ardem Patapoutian's group and Thomas Jentsch's group identified the leucine-rich repeat containing 8A (*LRRC8A*) gene as essential for VRAC function

using whole-genome siRNA screens coupled with high-throughput fluorescence assays [51, 52]. Other members of the *LRRC8* gene family include *LRRC8B*, *LRRC8C*, *LRRC8D*, and *LRRC8E* [51, 65]. Best available evidence suggests VRACs are hexameric channels consisting of LRRC8A (also referred to as SWELL1) and at least one other LRRC8 subunit [52, 66-70].

Over the past six years, the VRAC field has seen new insights in the channel's physiology, pathophysiology, structure, regulation, and pharmacology. I have summarized below many of these discoveries as well as discoveries made prior to the discovery of the LRRC8 gene.

Biophysics

There are several chloride channels that are activated in response to cell swelling that can be further categorized by their gating mechanism, voltage-dependent properties, anion permeability, and their pharmacology [30]. The swelling-activated chloride current, $I_{Cl,swell}$/$I_{Cl,vol}$, strictly refers the current produced by VRAC channels[61]. This current is measured using whole cell patch clamp electrophysiology, and is activated by exposing cells to hypotonic extracellular solutions or hypertonic intracellular pipette solutions [58]. $I_{Cl,swell}$ can be activated within a minute of hypotonic challenge, and take minutes to reach steady state [61]. During a hypotonic challenge in whole cell patch clamp electrophysiology, the cell will continuously swell due to clamping of an osmotic difference across the cell membrane by the extracellular bath solution and the intracellular pipette solution.

$I_{Cl,swell}$ is moderately outwardly rectifying and is specific for anions over cations (P_{cation}/P_{anion} ~0.02-0.04) [71-73]. $I_{Cl,swell}$ anion permeability follows the Eisenman's I sequence of $SCN^- > I^- > NO3^- > Br^- > Cl^- > F^-$ [53, 64, 74]. Furthermore, VRAC is permeable to various small charged organic osmolytes (e.g., taurine, gluconate, glutamate, pyruvate) with a Px/P_{Cl} of ~0.2-0.4 and uncharged organic osmolytes (e.g., *myo*-inositol, sorbitol), hence the name volume-sensitive organic osmolyte-anion channel [72, 75-79]. From Stoke's diameter of permeating anions, VRAC's pore diameter was estimated to be 1.1 nm wide [64]. A study using polyols came to a similar conclusion, estimating VRAC's pore to be 1.25 nm [80]. VRAC has also been shown to be

permeable to molecules such as HCO_3^-, water, and ATP, eluding to roles of pH regulation, water permeability and energy homeostasis, respectively [81-83].

In addition to being moderately outwardly rectifying, $I_{Cl,swell}$ shows time-dependent inactivation at positive voltages greater than 60 mV [84, 85]. This inactivation can be facilitated with more depolarizing pulses. The inactivation kinetics have been shown to vary across different cell types and may be due to the heterogeneity of subunit composition of VRAC ([61]; also see section **Structure/Function** below). Inactivation of $I_{Cl,swell}$ is due in part to the extracellular and intracellular ionic composition. Increasing extracellular divalent cations and protons have been found to facilitate inactivation [85-87] (low pH also activates a ubiquitously expressed proton-activated chloride channel that does not show current inactivation, and this current may be a contaminant in the pH-dependent studies of VRAC; [10, 11]), while decreasing extracellular chloride has a similar effect [85]. In addition, anionic substitution shows that the more permeable the anion, the less time-dependent inactivation is observed [85]. These observations are supported by studies showing VRAC inhibitors facilitate current inactivation and lessen voltage dependence for inactivation [71, 88, 89]. It should be noted that extracellular ATP inhibits VRAC currents in a voltage-dependent manner; however, inactivation does not occur with ATP inhibition, as with other inhibitors [84, 90]. Another variable that may affect $I_{Cl,swell}$ inactivation is the voltage clamp protocol used to elicit currents. A hyperpolarizing pre-pulse should be used to ensure all VRAC channels have recovered from inactivation due to a previous depolarizing pulse [91].

The unitary conductance of VRAC proved to be controversial in the early characterization of this channel. Early studies used stationary noise analysis on swelling-activated whole-cell currents to estimate the unitary conductance of VRAC and found that the channel had ~1 pS conductance at 0 mV [73, 92-95] whereas non-stationary noise analysis on swelling-activated whole-cell currents estimated ~15-20 pS at 0 mV [95]. This unitary conductance was corroborated by single channel measurements on excised patches and cell-attached recordings using double-patch configuration [84, 85, 96, 97]. The discrepancy between the unitary conductance estimated

from stationary noise analysis and the unitary conductance from single channel recordings was thought to be due to incorrect assumptions in open probability of the channel [6]. Stationary noise analysis assumed graded increases in macroscopic currents were due to graded increases in open probability of the channel; however, non-stationary noise analysis showed that open probability of VRAC most likely changed in stepwise fashion from 0 to near unity. This suggested that VRAC activation occurs by increasing the number of open channels over time rather than the increase of open probability over time [95]. The mechanism by which channel activation is regulated has yet to be elucidated.

In summary, these unique biophysical properties of outward rectification, time-dependent inactivation at positive voltages, permeability to inorganic ions and organic small molecules and moderate unitary conductance distinguish VRAC from other chloride channels that show activation following cell swelling such as bestrophins, CaCCs, CFTR, CLC-2 and Maxi-Cl [3].

Structure/Function

The LRRC8 protein family consists of five members: LRRC8A, LRRC8B, LRRC8C, LRRCD, and LRRC8E [65]. VRAC can be functionally reconstituted by expressing LRRC8A and at least one other LRRC8 subunit [51]. Various stoichiometry combinations of LRRC8 subunits give rise to different functional properties. Expression of the LRRC8D subunit has been shown to be important for the transport of platinum-based anticancer drugs, taurine, and blasticidin [98]. Studies on LRRC8A/LRRC8D heteromers showed they are important for the transport of uncharged myo-inositol, taurine, and GABA from cells, whereas LRRC8A/LRRC8E heteromers transport negatively charged aspartate [99]. LRRC8A/LRRC8E heteromers were also shown to be potentiated by intracellular oxidation while LRRC8A/LRRC8C and LRRC8A/LRRC8D heteromers were inhibited by intracellular oxidation [100]. Furthermore, LRRC8A/LRRC8E were found to inactivate at positive voltages, more so than LRRC8A/LRRC8C and LRR8A/LRRC8D heteromers [51]. VRAC activity can be measured if you knockout LRRC8C-E subunits from HCT116 cells; however, it is absent when heterologously expressing LRRC8A/LRRC8B

heteromers in quintuplet knock out of the LRRC8 proteins ($LRRC8^{-/-}$) [51]. One study suggests that LRRCB may serve as a Ca^{2+}-leak channel [101]. Singly expressing LRRC8B-E subunits into $LRRC8^{-/-}$ cells does not lead to surface expression, whereas singly expressing LRRC8A does although current is very small and shows little to no volume-sensitivity [51]. LRRC8A homomeric current can be amplified when coupling low ionic strength pipette solution with hypotonic bath solution ([70]; unpublished). When expressing LRRC8A/LRRC8C-E heteromers, decreasing LRRC8A cDNA during transfection results in larger currents compared to a 1:1 transfection ratio, suggesting subunit stoichiometry is important for channel function [102]. In studies of LRRC8 subunit expression in oocytes, constitutive VRAC activity in isotonic conditions was achieved by attached fluorescent proteins to the C-terminal end of LRRC8 subunits [103].

Four years after the genes that encode VRAC were discovered, four high-resolution cryo-EM structures of the LRRC8A homomer were published [67-70]. Two years later the structure of the LRRC8D homomer was published [66]. The LRRC8A structures varied slightly that may be explained by the different reagents used to generate the structures, as well as species used. LRRC8A can be broadly described by four regions: transmembrane region, extracellular region, intracellular region, and leucine-rich repeat (LRR) region. The transmembrane region is comprised of four transmembrane domains (TM1-4). The extracellular region is comprised of extracellular loop 1 and 2 (EL1-2). EL1 connects TM1 and TM2 and has one β-strand (EL1β), followed by one α-helix (EL1H). EL2 connects TM3 and TM4 and has two β-strands (EL2β1-2). The intracellular region is comprised of two intracellular loops (IL1-2). IL1 connects TM2 and TM3, and has three α-helices (IL1H1-3). IL2 connects TM4 and the LRR domain and has four α-helices (IL2H1-4). The leucine-rich repeat region is comprised of an N-terminus (containing one α-helix), 15 LRRs (LRR1-15) and a C-terminus (containing three α-helices). The LRRs form a crescent-shaped structure, as is observed in other LRR-containing proteins. The LRRC8A structure shows a hexameric assembly, as was predicted from homology comparison with Pannexins [65].

Likewise, a low-resolution structure of LRRC8A/LRRC8C heteromers showed a hexameric assembly [70]. The pore is comprised of TM1, TM2, EL1H, IL1H1, IL1H3 and the N-terminus. The diameter pore ranges from ~6 to 35 Å where the pore is narrowest towards the extracellular side and widest towards the intracellular side. The LRRC8D structure had four similar regions as LRRC8A. Some major differences between the LRRC8A structures and the LRRC8D structure were a larger pore, a resolved N-terminal α-helix inside the channel's pore, and a two-fold symmetry vs a three-fold or six-fold symmetry observed from the LRRC8A structures [66].

Prior to the cryo-EM structures of LRRC8A homomers, mutagenesis and cysteine accessibility studies demonstrated that LRRC8A T44 of TM1 was important for anion conduction. Mutating T44 to a cysteine increased I^- permeability, and reacting T44C with sodium (2-sulfonatoethyl)methanethiosulfonate (MTSES) inhibited VRAC current [52]. Further studies showed that mutating T44 to a cysteine in LRRC8C-E subunits also increased I^- permeability [104]. The cryo-EM structures confirmed T44 projects into the channel's pore [67-70]. Mutagenesis studies of the N-terminal domain of LRRC8A also altered permeability properties [105]. Mutating T5 to a cysteine increased I^- permeability and conferred MTSES inhibition [52, 69]. One of the LRRC8A structures showed a partial coiled region projecting towards the pore, but the rest of the N-terminus was unresolved [69]. The recent LRRC8D homomeric structure did have a resolved N-terminal helix, providing further evidence that the N-terminal region of LRRC8 subunits forms part of the channel's pore [66]. Mutagenesis studies guided by the cryo-EM structures of LRRC8A, identified LRRC8A R103, the residue found at the narrowest diameter of the pore, important for anion/cation permeability as well as for ATP and DCPIB block [67, 69]. Position R103 is replaced with a leucine in LRRC8C and LRRC8E and replaced with a phenylalanine in LRRC8D. The bulky phenylalanine was predicted to widen the pore, a property that may be important for the transport of organic osmolytes [70]. Indeed, the LRRC8D homomer structure had a wider pore at this position [66]. Mutating residues of LRRC8A EL1 with equivalent residues of LRRC8C and LRRC8E showed EL1 is important for voltage-dependent properties

and I^- permeability. Swapping regions of LRRC8A EL1 with LRRC8E EL1 and co-expression with LRRC8C conferred LRRC8E voltage-dependent inactivation properties, similar to those observed in LRRC8A/LRRC8E heteromers [106]. Chimera studies of LRRC8 subunits found that swapping IL1 and EL1 loops between subunits generated functional swelling-activated homomeric channels (e.g., LRRC8A-8C(EL1), LRRC8C-8A(IL1), LRRC8D-8A(IL1), LRRC8E-8A(IL1)) [102]. Interestingly, swapping 25 amino acids from LRRC8A IL1 into LRRC8C and LRRC8E IL1 generated functional VRACs [102].

It is important to note that the homomeric channels are not functional and may not exist in nature. However, the structures of homomeric LRRC8A and LRRC8D have provided great insight into the structure/function of these channels. In addition, chimeric approaches have yielded functional homomeric channels; however, again, VRAC exists as heteromeric assemblies of unknown stoichiometry.

Regulation

The process by which cell swelling leads to VRAC activation is still not fully resolved. Does cell swelling directly activate VRAC or are there intermediate signaling pathways? Perturbations in cell volume is accompanied by a multitude of changes including but not limited to changes in ionic strength, cytosolic inorganic ion composition, mechanical force at the cell membrane, membrane composition, molecular crowding, activation of protein kinases and Rho GTP-binding proteins, many of which have been shown to regulate VRAC activity in some manner.

Early studies suggested that intracellular anionic composition regulated VRAC activity; however, subsequent studies by the same group concluded that ionic strength rather than anion composition regulated VRAC by lowering the threshold for activation by swelling, or the volume set-point [75, 76, 107]. Other groups also found that ionic strength regulated VRAC in different cell types and suggested that reductions in ionic strength might be sufficient to activate VRAC [108-110]. The role of ionic strength is a topic of debate to this day. Studies using purified proteins reconstituted in lipid vesicles found that reductions in ionic strength in the absence of swelling led

to VRAC activation [104]. Ionic strength has been proposed to affect electrostatic properties of LRR domains of LRRC8 proteins and in turn affect LLR interactions with neighboring LLR domains [68-70]. Evidence for LRRs being the cell volume sensor is consistent with findings that attaching a fluorescent protein to the C-terminal end of LRRC8 proteins led to constitutive activity in absence of cell swelling [103]. However, this has not been tested further.

Studies have shown that intracellular ATP is required for swelling-activated VRAC activity. Increasing the intracellular concentration of ATP can accelerate VRAC activation, as well as lower the volume set-point [76, 111-113]. VRAC activation can also be achieved using non-hydrolyzable ATP analogs, such as AMP-PNP, AMP-PCP, and ATPγS, suggesting ATP binding, not ATP hydrolysis is necessary for channel activation [74, 112]. However, other studies suggest that ATP-dependent phosphorylation or both ATP-dependent phosphorylation and ATP binding is necessary for VRAC activation [89, 114, 115]. In addition, Mg-ATP is not sufficient for VRAC activation, and high intracellular Mg^{2+} concentrations inhibited VRAC [113]. The Mg^{2+} block is most likely due to the sequestration of free ATP from the cytosol. ATP has also been shown to regulate VRAC through paracrine and autocrine manners. Early studies in rat hepatoma cells showed that swelling-dependent release of ATP led to the activation of VRAC via purinergic P2Y receptors [116]. Later studies on astrocytes further supported this claim that ATP can activate VRAC, even in the absence of swelling [117]. The hypothesis was further expanded to include the activation of G_q-coupled G protein-coupled receptors (GPCRs) by ATP and other signaling molecules such as glutamate and bradykinin [74, 118-120].

Mechanical stretch of the cell membrane has been considered as an activating mechanism for VRAC; however, contradicting results have led others away from this hypothesis. Inducing sheer stress on the cell membrane led to the activation of Cl^- currents, but these currents did not follow the biophysical properties of $I_{Cl,swell}$ [121, 122]. Applying positive pressure through the patch pipette induced VRAC currents; however, it has been argued that cell swelling does not

lead to membrane stretch because cells normally possess extra membrane invaginations that may unfold during swelling [73, 91, 94, 123, 124].

The cytoskeleton and related components have also been investigated in the regulation of VRAC. Of note, the membrane microdomain, caveolae, has been implicated in the regulation of VRAC in a variety of contexts [74]. Annexin II, a calcium-dependent phospholipid binding protein important for the formation caveolae, was shown to regulate VRAC. The use of mimetic peptides reduced VRAC currents in vascular endothelial cells. It was proposed that annexin II peptides sequestered p11 ligand binding to endogenous annexin II [125]. Annexin II also forms a complex with another caveolae associated protein, caveolin 1 and expression of caveolin-1 was found to correlate with VRAC activity. Cells lacking caveolin 1 showed little $I_{Cl,swell,}$ which could be rescued by overexpression of caveolin 1 [126]. Introduction of a dominant negative form of caveolin 1 also reduced $I_{Cl,swell}$ [127].

Apoptosis and reactive oxygen species (ROS) have also been shown to regulate VRAC. During apoptosis, the cell undergoes cell shrinkage, a process mediated by a chloride current that fits the biophysical, pharmacological, and regulatory profile of $I_{Cl,swell}$ [128]. Proapoptotic stimuli such as staurosporine, TNFα, doxorubicin and ROS have been shown to induce $I_{Cl,swell}$ in the absence of cell swelling [128-132]. ROS production has also been proposed to occur during cell swelling in the absence of apoptosis [55]. $I_{Cl,swell}$ is reduced by inhibitors of the ROS-producer NAPDH oxidase (NOX). Additionally, ROS scavengers such as N-acetyl cysteine have been shown to block ROS-activated $I_{Cl,swell}$ [132]. Recent studies have shown that LRRC8A co-immunoprecipitates with NOX1 in vascular smooth muscle cells and functions as part of the NOX1 signaling complex [133]. As mentioned above, oxidation of heterologously expressed LRRC8A/LRRC8E heteromers leads to the activation of VRAC currents in Xenopus oocytes, further supporting a role for ROS as a regulator in the activation of $I_{Cl,swell}$ [100].

In summary, VRAC is regulated by a variety of processes and molecules. The complex regulatory process of VRAC led many laboratories to claim the incorrect molecular identify for the channel [134-138].

Physiology and pathophysiology

VRAC has been demonstrated to be important for cell volume regulation in a myriad of cell types [8, 53, 55]. This has recently been confirmed by genetic knockout of LRRC8A, the obligatory subunit of VRAC, leading to impaired RVD in cells [51]. VRAC has also been implicated in other physiological and pathophysiological processes; however, many of these studies were performed using poor pharmacological tools that are non-specific towards VRAC. For the purpose of this introduction, I will only be focusing on recent studies that used genetic evidence and genetic knockout approaches to establish and verify VRAC's role in these processes. It should be noted that genetic manipulations can lead to compensatory mechanisms and these studies should be carefully interpreted [139, 140].

The *LRRC8A* gene was initially discovered in a patient diagnosed with agammaglobulinemia, an immunodeficiency disorder characterized by defective B-cell development [141]. The patient had a singly mutated LRRC8A allele that truncated the last 91 amino acids and added 35 amino acids encoded by an intron, LRRC8A$^{\Delta 91/+35}$. The introduction of bone marrow cells expressing LRRC8A$^{\Delta 91/+35}$ into irradiated mice led to a significant decrease in B-cells [141]. Because the patient's unaffected allele encoded a WT LRRC8A, researchers concluded LRRC8A$^{\Delta 91/+35}$ may act in a dominant negative manner. Interestingly, later studies showed that LRRC8A$^{\Delta 91/+35}$ does not have VRAC activity, and when co-expressed with WT LRRC8A, VRAC activity is not repressed [52]. This suggests that LRRC8A$^{\Delta 91/+35}$'s role in B-cell development may not rely on VRAC activity. Additionally, LRRC8A KO mice only had a modest reduction in B-cells, and B-cell function was not affected [142]. These mice did exhibit reduced thymus development, decreased proliferation, increased apoptosis of thymocytes, and impaired

T-cell function [142]. In contrast to these findings, ébouriffé mice, which have a 2bp frame shift in *LRRC8A* that leads to a truncated form of LRRC8A, do not display impaired T-cell development and function. Interestingly, LRRC8A$^{ebo/ebo}$ T-cells lack $I_{Cl,swell}$ [143].

VRAC was recently demonstrated to play a role in innate immunity by facilitating the transport of cGAMP, a key molecule of the STING-mediated interferon response pathway, which is activated during DNA viral infection [144]. Activation of VRAC increased the interferon response to viral infection while LRRC8E knockout mice had a reduced response, suggesting that LRRC8E-containing VRACs are critical for this innate immune response [144]. Another study in bioRxiv suggests LRRC8C-containing VRACs are also important for this pathway [145].

VRAC has also been proposed to act as a regulator of the cell cycle and cell proliferation. $I_{Cl,swell}$ amplitudes have been demonstrated to fluctuate within the cell cycle [146, 147]. Furthermore, knockdown of the obligatory subunit of VRAC, LRRC8A, in glioblastoma cells was also able to slow cell proliferation [148]. This study supports previous pharmacological studies of VRAC showing non-specific pharmacological inhibitors are able to slow cell proliferation in different of cell types [149-153].

As mentioned above, VRAC has been implicated in apoptosis by mediating apoptotic volume decrease (AVD) [128]. Recently, genetic knockout studies LRRC8A impaired apoptosis and AVD induced by proapoptotic drugs such as cisplatin and staurosporine [98]. LRRC8A and LRRC8D knockout studies also showed reduced uptake of proapoptotic drugs such as platinum-based anticancer drugs cisplatin/carboplatin, suggesting a dual role in drug-induced apoptosis [98]. Additionally, analysis of the Cancer Genome Atlas showed patients with reduced expression of LRRC8D, but not LRRC8A, had lower survival rates suggesting a role in cancer and response to cancer treatments [98]. In addition to proapoptotic drugs, the antibiotic drug, blasticidin, was also found to enter cells through LRRC8D-dependent VRACs [98, 154].

Early studies suggested that VRACs play a role in the excitability of pancreatic beta cells and insulin secretion. Pancreatic beta cells regulate the secretion of insulin from the pancreas in

response to elevated blood glucose levels. As blood glucose levels rise, glucose is transported into beta cells, leading to increased glycolysis and an increase in the ATP/ADP ratio. This leads to the inhibition of K_{ATP} channels and a depolarization of the plasma membrane. Depolarized membrane potentials activate voltage gated Ca^{2+} channels, and the subsequent influx of Ca^{2+} causes insulin-containing vesicles to fuse to the cell membrane, releasing their contents for blood circulation [155, 156]. In addition to K_{ATP} currents, other glucose-stimulated currents have been measured including swelling-activated chloride currents [155]. Characterization of these chloride currents implicated VRAC; however, inconsistent anion permeability data suggested a different chloride channel may be responsible [157]. In addition, these studies relied on various non-specific inhibitors of VRAC [155]. Nevertheless, two recent studies supported this hypothesis and found that LRRC8A knockout mice had lost swelling-activated chloride currents from beta cells and had decreased glucose tolerance *in vivo* [158, 159]. One of these studies found that LRRC8A knockout from beta cells abolished glucose-dependent Ca^{2+} activity and insulin secretion from beta cells [158] while the other found that these processes were delayed [159]. The reasons for the discrepancies in these findings are currently unknown. Regardless, these studies show VRAC plays an important role in glucose homeostasis and may serve as therapeutic target for diseases such as type-2 diabetes.

LRRC8A knockout studies in mouse adipocytes abolished $I_{Cl,swell}$ and found VRAC is critical for adipocyte expansion and potentiating insulin signaling in the context of obesity [160]. Adipocyte glucose uptake and lipid synthesis is regulated by the insulin-PI3K-AKT2-GLUT4 signaling pathway. LRRC8A was found to regulate this pathway by interactions with growth factor receptor bound-2 (GRB2) and caveolin 1 via LRR domains of LRRC8A. GRB2 knockout was able to rescue insulin-PI3K-AKT2-GLUT signaling in LRRC8A KO adipocytes [160]. Authors proposed VRAC activation led to increased signaling through this pathway. *In vivo*, LRRC8A knockdown or adipocyte specific LRRC8A knockout reduced adiposity, adipocyte size, and impaired systemic glycemia and insulin sensitivity in obese mice [160]. These studies are in line with previous

findings that LRRC8C is important for high-fat diet-induced weight gain and insulin resistance. Interestingly, a study published while this dissertation was being written shows that LRRC8A plays a similar role in skeletal muscle by regulating the insulin/stretch-PI3K-AKT2 pathway in myocytes as well myogenic differentiation [161]. VRAC's role in myocyte differentiation was also studied recently in C2C12 cells, showing VRAC activation early in myocyte differentiation [162].

Numerous studies have implicated astrocytic VRAC in the pathogenesis of stroke as well as contributing to normal, physiological release of excitatory amino acids for astrocyte-neuron communication [74, 163]. Ischemic stroke leads to astrocyte swelling, VRAC activation, and release of glutamate, via VRAC, into the extracellular space. Glutamate release into synapses can activate NMDA receptors, triggering calcium influx and excitotoxic cell death [163]. Genetic knockdown and knockout studies of LRRC8A in astrocytes abolishes VRAC-dependent chloride currents and glutamate release in cultures and *in vivo* [164, 165]. In the latter study, astrocytic LRRC8A knockout reduced total infarct size, as well as improved neurological scores compared to wildtype mice following experimental stroke [165]. These results are supported by pharmacological experiments using tamoxifen and DCPIB to inhibit VRAC [166-172]. However, the lack of specificity of these compounds raises concerns about potentially confounding off-target effects of the drugs [173-177]. In the same study with astrocyte-specific ablation, the group found that glutamatergic transmission was diminished due to a decrease in release probability and available ambient glutamate. This suggests VRAC plays a role in tonic release of glutamate at these synapses.

LRRC8A knockout mice were found to have a variety of phenotypes including infertility, high pre- and postnatal mortality, growth retardation, curly hair and multiple severe tissue abnormalities [142]. Subsequent studies on germ-line specific LRRC8A knockout mice showed that infertility in male mice is caused by impaired volume regulation in sperm that led to disorganized mitochondrial sheaths, malformed flagella, and reduced motility [178, 179]. Studies in ébouriffé mice also found they are infertile and have similar sperm defects as LRRC8A knockout

mice [143]. A patient with a heterozygous mutation in LRRC8A (R545H) was also found to have a fertility disorder, called Sertoli-cell only disorder [179]. Studies in Xenopus oocytes found that this mutation led to a reduction in currents when co-expressed with LRRC8C or LRRC8D. However, these studies used fluorescently tagged LRRC8 subunits to activate currents, and also showed 1:1 co-expression of LRRC8A R545H and LRRC8A WT had no effect on currents [179]. Therefore, further studies of how this mutation causes infertility is warranted.

In summary, VRAC current as well LRR8A-dependent protein-protein interactions have been implicated in health and disease. These molecular studies provide some of the first steps in validating VRACs as potential therapeutic targets. Due to their ubiquitous expression, it is difficult to imagine targeting VRACs in a specific tissue type; however, this may become possible as we continue to learn more about the subtype-specific roles (i.e., LRRC8D-dependent vs. LRRC8E-dependent) as well as the possibility of distinguishing such subtypes pharmacologically or genetically.

Pharmacology

For nearly 30 years researchers have relied on non-specific modulators to study the pharmacology of VRAC, which is a common problem faced for many chloride channels. The lack of specific modulators hampered many physiological studies prior to the molecular cloning of VRAC and continues to impede the understanding of VRAC as a potential therapeutic target. Therefore, the VRAC field would greatly benefit from studies aimed at developing the pharmacology of these important channels.

The best-in-class inhibitor of VRAC to date is the ethacrynic-acid derivative DCPIB (4-(2-butyl-6,7-dichlor-2-cyclopentyl-indan-1-on-5-yl)oxybutyric acid) [173]. DCPIB inhibits VRAC in various cell types, including HEK293 cells, HELA cells, HCT116 cells (unpublished), calf bovine pulmonary artery endothelial cells, mouse astrocytes, Xenopus oocytes, guinea-pig atrial cardiomyocytes, and rat pancreatic beta cells, in a voltage-independent, fully reversible manner with an IC_{50} in the range of 2-5 μM [118, 173, 180-184]. DCPIB is preferred over other VRAC

inhibitors due to its specificity towards VRAC over other chloride channels such as CFTR, CaCCs, CLCs, Maxi-Cl, and PAC [173, 185-187]. However, it has been shown to have several off-target effects such as, K_{ir} channels, TREK K^+ channels, H^+/K^+-ATPase, connexin hemichannels, glutamate transporter GLT-1, and most recently our lab has found DCPIB also inhibits mitochondrial function [175-177, 188, 189].

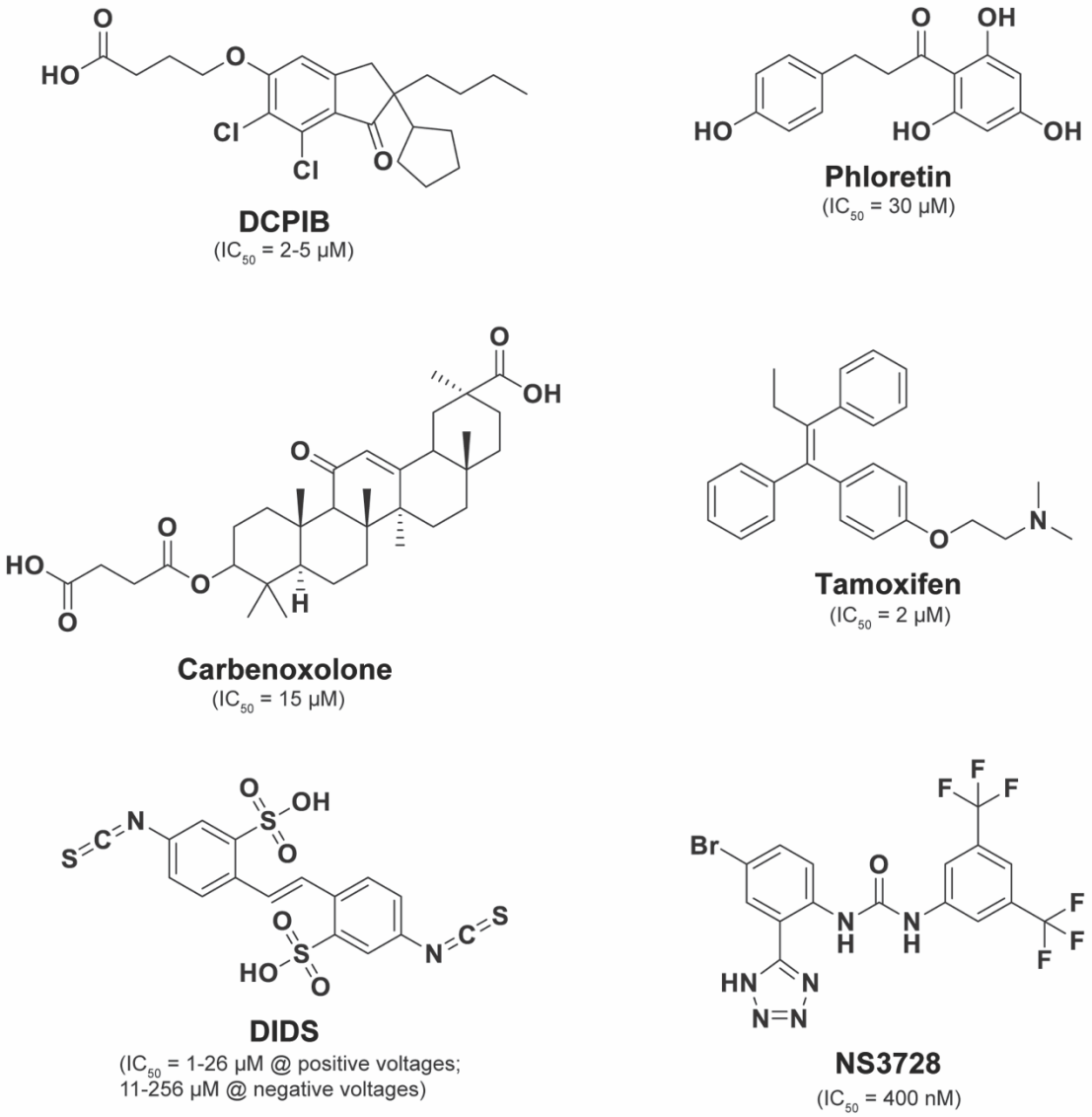

Figure 3. Commonly used VRAC inhibitors

The potassium-chloride cotransporter (KCC) antagonist, R-(+)-[(2-n-butyl-6,7-dichloro-2-cyclopentyl-2,3-dihydro-1-oxo-1H-inden-5-yl)-oxy] acetic acid (DIOA) is structurally related to

DCPIB, only differing in the length of its oxy-carbonic acid group (DCPIB has an extra carbon in the linker). DIOA inhibits VRAC in rat thymocytes [190] and HeLa cells with an IC50 of 20 mM [187]. The differences in potency between DCPIB suggest the length of the oxy-carbonic acid group is important for VRAC inhibition.

The acidic di-aryl urea small molecules were found to inhibit VRAC, with NS3728 being the most potent with an IC_{50} of 400 nM. However, NS3728 was also found to inhibit CaCCs [191, 192].

The natural phenol, phloretin was shown to inhibit VRAC in a voltage-independent and reversible manner with an IC_{50} of 30 μM [193]. The inhibitory effects were only observed when phloretin was applied extracellularly; intracellular application through the pipette solution did not inhibit VRAC [193]. Phloretin was also shown to inhibit CFTR at high concentrations, but not inhibit CaCCs. Additional off-targets include cation channels, aquaporins and transporters [193].

The estrogen receptor modulator, tamoxifen, has also been shown to inhibit VRAC in various different cell types such as astrocytes, endothelial cells, epithelial cells, macrophages, fibroblasts, mouse cortical collecting duct cells with an IC_{50} of 2 μM [89, 147, 151, 192, 194-197]. Tamoxifen inhibition of VRAC was found to be voltage-independent and reversible. Interestingly, despite the ability of tamoxifen to inhibit VRAC in a variety of different cell types, it was unable to inhibit neuronal VRAC [97, 198, 199].

The gap junction/hemichannel inhibitor, carbenoxolone, was also found to inhibit VRAC with an IC_{50} of 15 uM [200].

Conventional non-specific anion channel inhibitors such as SITS (4-acetamido-4’-isothio-cyanato-2,2’-stilbenedisulfonic acid), DIDS (4,4'-diisothiocyano-2,2'-stilbenedisulfonic acid), NFA (niflumic acid), FFA (fluflemic acid), NPPB (5-nitro-2-(3-phenylpropylamino)benzoic acid), DPC (diphenylamine-2-carboxylate), 9-AC (9-Anthracenecarboxylic acid), NPA (N-phenylanthracillic acid), have been shown to inhibit VRAC with IC_{50}s in the single micromolar range to the 100s of

micromolar range [184, 187, 192, 197, 201-203]. SITS and DIDS, inhibited VRAC in a voltage-dependent manner, with higher potency at positive voltages compared to negative voltages [94, 201, 204]. This voltage-dependency suggests that these compounds inhibit VRAC in an open-state-dependent manner, which is supported by the approximate effective radii of these compounds being similar the predicted VRAC pore size [80, 205].

ATP also inhibits VRAC on the extracellular side with voltage-dependence with an IC_{50} of 2-5 uM at positive voltages, suggesting pore block [90, 206]. Mutagenesis of LRRC8A pore lining residue, R103, was able to abolish block by ATP [69].

In summary, several molecules inhibit VRAC with varying potencies and specificities (Figure 3). Their anion channel specificity has been important when using these compounds to define physiological and pathophysiological roles of VRACs. With the recent discovery of the genes that encode VRAC, many of these roles have been verified using genetic approaches. Additionally, the completed structures of LRRC8 proteins have provided insight into the mechanism of action of these compounds. Recently, a DCPIB-bound LRRC8A homomeric structure was published, showing DCPIB interacting with pore-lining residue R103 [67]. Understanding the binding site of VRAC inhibitors may point to structural changes that can be made to these molecules that my potentially increase potency and specificity towards VRAC. Moreover, the ability to generate VRAC knockout cells provides the opportunity to better test the specificity of compounds.

GOALS OF THIS THESIS

Volume-regulated anion channels (VRACs) play important roles in human physiology and pathophysiology. The recent cloning of the genes that encode VRACs provide unprecedented opportunities for studying the molecular physiology of these important channels. My thesis project will employ leading-edge techniques in electrophysiology, site-directed mutagenesis, and high-throughput fluorescence assays, to develop the molecular pharmacology of VRAC channels.

CHAPTER 2. CYSTL1 RECEPTOR ANTAGONISTS PRANLUKAST AND ZAFIRLUKAST INHIBIT LRRC8-MEDIATED VOLUME REGULATED ANION CHANNELS INDEPDENTLY OF THE RECEPTOR

Work presented in this chapter was published in American Journal of Physiology-Cell Physiology [45].

Abstract

Volume Regulated Anion Channels (VRACs) encoded by the LRRC8 gene family play critical roles in myriad cellular processes and might represent druggable targets. The dearth of pharmacological compounds available for studying VRAC physiology led us to perform a high-throughput screen (HTS) of 1,184 of FDA-approved drugs for novel VRAC modulators. We discovered the cysteinyl leukotriene receptor 1 (CysLT1R) antagonist, Pranlukast, as a novel inhibitor of endogenous VRAC expressed in HEK293 cells. Pranlukast inhibits VRAC voltage-independently, reversibly, and dose-dependently with a maximal efficacy of only ~50%. The CysLT1R pathway has been implicated in activation of VRAC in other cell types, prompting us to test whether Pranlukast requires the CysLT1R for inhibition of VRAC. Quantitative PCR analysis demonstrated that *CYSLTR1* mRNA is virtually undetectable in HEK293 cells. Furthermore, the CysLT1R agonist LTD4 had no effect on VRAC activity and failed to stimulate Gq-coupled receptor signaling. Heterologous expression of the CysLT1R reconstituted LTD4-CysLT1R-Gq-calcium signaling in HEK293 cells but had no effect on VRAC inhibition by Pranlukast. Finally, we show the CysLT1R antagonist Zafirlukast inhibits VRAC with an IC_{50} of ~17 μM and does so with full efficacy. Our data suggest that both Pranlukast and Zafirlukast are likely direct channel inhibitors that work independently of the CysLT1R. This study provides clarifying insights into the putative role of leukotriene signaling in modulation of VRAC and identifies two new chemical scaffolds that can be used for development of more potent and specific VRAC inhibitors.

Introduction

The ability of a cell to regulate its volume in response to changes in swelling or shrinkage is an early evolutionary adaptation required for homeostasis [53-57]. Cell swelling induced by hypo-osmotic shock activates a process known as regulatory volume decrease (RVD) that restores the cell to its normal volume. Volume-regulated anion channels (VRACs) enable RVD by mediating the efflux of chloride (Cl-) and small organic osmolytes (e.g. taurine) from the cell, which creates an outwardly directed osmotic driving force that promotes water efflux from the cell [53-57].

VRAC function has been studied extensively using electrophysiological techniques for nearly three decades [59, 207]. VRACs are ubiquitously expressed in mammalian cells and have been implicated in diverse functions, in addition to cell volume regulation, such as cell proliferation [146, 208, 209], cell migration [210, 211], regulation of endothelial cell calcium signaling [212], release of excitatory amino acids in the brain [72, 165, 169, 213], and regulation of insulin secretion from pancreatic beta cells [155, 158, 159, 214, 215].

The identity of the genes encoding VRACs has been highly controversial [6], and only recently has the gene family been definitively established. In genome-wide RNA interference screens, the laboratories of Patapoutian and Jentsch found that the leucine-rich repeat containing 8A (LRRC8A) gene is essential for VRAC activity in mammalian cells [51, 52]. Other gene family members include LRRC8B, LRRC8C, LRRC8D, and LRRC8E. The best available evidence suggests that VRACs are hexamers containing a LRRC8A subunit and at least one other LRRC8 subunit [51, 67-70]. The identification of the genes encoding VRAC creates unprecedented opportunities for studying the molecular and integrative physiology and therapeutic potential of these important channels.

Emerging evidence raises the intriguing possibility that VRAC might represent a druggable target in certain disease states (reviewed in Strange et al., 2019). For example, several studies have suggested that VRAC expressed in astrocytes might be a therapeutic target in stroke [74,

163]. Ischemic stroke leads to astrocyte swelling, VRAC activation, and release of glutamate, via VRAC, into the extracellular space. Glutamate release into synapses can activate NMDA receptors, triggering calcium influx and excitotoxic cell death [163]. Genetic knockdown and knockout studies of LRRC8A in astrocytes abolishes VRAC-dependent chloride current and glutamate release in cultures and *in vivo* [164, 165]. In the latter study, astrocytic LRRC8A knockout reduced total infarct size, as well as improved neurological scores compared to WT mice following experimental stroke [165]. These results are supported by pharmacology experiments using tamoxifen and DCPIB to inhibit VRAC [166-172]. However, the lack of specificity of these compounds raises concerns about potentially confounding off-target effects of the drugs [173-177]. To fully establish the safety and efficacy of VRAC inhibition in stroke and other therapeutic areas, more potent and specific inhibitors of VRAC must be developed.

In this study, we performed a high throughput screen with HEK293 cells for novel small-molecule modulators of VRAC. By interrogating a library of 1,184 FDA-approved drugs, we identified the CysLT1 receptor (CysLT1R) antagonist, Pranlukast, as a novel inhibitor of VRAC. Interestingly, CysLT1R has been implicated in the modulation of VRAC [216], however, we show that HEK293 cells do not functionally express the CysLT1 receptor. In addition, we show the structurally distinct CysLT1R inhibitor, Zafirlukast, also inhibits VRAC. These studies provide clarifying insights into the putative role of CysLT1 receptor signaling in regulation of VRACs and identify CysLT1R antagonists as structurally novel small-molecule inhibitors of LRRC8 channels.

Materials and Methods

Chemicals

Pranlukast was purchased from Sigma-Aldrich (St. Louis, MO). All salts were purchased from Sigma-Aldrich and were of the highest grade available.

Molecular biology

The CysLT1R-pCMV6 plasmid was purchased from Origene Technologies. The YFP(H148Q/I152L) plasmid was generously provided by Dr. David Weaver (Vanderbilt University). We introduced an additional mutation (F46L) to increase yellow fluorescent protein (YFP) fluorescence emission and halide sensitivity [50] using a QuickChange Mutagenesis Kit (Agilent Technologies). The YFP(F46L/H148Q/I152L) cDNA was fully sequenced to ensure that the intended mutations were present and that no spurious mutations had occurred during the PCR amplification. LRRC8AKO-HEK293 cells were a kind gift from Dr. Rajan Sah (Washington University, St. Louis, MO). LRRC8A knockout was generated by a CRISPR-Cas9 mediated approach [217].

Quantitative real-time PCR

For mRNA quantification of HEK293, HEK293-Ozzy, and THP-1 cells, total RNA was isolated using TRIzol (Life Technologies). FAM labeled Taqman probes against human *LRRC8A* (Cat no. 4331182), human *LRRC8B* (Cat no. 4331182), human *LRRC8C* (Cat no. 4331182), human *LRRC8D* (Cat no. 4351372), human *LRRC8E* (Cat no. 4331182), and human *ACTB* (Cat no. 4331182) were purchased from Applied Biosystems (Foster City, CA). *qSTAR* qPCR primer pairs against human *CysLT1R* (Cat no. HP209551) and *GAPDH* (Cat no. HP205798) were purchased from Origene Technologies. The SsoAdvanced Universal Probes Supermix was used as a qPCR reagent for *LRRC8A-E and* ACTB (BioRad, Hercules, CA). The iTaq Universal SYBR Green One-Step Kit was used as a qPCR reagent for *CYSLT1R* and *GAPDH* (Bio-Rad, Hercules, CA). Reactions containing 500 ng RNA were run from at least 2 biological replicates in duplicate in 10 µL reactions according to the manufacturer's specifications using a Bio-Rad CFX96 instrument (Bio-Rad, Hercules, CA). *ACTB* and *GAPDH* were used as reference genes. Normalizations were done using the $2^{-\Delta\Delta CT}$ method.

Cell Culture and transient transfection

HEK293 cells were cultured in 75 cm^2 flasks with Dulbecco's Modified Eagle Medium (DMEM) supplemented with 10% Fetal Bovine Serum (FBS) 1% Penicillin/Streptomycin (P/S). HEK293 cells stably transfected with the YFP(F46L/H148Q/I152L) fluorophore (i.e. HEK293-Ozzy cells) were cultured in the same medium supplemented with 700 µg/mL G418 Sulfate (Corning, Corning, NY). For patch clamp experiments, HEK293 cells plated in 35-mm Nunclon dishes (Thermo Fisher Scientific, Rochester, NY) were co-transfected with 1 µg CysLT1R plasmid DNA and 0.5 µM GFP (transfection marker) using Lipofectamine LTX and studied the next day. For calcium imaging experiments, HEK293 cells were transfected with 8 µg CysLT1R plasmid DNA in T-75 flasks (Thermo Fisher Scientific, Rochester, NY), plated in 384-well plates (Corning; see below) the next day, and allowed to recover for an additional 24 hours before experiments.

Patch clamp electrophysiology

The day of experiments, parental or transfected (see above) HEK293 cells were rinsed with divalent-free Hank's Balanced Salt Solution (HBSS), dissociated using 0.25% trypsin/1 mM EDTA for approximately 30-sec, diluted with complete medium, plated on poly-L-lysine-coated round glass coverslips, and allowed to recover at 37ºC in a 5% CO_2 incubator for at least 1 h before experiments. Patch pipettes were pulled from Clark Custom 8520 Patch Glass (1.5 o.d. × 1.16 i.d.) (Harvard Apparatus, Holliston, MA) using a P-1000 Flaming/Brown Microelectrode puller (Sutter Instruments) to a resistance of 2 – 4 MΩ when filled with the following solution (in mM): 126 CsCl, 2 MgSO4, 20 HEPES, 1 EGTA, 2 Na_2ATP, 0.5 GTP (pH 7.2 adjusted with CsOH, 275 mOsm). The isotonic bath solution contained (in mM): 75 CsCl, 5 MgSO4, 1 Calcium-D-gluconate, 12 HEPES, 8 Tris base, 5 glucose, 2 glutamine, and 95 sucrose (pH 7.4 adjusted with CsOH, 300 mOsm). Hypotonic bath (250 mOsm) was made by excluding sucrose from the isotonic bath.

Macroscopic currents were recorded under voltage-clamp conditions using an Axopatch 200B amplifier (Molecular Devices, Sunnyvale, CA). Cells were voltage clamped at a holding potential of -30 mV and whole-cell currents were elicited by a voltage ramp or step protocol. For

voltage ramps, membrane potential was first stepped to -100 mV for 50 msec and then ramped over 1 sec to +100 mV. This was followed by a step back to 0 mV for 4 sec before this protocol was repeated. Step changes in membrane voltage were induced by stepping membrane voltage to -120 mV to +120 mV in 800 msec, 20 mV increments. Data were collected at 5 kHz and filtered at 1 kHz. Data acquisition and analysis were performed using pClamp 9.2 software suite (Molecular Devices). Percent inhibition of compounds was determined by normalizing data to currents inhibited by 10 μM DCPIB. Initial rate of swelling-induced VRAC activation was calculated by determining the linear slope of increasing current during the first 180 seconds following hypotonic solution addition.

Fluorescence reporter assay of VRAC function

HEK293-Ozzy cells were dissociated using 0.25% trypsin/1 mM EDTA and plated at a density of 20,000 cells/well in clear bottomed, black-walled Corning PureCoat amine coated 384 well plates (Corning, Corning, NY) and cultured overnight at 37ºC in a 5% CO_2 incubator. The following day cells were washed with isotonic solution containing (in mM): 140 NaCl, 5 KCl, and HEPES (pH 7.4, 310 mOsm). Compounds from the FDA library were dissolved in hypotonic solution containing (in mM): 5 KCl, 20 HEPES, and 90 mannitol (pH 7.4, 120 mOsm) and added simultaneously to all 384-wells at a final screening concentration of 10 μM. After 5 min allowed for cell swelling and VRAC activation, 100 mM NaI was added to all 384-wells simultaneously and Ozzy fluorescence was measured at 1Hz using a Panoptic kinetic imaging plate reader (WaveFront Bioscience, Franklin, TN, USA). Fluorescence values from each well were normalized to baseline readings (i.e. average of the first 5 readings before hypotonic solution is added). Percent fractional quenching was calculated by subtracting fluorescence readings obtained before and after NaI addition. Data were plotted with GraphPad Prism version 7.03 (GraphPad Software, San Diego, CA) to generate representative experiment traces and CRCs using a non-linear regression analysis.

Calcium imaging

Parental HEK293 cells or HEK293 cells transiently transfected with CysLT1R (see above) were dissociated and plated in 384-well plates as described above. The next day, the cells are washed and incubated in assay buffer (HBSS + 20 mM HEPES) containing a final concentration of 2 μM Fluo-8 AM. The cells were incubated with dye for 1 hour at room temperature and washed with assay buffer. Compounds in assay buffer were added at 2X concentrations to reach final concentrations indicated in the figure legends. Fluo-8 fluorescence was measured using a Panoptic plate reader and normalized to baseline (average of the first 5 readings before solution addition).

Statistics

All data are presented as means ± SEM; n represents the number of cells in patch-clamp recordings, the number of plates in high throughput screens, or the number of wells in fluorescence-based assays. Statistical significance was determined by using Student's t test for unpaired means for two groups. For groups greater than two, one-way analysis of variance (ANOVA) and Kruskal-Wallis post-hoc test was used.

Results

Development of a VRAC reporter assay for HTS

We developed a quantitative, fluorescence-based "quenching" assay that reports endogenous VRAC activity in HEK-239 cells to support an HTS campaign for novel channel modulators. qPCR analysis revealed expression of all *LRRC8* gene family members, where *LRRC8D* was the predominate subunit expressed at the mRNA level (n=4; Fig. 4A). The assay was adapted from those used to identify the *LRRC8* gene family in genome-wide siRNA screens [51, 52]. Stably transfected HEK293 cells expressing a iodide-sensitive YFP mutant, termed Ozzy, were plated in 384-well plates, exposed to hypotonic medium for 5 min to induce VRAC activation, and then treated with iodide-containing buffer to induce inwardly directed iodide flux through

VRAC and quenching of the Ozzy fluorophore (Fig. 4B; black line). The degree of iodide-induced quenching was dramatically reduced in HEK293 cells lacking the essential VRAC subunit LRRC8A (Fig. 4B; grey line), indicating that most of the quenching signal reflects iodide flux through VRAC.

We evaluated the assay's ability to quantify inhibition of VRAC by the known inhibitor carbenoxolone (CBX; [103, 200, 218]). CBX inhibited VRAC-mediated iodide quenching (e.g. Fig. 4C) in a dose-dependent manner with a mean ± SEM IC_{50} of 18 ± 0.54 μM (n=10; Fig. 4D), which is close to the value reported by others using electrophysiological techniques [200]. Using CBX as a control inhibitor, we performed a so-called "checkerboard" assay to evaluate the uniformity and reproducibility of the assay. Every other well of a 384-well plate was treated with hypotonic media alone or hypotonic media containing 50 μM CBX. As shown in Fig. 4E, there was a clear separation of iodide-induced quenching observed in blocked vs. unblocked population of wells (Fig. 4D). The mean ± SEM Z' value calculated from 8 plates over 3 days was 0.70 ± 0.03, indicating the assay is robust enough to support high-confidence hit-picking in a high-throughput screen. Finally, we found that the assay is tolerant to the small-molecule solvent DMSO at concentrations ranging between 0.0046 and 0.12 % (v/v) (Figure 4F), ruling out the possibility of DMSO having direct, confounding effects at the screening concentration of 0.01% v/v.

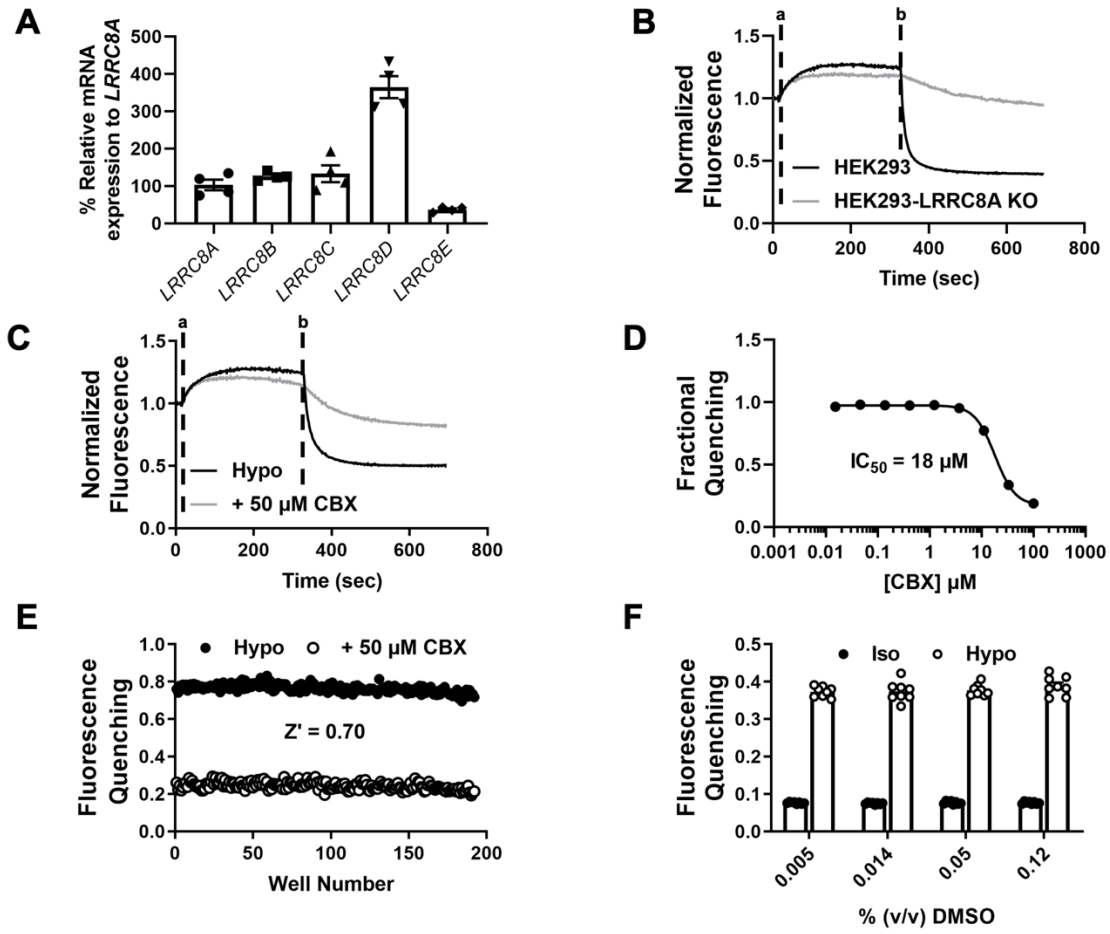

Figure 4. Ozzy assay development

A) qPCR quantification of LRRC8A-E mRNA in Ozzy-HEK293 cells (n=4). B) Representative traces of Ozzy-quenching assay using HEK293 cells and HEK293-LRRC8A KO cells. Hypotonic solutions were added at time "a" and NaI was added at time "b". C) Representative traces of an Ozzy-quenching assay using the known VRAC inhibitor carbenoxolone (CBX). Hypotonic solutions (hypotonic (hypo) bath; hypotonic bath + 50 µM CBX) were added at time "a" and NaI was added at time "b". D) CBX CRC generated using Ozzy-quenching assay (mean ± SEM IC50 = 18 ± 0.54 µM; n=10). E) Scatter plot of "checkerboard" analysis for Ozzy-quenching assay (mean ± SEM Z'=0.70 ± 0.03; 8 plates over 3 days). F) The effect of DMSO concentration in isotonic and hypotonic bath solutions on Ozzy fluorescence quenching (n=8).

Discovery and characterization of Pranlukast as an inhibitor of VRAC

We screened 1,184 compounds from the SelleckChem FDA-approved drug collection for novel inhibitors of VRAC. The mean ± SEM Z' for the 6-plate run was 0.64 ± 0.01, indicating the assay performed well during the screen. The only reproducible inhibitors identified in the screen was Pranlukast (Fig. 5A), an antagonist of the cysteinyl leukotriene receptor 1 (CysLT1) used for the treatment of asthma [219, 220]. As shown in Fig. 5B, Pranlukast inhibited VRAC-mediated iodide quenching dose-dependently and with partial efficacy (n=5). We could not derive an IC_{50} because Pranlukast does not fully inhibit the channel.

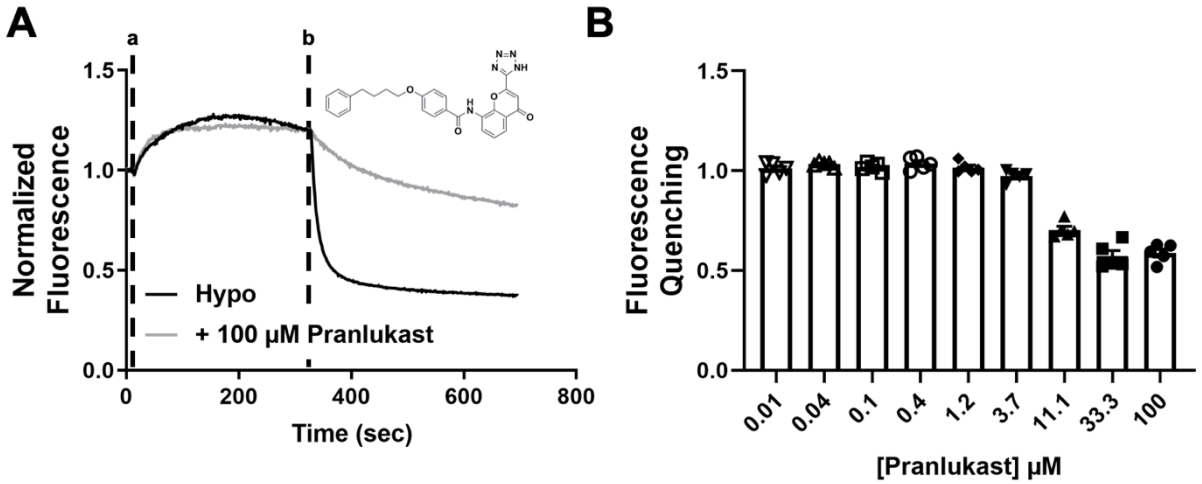

Figure 5. Discovery of Pranlukast in a HTS of the FDA library

A) Representative traces of an Ozzy-quenching assay with Pranlukast. Hypotonic solutions (hypotonic (hypo) bath; hypotonic bath + 100 µM Pranlukast) were added at time "a" and NaI was added at time "b". Inset: structure of Pranlukast. B) Dose-dependent inhibition of VRAC using Ozzy-quenching assay (n=5).

We confirmed and extended these observations using whole-cell patch electrophysiology techniques to measure VRAC function and inhibitory characteristics of Pranlukast. HEK293 cells were patch clamped with intracellular and extracellular solutions designed to isolate chloride currents under isotonic conditions (300 mOsm) and then subjected to a 200-250 mOsm hypotonic stimulus to induce cell swelling. As shown in Fig. 6A, cell swelling led to the activation of outwardly rectifying chloride current exhibiting time-dependent inactivation at positive potentials that is characteristic of VRAC [7]. Bath application of 3 μM Pranlukast, which is close to the solubility limit of Pranlukast in these buffers, led to a reduction in VRAC current amplitude (Fig. 6A). Inhibition was dose-dependent with a mean ± SEM maximal efficacy at 3 μM of 51 ± 6% ($n \geq 4$; Fig. 6B). We evaluated the voltage-dependency of Pranlukast inhibition in voltage-ramp experiments (Fig. 6C), which revealed that VRAC inhibition is voltage-independent (Fig. 6D). Pranlukast-dependent inhibition occurred with a mono-exponential time course (Fig. 6E) and mean ± SEM time constant of 61 ± 15 sec ($n=7$; Fig. 6F) and was fully reversible (Fig. 6E).

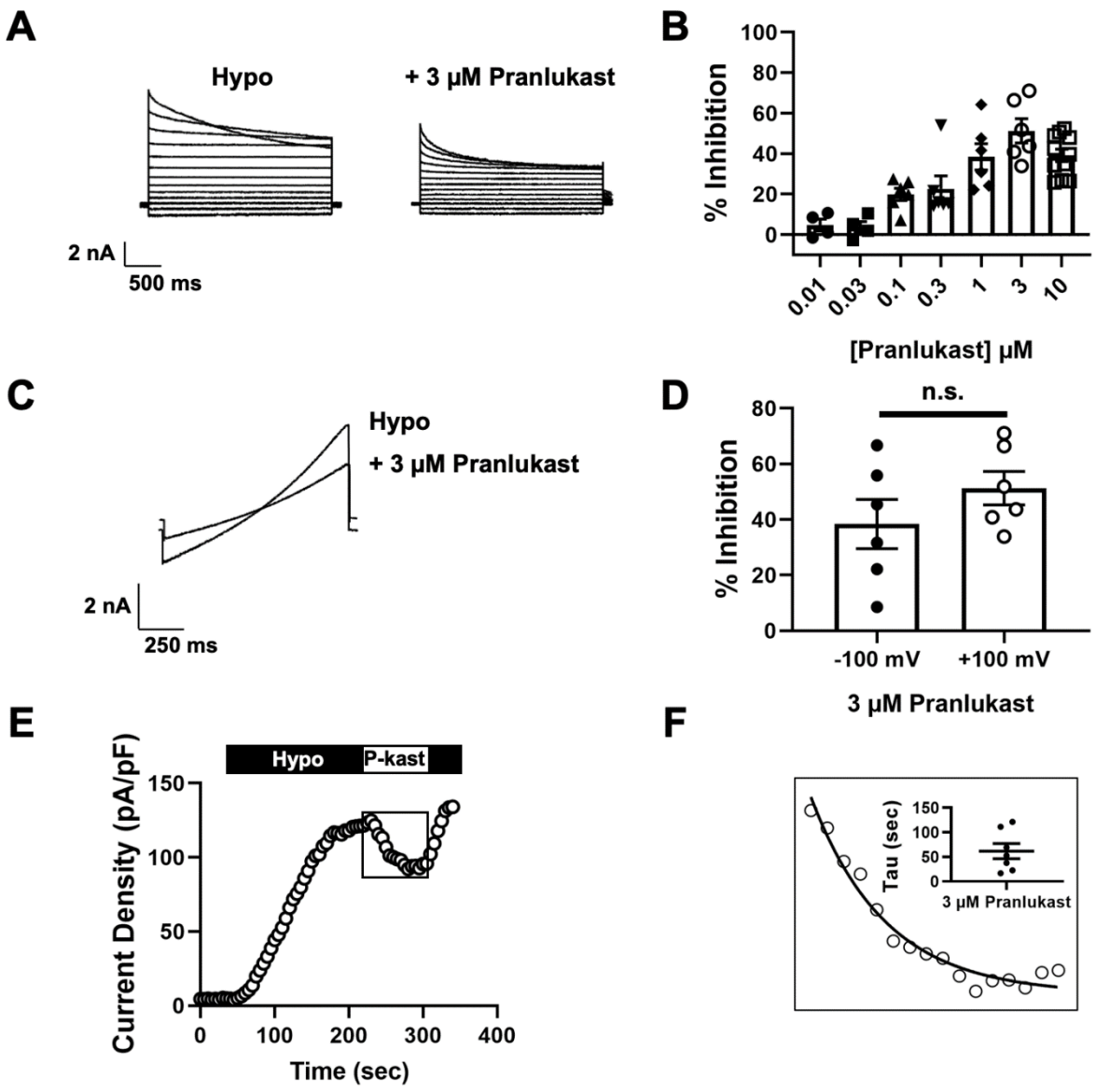

Figure 6. Pranlukast inhibits VRAC currents

A) Whole-cell currents from HEK293 cells were measured using a step protocol from -120 mV to +120 mV, with 20 mV steps. Cells were exposed to hypotonic bath and hypotonic bath + 3 μM Pranlukast. B) Dose-dependent inhibition of VRAC with Pranlukast from whole-cell patch clamp electrophysiology (max efficacy at 3 μM = ~50%; n≥4) C) Whole-cell currents from HEK293 cells were measured using a ramp protocol from -100 mV to +100 mV. Cells are exposed to hypotonic bath and hypotonic bath + 3 μM Pranlukast. D) Analysis of VRAC currents with 3 μM Pranlukast at -100 mV and +100 mV from applying the voltage ramp protocol. E) Exemplar time course of VRAC activation under hypotonic solution exposure, 3 μM Pranlukast, and wash (hypo) treatment F) 3 μM Pranlukast-dependent current inhibition time constant (mean ± SEM τ=62 ± 16 sec; n=7).

In control hypotonic buffer, inactivation of VRAC current at 120 mV is described by a single exponent with a mean ± SEM time constant of 1.7 ± 0.1 sec (n=17; Fig. 7A-B). In contrast, bath application of 3 μM Pranlukast led to the appearance of a second, statistically significantly faster (P=0.003) inactivation time constant (Fig. 7A-B). There was no significant difference (P<0.05) between the slower time constant in the presence of Pranlukast and the single time constant measured in control buffer (Fig. 7A-B). Taken together, these data are consistent with Pranlukast being an authentic albeit partially efficacious inhibitor of VRAC activity.

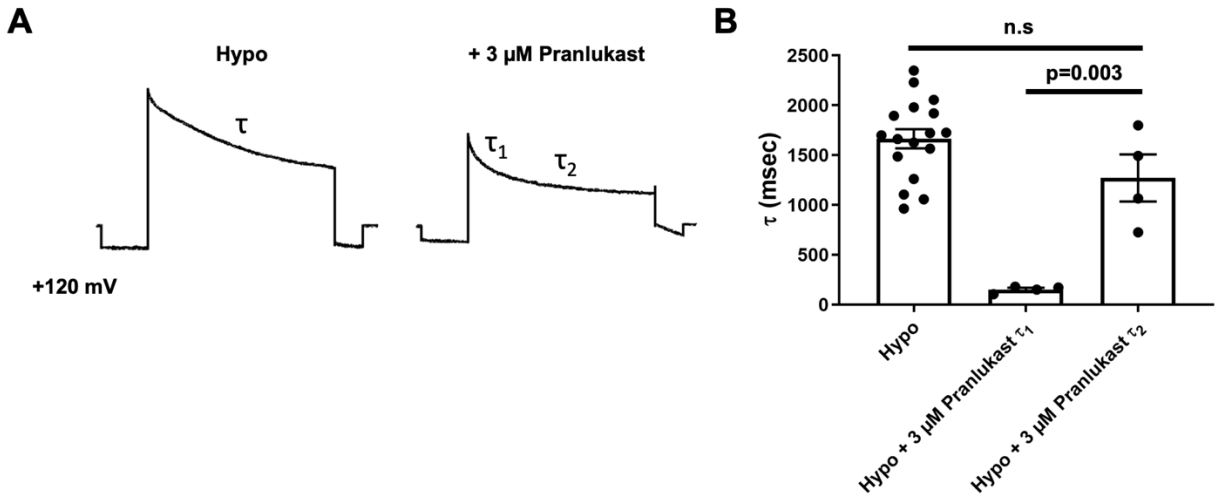

Figure 7. Pranlukast-dependent VRAC inhibition induces a second inactivation time constant

A) Whole-cell currents from HEK293 cells exposed to hypotonic and hypotonic + 3 μM Pranlukast were measured using a step protocol at +120 mV. B) Quantification of inactivation time constants generated from exponential fit curves (p=0.003; Hypo + 3 μM Pranlukast τ1 vs Hypo + 3 μM Pranlukast τ2, One-way ANOVA and Kruskal-Wallis post-hoc test; n≥4).

Pranlukast inhibits VRAC independently of the CysLT1 receptor

A previous study implicated leukotriene signaling and the CysLT1R pathway in VRAC modulation [216], raising the possibility that Pranlukast inhibits VRAC indirectly via the CysLT1 receptor. We therefore systematically tested if Pranlukast-dependent VRAC inhibition requires the expression and function of CysLT1R. Quantitative PCR was used to measure the abundance of CysLTR1 mRNA expression in the same HEK293 cell line that was used for patch clamp

experiments (Fig. 6) and the THP-1 monocytic cell line in which CysLT1R is known to be expressed [221, 222]. Whereas abundant CysLT1R mRNA expression was detected in THP-1 cells, there was virtually no detectable mRNA expression present in HEK293 cells (n=7; Fig. 8).

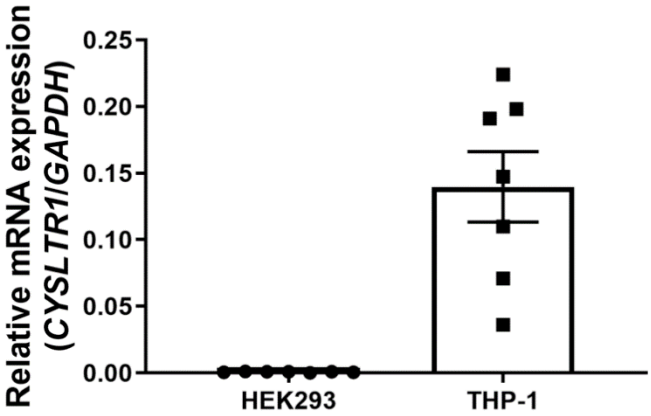

Figure 8. CysLT1R mRNA expression in HEK293 and THP-1 cells

qPCR quantification of CYSLTR1 mRNA in HEK293 and THP-1 cells (positive control) (n=7).

We determined if despite the low abundance of CysLT1R mRNA in HEK293 cells (Fig. 8) that there is enough receptor protein expression present to mediate effects of Pranlukast on VRAC activity. CysLT1R is a Gq-coupled GPCR that leads to increases in intracellular calcium following receptor stimulation, enabling us to test for receptor function using a fluorescence calcium assay. We first confirmed that the Gq-PLC-PIP_2-IP_3-calcium system is intact in HEK293 cells by taking advantage of the endogenous expression of the M3 muscarinic receptor, another Gq-coupled GPCR. HEK293 cells were plated in 384-well plates, loaded with the fluorescence indicator dye Fluo-8 AM, and then treated with escalating doses of acetylcholine (ACh). As shown in Figs. 9A-B, ACh addition led to a dose-dependent increase in intracellular calcium, with a mean ± SEM EC_{50} of 693 ± 0.05 nM (n=5). In striking contrast, addition of the endogenous CysLT1R agonist LTD4 had no effect on intracellular calcium at doses up to 100 nM (n=5; Figs. 9D; blue line). However, transfecting HEK293 cells with a plasmid encoding the CysLT1 receptor conferred

sensitivity to LTD4 and led to a dose-dependent increase in intracellular calcium with LTD4 (Fig. 9C; Fig. 9D; red line).

It has been postulated that cell swelling leads to the synthesis of leukotrienes and potentiation of VRAC via the CysLT1 receptor [216]. Therefore, as another test of CysLT1R functional expression, we tested if LTD4 activates VRAC in the absence of cell swelling. These experiments were performed using the Ozzy quenching assay. As shown in Figs. 9E-F, 100 nM LTD4 in isotonic buffer failed to increase iodide-induced quenching compared to isotonic buffer alone, whereas hypotonic media led to robust fluorescence quenching. Taken together, the results of these experiments are consistent with the interpretation that HEK293 cells lack both CysLT1R mRNA and protein expression needed for receptor-mediated inhibition of VRAC by Pranlukast.

Finally, we tested if heterologous expression of CysLT1R increases sensitivity of the VRAC current to inhibition by Pranlukast. HEK293 cells were transfected with either GFP (control) or CysLT1R and GFP and patch clamped in the whole-cell configuration. There was no statistically significant difference in VRAC inhibition by 1 μM Pranlukast in HEK293 cells transfected with GFP (30.8 ± 4.5%; n=4) or CysLT1R plasmid (30.4 ± 5.2%; n=4). In addition, the initial rate of activation between HEK293 cells transfected with GFP or CysLT1R showed no difference, 0.08 ± 0.009 pA/pF/sec and 0.08 ± 0.004 pA/pF/sec, respectively.

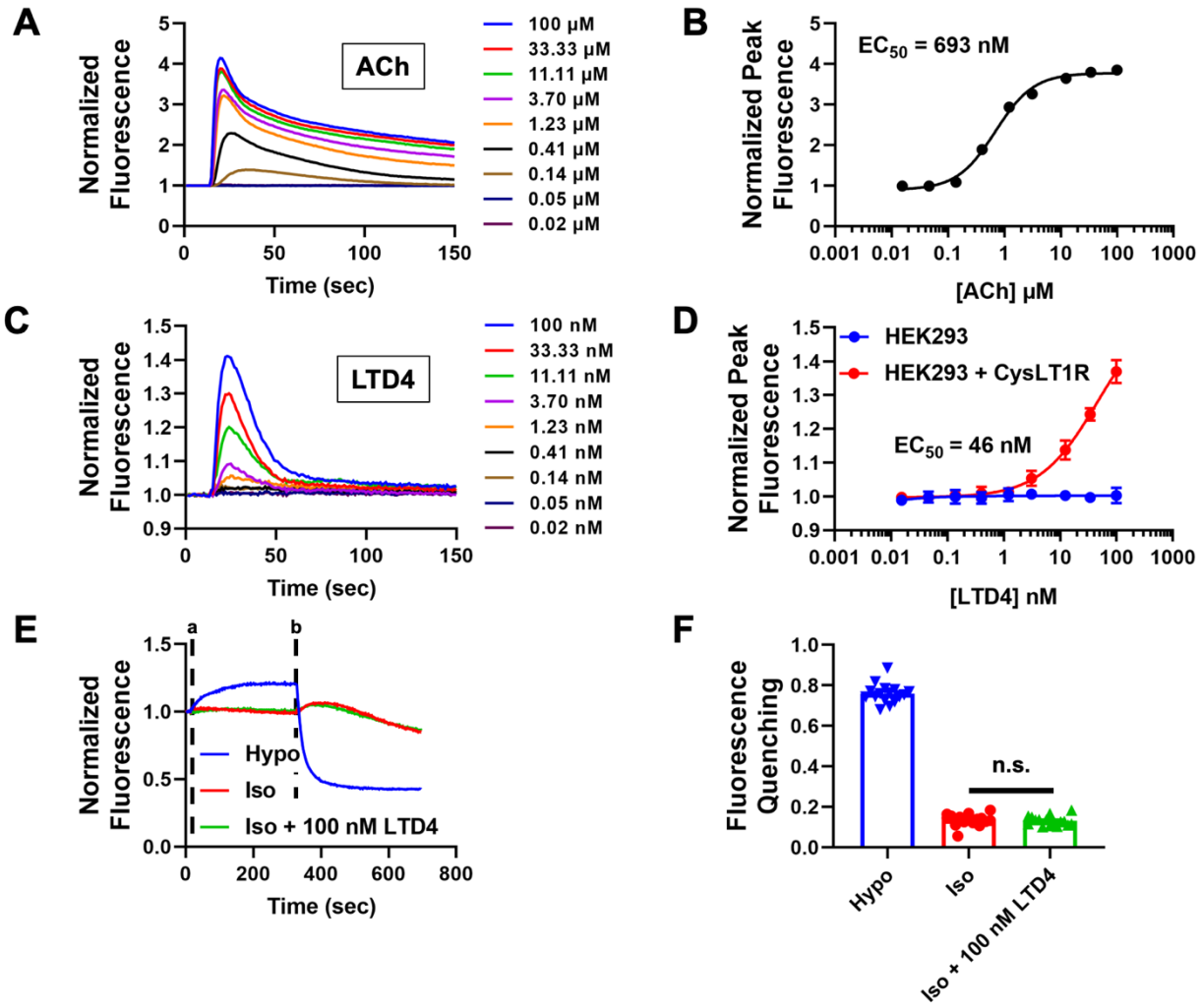

Figure 9. CysLT1 receptors are not functionally expressed in HEK293 cells

A) Representative traces of acetylcholine (ACh) CRC in HEK293 cells using Fluo-8 calcium assay B) ACh CRC in HEK293 using Fluo-8 calcium assay (mean ± SEM EC50 = 693 ± 0.05 nM; n=5) C) Representative traces of LTD4 CRC in HEK293 cells transiently transfected with CysLT1R using Fluo-8 calcium assay (HEK293 cells alone did not show a response to LTD4) D) LTD4 CRC in HEK293 and HEK293 cells transiently transfected with CysLT1R (mean ± SEM EC50 = 46 ± 19 nM in HEK293 + CysLT1R cells; n=5) using Fluo-8 calcium assay E) Representative traces of HEK293 cells treated with hypotonic, isotonic, or isotonic + 100 nM LTD4 solutions using Ozzy-quenching assay. Solutions are added at time a and NaI added at time b (n=16). F) Ozzy-quenching assay summary data from panel E. There was no significant difference between isotonic and isotonic + 100 nM LTD4 groups (One-way ANOVA and Kruskal-Wallis post-hoc test).

VRAC is also inhibited by the structurally distinct CysLT1R antagonist Zafirlukast

Holm *et al.* (2013) reported that the CysLT1R antagonist, Zafirlukast, which is structurally distinct from Pranlukast (Fig. 10A), inhibits hypotonic-induced regulatory volume decrease (RVD) and taurine release from A549 lung epithelial cell line [216]. Given that VRAC plays key roles in both of these physiological processes [6], we determined if Zafirlukast inhibits VRAC in HEK293 cells. In fluorescence assays, Zafirlukast inhibited iodide-induced Ozzy quenching dose-dependently with a mean ± SEM IC_{50} of 17.0 ± 0.6 μM (n=10). Similarly, patch clamp experiments revealed that Zafirlukast acutely and reversibly inhibited swelling-induced VRAC activity with a mean ± SEM IC_{50} of 17.2 ± 4.0 μM (n≥4; Figs. 10B, 10C, and 10D). Importantly, however, and in contrast to Pranlukast, Zafirlukast fully inhibits VRAC at higher concentrations.

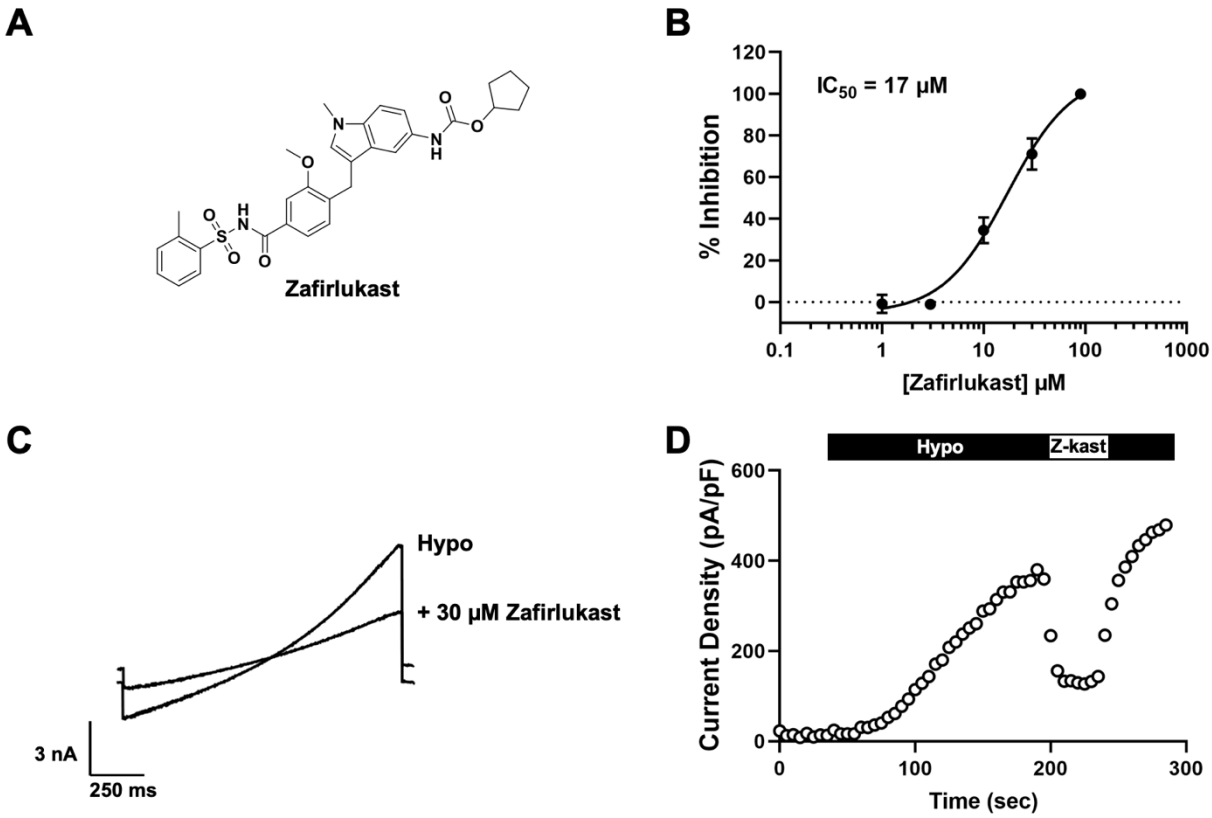

Figure 10. The CysLT1R antagonist, Zafirlukast, inhibits VRAC

A) Structure of Zafirlukast. B) Zafirlukast concentration response curve generated from whole-cell patch clamp electrophysiology (mean ± SEM IC50 = 17 ± 4 µM; n≥4). C) Whole-cell currents from HEK293 cells were measured using a ramp protocol from -100 mV to +100 mV. Cells were exposed to hypotonic bath and hypotonic bath + 30 µM Zafirlukast. D) Exemplar time course of VRAC activation under hypotonic solution exposure, 30 µM Zafirlukast, and wash (hypo) treatment.

Discussion

Since the initial discovery of VRAC currents nearly 30 years ago [59, 207], studies aimed at understanding the physiological roles of this channel have relied heavily on nonspecific inhibitors such as DCPIB, DIDS, niflumic acid, and tamoxifen [174, 187]. DCPIB is the best-in-class inhibitor with an IC_{50} of approximately 5 μM, and relatively little activity on other anion channels [174]. However, recent studies have shown that DCPIB has promiscuous activity toward several other classes of transport proteins, including glutamate transporters, inward rectifier potassium channels, proton-potassium ATPase transporters, and connexin channels [175-177, 189]. With the recent discovery of the LRRC8 gene family, genetic approaches have been used to uncover new and potentially druggable physiological and pathophysiological roles (see below) of VRAC, however compensatory changes in gene expression could potentially confound conclusions about the therapeutic potential of VRAC in certain disease settings. Therefore, fully understanding how acute pharmacological modulation of VRAC function in wild type animals might impact disease progression will require the development of potent, specific, and *in vivo*-active inhibitors and activators of the channel. This was the motivation behind the present work.

We took a molecular target-based HTS approach to discover new small-molecule modulators of VRAC. The functional assay was modeled after those employed by the Jentsch and Patapoutian groups to discover the LRRC8 gene family in whole-genome siRNA screens [51, 52]. Target-based assays are typically developed around a cell line in which the molecular target of interest is massively overexpressed. While this approach is useful for increasing the signal-to-noise ratio of an assay, it can oversimply the molecular complexity of a target protein in its native environment. For example, it appears that VRAC channels are hexamers comprised of the essential LRRC8A subunit and at least one other subunit from the gene family (i.e. LRRC8B-E). The subunit composition and stoichiometry of native VRAC channels are currently unknown and may vary between cell types [6]. To avoid biasing our assay toward an overexpressed target that might not represent the endogenously expressed channel, we developed the assay against the

native VRAC expressed in HEK293 cells. Future studies will examine whether heterologously expressed VRACs of specific subunit composition (e.g. LRRC8A/C, LRRC8A/D, LRRC8A/D) exhibit unique pharmacological profiles.

We discovered Pranlukast as a novel inhibitor of VRAC in a screen of 1,184 FDA-approved drugs. Pranlukast is a nanomolar-affinity antagonist of the CysLT1 receptor, a Gq-coupled receptor expressed in airway smooth muscle cells and other cell types [219, 220]. CysLT1 receptor stimulation by the endogenous ligand LTD4 leads to airway constriction, inflammation, and airway damage associated with asthma [223]. Pranlukast has been used clinically for decades to treat asthma and works as a competitive antagonist of LTD4 binding to CysLT1R and inhibition downstream of Gq-PLC-IP_3-IP_3R-calcium signaling. Interestingly, LTD4 has also been shown to stimulate calcium signaling and augment cell volume regulation in Ehrlich ascites tumor cells [224, 225]. While the effect of LTD4 on cell volume regulation appears to be independent of intracellular calcium and mediated primarily by cell volume-sensitive potassium channels [226], we systematically explored whether inhibition of VRAC by Pranlukast is dependent on the expression and function of CysLT1R. We reasoned that if the inhibition of VRAC by Pranlukast is dependent on the CysLT1R pathway, 1) the receptor must be expressed in HEK293 cells, which were used to discover Pranlukast and characterize its effects on VRAC function, 2) the receptor should be functional such that its stimulation elicits Gq-coupled calcium signaling HEK293 cells, and 3) stimulation of the receptor should enhance VRAC activity.

Quantitative PCR analysis clearly showed that mRNA for *CYSLTR1* is virtually undetectable in HEK293 cells, which is in striking contrast to the THP-1 monocytic cell line that was used as a positive control for *CYSLTR1* expression. Our results agree with another study that found undetectable levels of *CYSLTR1* mRNA expression in HEK293 cells [227]. Although we showed that stimulation of the endogenously expressed Gq-coupled M3 muscarinic receptor with acetylcholine leads to a dose-dependent increase in intracellular calcium, LTD4 application was without effect on intracellular calcium in parental HEK293 cells. Transient transfection of the

CysLT1 receptor was able to reconstitute Gq-coupled calcium signaling in HEK293 cells, but LTD4 had no effect on swelling-induced iodide quenching under these conditions. In addition, we observed clear VRAC inhibition in whole-cell patch clamp experiments in which intracellular calcium was buffered to vanishingly low concentrations that would not support Gq-coupled calcium signaling. Finally, hypotonic cell swelling has been reported to induce the synthesis of leukotrienes in Ehrlich ascites tumor cells [228], raising the possibility that heterologous expression of the CysLT1R might increase the sensitivity of VRAC to inhibition by Pranlukast. However, we found no evidence of this in the present study. Taken together, these data support the conclusion that inhibition of VRAC by Pranlukast requires neither the expression nor function of the CysLT1 receptor in HEK293 cells.

We propose that Pranlukast inhibits VRAC through direct interactions with the channel protein, for the following reasons. First, as noted above, Pranlukast does not require its cognate receptor for VRAC inhibition. Second, the concentrations of Pranlukast required to inhibit VRAC 0.1-10 μM are approximately 25-2500-fold higher than that need for inhibition of CysLT1R (IC_{50} = 4.3 nM) [229]. These differences are even greater for Zafirlukast (VRAC IC_{50} = 17 μM vs CysLT1R IC_{50} = 1.9 nM; >8,000-fold difference) indicating the binding sites for VRAC inhibition are fundamentally different and probably not located on the CysLT1 receptor. Third, Pranlukast inhibits VRAC rapidly (τ ~ 1 min) and reversibly, as would be expected for a direct channel inhibitor. Fourth, Pranlukast altered the kinetics VRAC inactivation at positive potentials. While it is formally possible that Pranlukast-dependent changes in inactivation are mediated by some unknown signaling pathway or changes in cell membrane properties, for example, we feel it is more likely that this reflects interactions of the small molecule with the VRAC protein. Jentsch and colleagues showed that the inactivation properties of heterologously expressed VRAC currents are dependent on the subunit combination [51] and identified charged residues near the extracellular pore mouth that regulate the inactivation properties of the channel [106]. Interestingly, these amino acids are near a residue in LRRC8A (i.e. Arginine 103) that was

recently proposed to comprise the biding site for DCPIB [67]. Studies are underway to test the role of R103 and other pore-lining residues in VRAC inhibition by Pranlukast and Zafirlukast.

Although Pranlukast and Zafirlukast are used clinically to treat asthma, we believe it is unlikely that their therapeutic efficacy is related to inhibition of VRAC currents. Whole-plasma concentrations after a single dose range between 0.5 – 1.0 μM [230-232]. However, greater than 99% of both drugs is bound by serum protein, reducing the free fraction of drugs capable of engaging VRAC to less than 10 nM. This concentration is well below the dose required to inhibit VRAC.

The discovery of Pranlukast and Zafirlukast represent critical first steps in developing more potent and specific inhibitors of VRAC using medicinal chemistry approaches. Each drug represents a distinct chemical scaffold from which diverse analog libraries can be synthesized for testing. The fluorescence quenching assay described in this work will be ideal for testing compound libraries for analogs with improved potency and efficacy. Immediate chemical synthetic goals for Pranlukast are improving VRAC inhibitory efficacy while maintaining potency. Goals for Zafirlukast will be maintaining full inhibitor efficacy while improving potency. Both programs should strive toward eliminating activity toward CysLT1R. Studies of structure-activity relationships of Pranlukast and Zafirlukast could identify a common minimal pharmacophore required for VRAC inhibition and help synthesize structurally unique inhibitors with improved potency, efficacy, and selectivity.

In conclusion, the recent discovery of the LRRC8 gene family that encodes VRAC has renewed interest in developing the molecular pharmacology for this important channel. We provide proof-of-concept that the iodide-quenching assay can be used to discover new pharmacological modulators in high-throughput screens of small-molecule libraries. The development of potent, specific, and *in vivo*-active small-molecule tools will provide important new tools for probing the integrative physiology, druggability, and therapeutic potential of VRAC in stroke [165], pain [217], and metabolic regulation [158-160, 233].

CHAPTER 3. ZINC PYRITHIONE POTENTIATES THE VOLUME-REGULATED ANION CHANNEL (VRAC) BY A REACTIVE OXYGEN SPECIES-DEPENDENT MECHANISM

Abstract

LRRC8-containing volume-regulated anion channels (VRACs) play important roles in human physiology and may serve as therapeutic targets for disease. To date there are no known potentiators of VRAC, despite the need for such tool compounds to better probe the physiology and druggability of these channels. This led us to perform a high-throughput screen against the FDA-approved drug library to identify novel potentiators of VRAC. We identified zinc pyrithione (ZPT) as a novel potentiator of VRAC in HEK293 cells. Using whole-cell patch clamp electrophysiology, we show that ZPT increases the rate of activation of VRAC currents in HEK293 cells and HCT116 cells. In addition, ZPT is able to potentiate steady-state swelling-activated currents in an acute and reversible manner and activate VRAC in the absence of cell swelling. ZPT has been previously identified as a therapeutic agent in the treatment against cancer because of its ability to induce apoptosis. Staurosporine is a distinct anticancer drug that also induces apoptosis and has been previously shown to activate VRAC via a reactive oxygen species (ROS) dependent mechanism. Using a ROS scavenger and a general inhibitor of NADP(H) oxidases, we were able to fully and partially block ZPT-mediated VRAC activation, respectively. This study suggests ZPT activates VRAC in a ROS-dependent mechanism, thus providing a novel tool compound to study VRACs.

Introduction

The preservation of cell volume following osmotic perturbations is an essential process for animal cells. Uncontrolled cell swelling can lead to the dilution of intracellular contents, destructive morphological changes, and eventually cell rupture [53, 55, 57]. Cell swelling activates a process known as regulatory volume decrease (RVD) whereby chloride and potassium ions, organic osmolytes (e.g., glutamate, taurine), and osmotically obliged water are transported out of the cell, returning cell volume back to its normal state. The volume regulated anion channel, or VRAC, plays a critical role in RVD and other physiological process related to cell volume, including cell division, migration, and apoptotic cell death [6, 8, 128, 234].

Since its initial discovery in T-lymphocytes and human intestinal epithelial cells in 1988, extensive biophysical and cell physiological studies have been carried out [59, 60]. However, it was not until 2014 that two groups independently identified the leucine-rich repeat containing 8A (*LRRC8A*) gene as an essential component of VRAC using genome-wide siRNA screens [51, 52]. The *LRRC8* gene family is comprised of five members and gives rise to five paralogs LRRC8A-LRRC8E [65]. VRAC can be functionally reconstituted by heterologous expression of the obligatory subunit LRRC8A together with at least one other LRRC8 subunit LRRC8C/D/E [51]. Recent cryo-EM structures of LRRC8A and LRRC8D homomers suggest VRACs are hexameric channel assemblies, a feature shared by homologous channels, pannexins and innexins [65, 67-70]. Heterologous co-expression of LRRC8A/LRRC8C, LRRC8A/LRRC8D, or LRRC8A/LRRC8E heteromers give rise to VRACs with distinct functional and regulatory properties. For example, studies performed in *Xenopus* oocytes found that LRRC8A/LRRC8E heteromers are potentiated by intracellular oxidation, whereas LRRC8A/LRRC8C and LRRC8A/LRRC8D heteromers are inhibited [100].

The identification of the LRRC8 gene family has led to a revitalization of the VRAC field, by confirming previously suspected roles and discovering new roles in adipocyte physiology, insulin signaling, vascular physiology, sperm development, drug uptake, immune responses to

virus infection, and neurotransmitter release in the brain [98, 133, 144, 158-161, 165, 178, 179]. Many of these studies have highlight the need for developing potent and specific pharmacological tools for probing the physiology and therapeutic potential of VRAC in human diseases. We recently reported the discovery in a high-throughput screen (HTS) of two cysteinyl leukotriene 1 receptor (CysLT1) antagonists, Pranlukast and Zafirlukast, that inhibit VRAC independently of CysLT1 receptor [45]. This discovery not only adds to the growing toolkit of inhibitors available for studying VRAC, but it also demonstrates the value of HTS for developing VRAC pharmacology.

There have been no small molecule potentiators of VRAC reported to date, which prompted us to interrogate a library of 1,184 FDA-approved drugs for compounds that enhance VRAC activity. The most potent potentiator identified in this screen was the antifungal, bacteriostatic compound found in some antidandruff shampoos, zinc pyrithione (ZPT). ZPT activates VRAC activity under isotonic conditions and dramatically enhances the rate of channel activation during hypotonic cell swelling in a reversible manner. Experiments with scavengers of reactive oxygen species (ROS) either partially or completely blunted the effects of ZPT on VRAC but had no effect on swelling-induced channel activation. Taken together, this study identifies a commonly used topical drug that leads to VRAC potentiation at least in part through ROS-dependent mechanisms.

Materials and Methods

Chemicals

Zinc pyrithione (1-Hydroxypyridine-2-thione zinc salt) and N-acetyl cysteine (NAC) were purchased from Sigma-Aldrich (St. Louis, MO). Diphenyleneiodonium chloride (DPI) was purchased from TOCRIS (Minneapolis, MN). All salts were purchased from Sigma-Aldrich and were of the highest grade available.

Cell culture

HEK293 cells were cultured in 75 cm^2 flasks with Dulbecco's Modified Eagle Medium (DMEM) supplemented with 10% Fetal Bovine Serum (FBS) and 1% Penicillin/Streptomycin (P/S). HEK293 cells stably transfected with the YFP(F46L/H148Q/I152L) fluorophore (i.e. HEK293-Ozzy cells) [45] were cultured in the same medium supplemented with 700 µg/mL G418 Sulfate (Corning, Corning, NY). HCT116 cells were cultured in 75 cm^2 flasks with McCoy's 5A Medium supplemented with 10% Fetal Bovine Serum (FBS) and 0.5% Penicillin/Streptomycin (P/S).

Patch clamp electrophysiology

On the day of experiments, HEK293 or HCT116 cells were rinsed with divalent-free Hank's Balanced Salt Solution (HBSS), dissociated using 0.25% trypsin/1 mM EDTA for approximately 10-sec, diluted with respective complete medium, plated on poly-L-lysine-coated round glass coverslips, and allowed to recover at 37ºC in a 5% CO_2 incubator for at least 1 h before experiments. Patch electrodes were pulled from 1.5-mm–outer diameter silanized borosilicate microhematocrit tubes; electrode resistance ranged from 1 to 3 MΩ when filled with the following solution (in mM): 126 CsCl, 2 MgSO4, 20 HEPES, 1 EGTA, 2 Na_2ATP, 0.5 GTP (pH 7.2 adjusted with CsOH, 275 mOsm). The isotonic bath solution contained (in mM): 75 CsCl, 5 MgSO4, 1 Calcium-D-gluconate, 12 HEPES, 8 Tris base, 5 glucose, 2 glutamine, and 95 sucrose (pH 7.4 adjusted with CsOH, 300 mOsm). Hypotonic bath (200-250 mOsm) was made by excluding sucrose from the isotonic bath. DMSO, ZPT, and DPI were added directly to bath solutions for experiments. Bath solutions containing NAC were made separately to ensure correct pH and osmolality.

Macroscopic currents were recorded under voltage-clamp conditions using an Axopatch 200A (Molecular Devices, Sunnyvale, CA) patch-clamp amplifier. Electrical connections to the patch-clamp amplifier were made by using Ag/AgCl wires and 3 M KCl/agar bridges. Series resistance was compensated by >85% to minimize voltage errors. Data were collected at 5 kHz

and filtered at 10 kHz. Data acquisition and analysis were performed by using pClamp 10 software (Axon Instruments).

Cells were voltage clamped at a holding potential of -30 mV and whole-cell currents were elicited by a voltage ramp or step protocol. For voltage ramps, membrane potential was first stepped to -100 mV for 50 msec and then ramped over 1 sec to +100 mV. This was followed by a step back to 0 mV for 4 sec before this protocol was repeated. Step changes in membrane voltage were induced by stepping membrane voltage to -120 mV to +120 mV in 2 sec, 20 mV increments. Percent inhibition of compounds was determined by normalizing data to currents inhibited by 10 μM DCPIB.

As previously described [111], initial rate of swelling-induced VRAC activation was calculated by determining by linear regression analysis of whole cell currents over 60 seconds following current activation. Current activation is defined as the point for which current continuously increases above current baseline (i.e., current measured with little fluctuation since the start of the experiment).

Cell volume measurements

Cell volume measurements were determined as previously described [102]. Patch-clamped cells were visualized and image-captured by video-enhanced differential interference contrast microscopy by using a Nikon TE300 microscope and Nikon Plan Fluor 60×/0.7 numerical aperture extra-long working distance lens and a Dage-MTI CCD camera. The diameter of cells was measured at a single focal plane that showed maximum cell diameter. Cell morphology was assumed to approximate a sphere, and cell volume was calculated as $4/3 \times \pi \times r^3$, where r is the cell radius. Cell volumes were normalized to cell volume 1 minute prior to solution exchange (i.e., time = -1 min).

Fluorescence reporter assay of VRAC function

HEK293-Ozzy cells were dissociated using 0.25% trypsin/1 mM EDTA and plated at a density of 20,000 cells/well in clear bottomed, black-walled Corning PureCoat amine coated 384 well plates (Corning, Corning, NY) and cultured overnight at 37ºC in a 5% CO_2 incubator. The following day cells were washed with isotonic solution containing (in mM): 140 NaCl, 5 KCl, and HEPES (pH 7.4, 310 mOsm). Compounds from the FDA library were dissolved in hypotonic solution containing (in mM): 5 KCl, 20 HEPES, and 90 mannitol (pH 7.4, 130 mOsm; 165 mOsm solution was used for submaximal activation of VRAC) and added simultaneously to all 384-wells at a final screening concentration of 10 μM. After 5 min allowed for cell swelling and VRAC activation, 100 mM NaI was added to all 384-wells simultaneously and Ozzy fluorescence was measured at 1Hz using a Panoptic kinetic imaging plate reader (WaveFront Bioscience, Franklin, TN, USA). Fluorescence values from each well were normalized to baseline readings (i.e. average of the first 5 readings before hypotonic solution is added). Peak fluorescence was calculated by taking the average trace recording from each compound screened on the plate and subtracting it from each compound trace of the same plate. The local maximum or minimum following NaI addition is determined and reported as peak fluorescence values. Percent quenching was calculated by normalizing slope values following NaI addition to DMSO control. Data were plotted with GraphPad Prism version 7.03 (GraphPad Software, San Diego, CA) to generate representative experiment traces and CRCs using a non-linear regression analysis.

Statistics

All data are presented as means ± SEM; n represents the number of cells in patch-clamp recordings or the number of wells in fluorescence-based assays. Statistical significance was determined by using two-way analysis of variance (ANOVA) and Sidak's multiple comparisons test was used, *$p<0.05$, **$p<0.01$, ***$p<0.001$, ****$p<0.0001$.

Results

Discovery and characterization of ZPT as a novel VRAC potentiator

We recently reported the discovery of the CysLT1 receptor antagonist Pranlukast as a novel VRAC inhibitor in a screen of the SelleckChem collection of 1,184 FDA-approved drugs [45]. The HTS assay utilized in this screen reports the quenching of the YFP variant Ozzy by iodide as the anion enters osmotically swollen HEK293 cells through endogenously expressed VRACs (see Methods). We reasoned that compounds from the FDA library that potentiate VRAC activity should increase the rate and/or peak of iodide-induced Ozzy quenching. Figure 11A shows a scatter plot of the peak fluorescence difference from baseline for all 1,184 wells in the screen. Wells that exhibited a peak fluorescence difference three standard deviations away from the mean are shown lying above (inhibitors) or below (activators/potentiators) the dashed lines. Zinc pyrithione (ZPT), which led to the greatest apparent potentiation of VRAC of any compound in the screen, is indicated with a black circle.

ZPT was ordered as a powder, freshly dissolved, and re-tested in Ozzy quenching assays. Figure 11B shows that compared to wells treated with the solvent control DMSO, addition of 10 μM ZPT during the 5-min hypotonic stimulus period led to an increase in the rate and extent of iodide-induced quenching. ZPT potentiated Ozzy quenching in a dose dependent manner when evaluated at concentrations between 0.01 μM and 50 μM. Fitting these dose-response data with a 4-parameter logistical function generated a 50% activation concentration (EC_{50}) value of 5.7 ± 1.1 μM (Figure 11C-D; n=13).

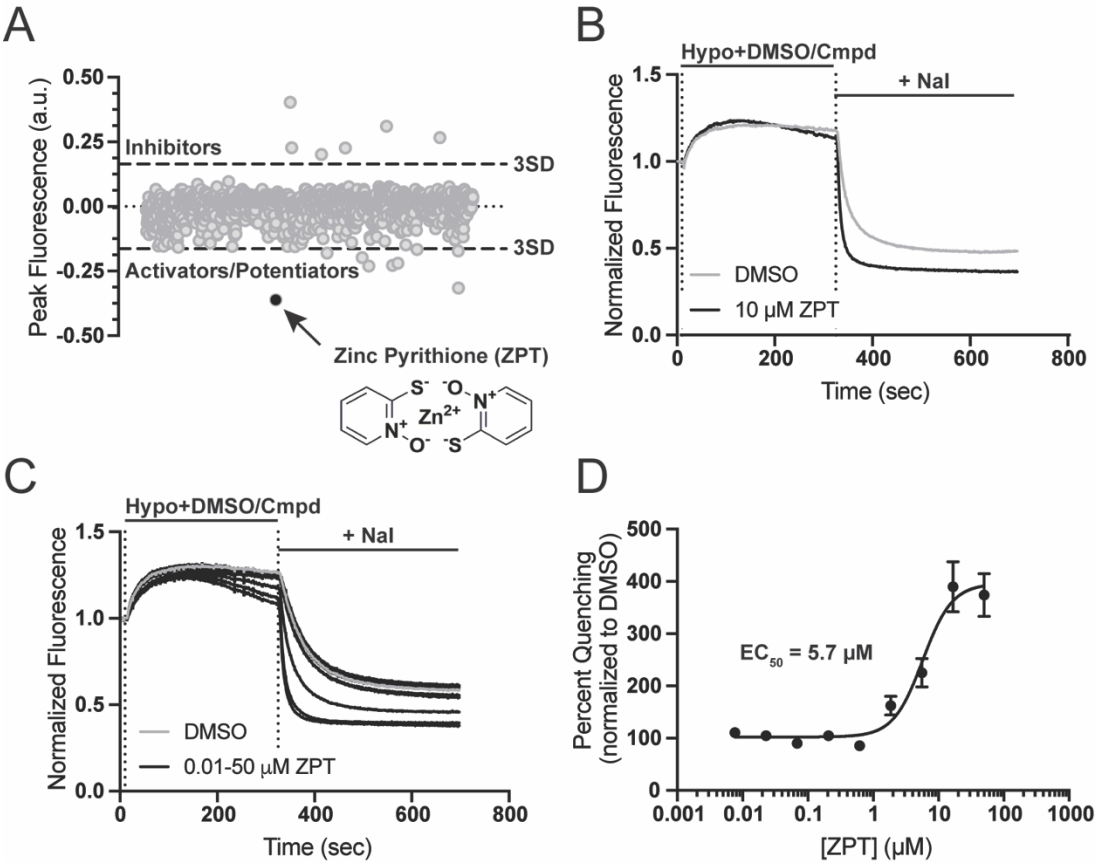

Figure 11. Discovery of zinc pyrithione in a HTS of the FDA library

A) Scatter plot of the 1,184 FDA drug compounds screened. A three-standard deviation from the mean cutoff was implicated to identify compounds as "hits". Compounds that slowed the rate of fluorescence quenching had positive values and compounds that increased fluorescence quenching had negative values. Zinc pyrithione is depicted as a black dot on the scatter plot. B) Representative traces of Ozzy-quenching assay with 10 μM zinc pyrithione (ZPT). Traces were normalized to mean of five baseline fluorescent measurements taken at the start of the experiment. Hypotonic solution (130 mOsm) containing DMSO (vehicle) or drug compound were added 10 sec after the start of the experiment. After 5 min incubation period, 100 mM NaI is added and fluorescence quenching is observed. Fluorescence measurements were taken throughout the entirety of the experiment. C) Representative traces of ZPT dose-dependent fluorescence quenching using the Ozzy-quenching assay. D) ZPT concentration response curve (CRC) generated from Ozzy-quenching assay using an EC_{50} osmolality solution (165 mOsm; mean ± SEM EC_{50} of 5.7 ± 1.1 μM; n=13).

Confirmation of ZPT activity with patch clamp electrophysiology

To confirm that ZPT is a *bona fide* VRAC potentiator and does not enhance iodide-induced Ozzy quenching through some other mechanism unrelated to the channel, we confirmed its ability to potentiate VRAC activity in "gold standard" whole-cell patch clamp experiments. In these

experiments, cells were bathed and patch clamped with cesium chloride-based solutions that isolate VRAC (and potentially other chloride currents) from contaminating potassium currents. Cell swelling was initiated by reducing bath osmolality from 300 mOsm (isotonic) to 200-250 mOsm (hypoosmotic) by removing sucrose. Figure 12A shows the time course of swelling-induced activation of VRAC currents recorded at +100 mV or -100 mV from HEK293 cells treated with a 200 mOsm bath solution containing either DMSO (n=6) or 30 μM ZPT (n=5). In contrast to DMSO-treated control cells, in which VRAC currents continue to activate over a 6-min period, VRAC currents in ZPT-treated cells reached a steady state within a few minutes after switching to hypotonic bath. The initial rate of current activation in the two treatment groups was quantitated by a linear regression fit analysis to current density recorded over the first min of VRAC activation (Figure 12B). Mean and individual activation rates ± SEM are shown in Figure 12C. VRAC in ZPT-treated cells activated approximately 8-fold faster than that in DMSO-treated cells. These differences were significantly different between the two groups at -100 mV ($P<0.05$) and +100 mV ($P<0.001$) (Figure 12C and Table 1). ZPT increased the rate of current activation significantly at both -100 mV ($P<0.05$) and +100 mV ($P<0.05$) by greater than 10-fold when cells were swollen with a more gentle hypotonic stimulus (i.e. 250 mOsm) (Table 1). Because the subunit composition of heteromeric VRAC channels is hypothesized to vary between cell types [235], which can alter regulatory properties of the channel [51, 235], we tested whether PTZ could also potentiate VRAC currents expressed in HCT116 colorectal carcinoma cells. As shown in Figs. 12D-F, 30 μM led to a significant ($P<0.05$) potentiation of swelling-induced VRAC activation compared to DMSO-treated cells. Thus, the effects of ZPT on VRAC do not appear to be cell-type specific.

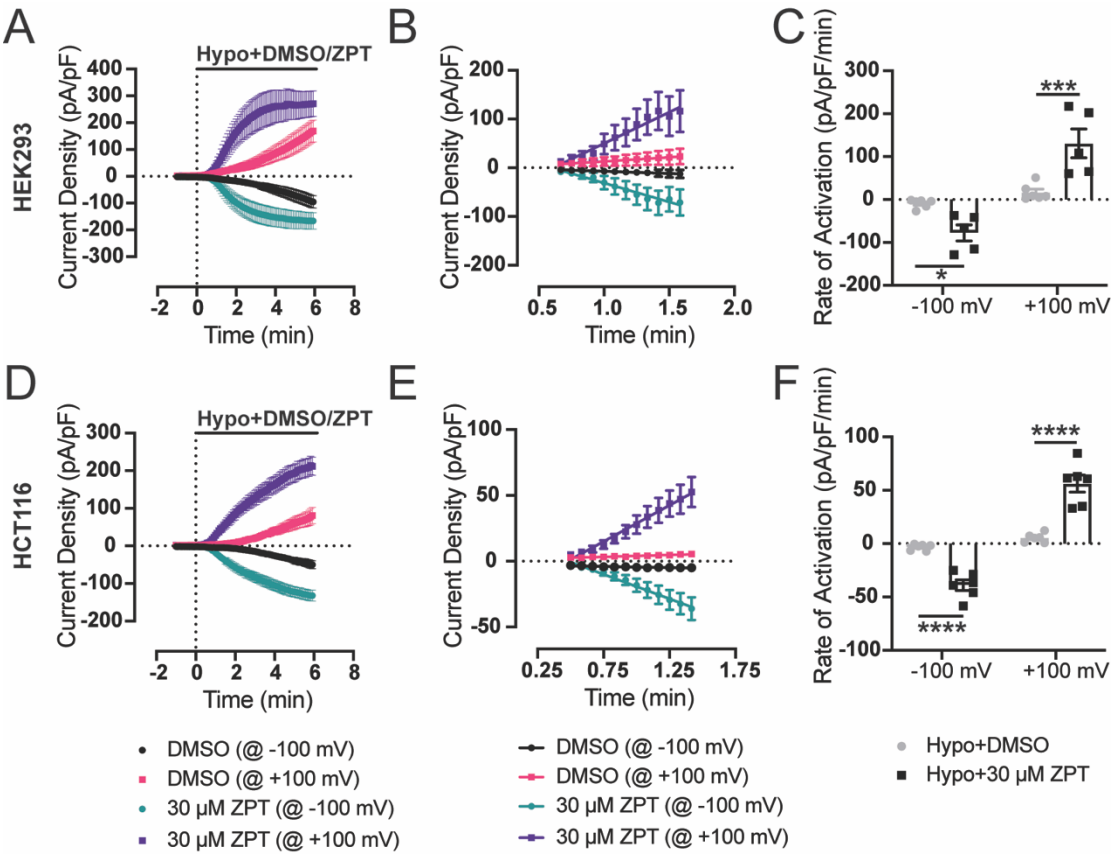

Figure 12. Zinc pyrithione potentiates the rate of activation of swelling-activated VRAC currents

A) Time course of swelling-activated whole-cell Cl- currents from HEK293 cells. Currents were measured using a ramp protocol from -100 mV to +100 mV. Cells are exposed to a hypotonic bath (200 mOsm) containing DMSO (vehicle) (n=6) or 30 μM ZPT (n=5) at time = 0 min. B) Fitting initial current activation at -100 mV and +100 mV of DMSO-treated (n=6) and ZPT-treated (n=5) cells with linear regression lines. C) Summary of rate of activation at -100 mV and +100 mV for individual DMSO-treated (@ -100 mV mean ± SEM -9.2 ± 4.1 pA/pF/min, @ +100 mV mean ± SEM 16.6 ± 7.6 pA/pF/min; n = 6) and ZPT-treated cells (@ -100 mV mean ± SEM -77.6 ± 18.9 pA/pF/min @ +100 mV mean ± SEM 130 ± 33.4 pA/pF/min; n=5). D) Time course of swelling-activated whole-cell Cl- currents from HCT116 cells. Currents were measured using a ramp protocol from -100 mV to +100 mV. Cells are exposed to a hypotonic bath (250 mOsm) containing DMSO (vehicle) (n=6) or 30 μM ZPT (n=6) at time = 0 min. E) Fitting initial current activation at -100 mV and +100 mV of DMSO-treated (n=6) and ZPT-treated (n=6) cells with linear regression lines. F) Summary of rate of activation at -100 mV and +100 mV for individual DMSO-treated (@ -100 mV mean ± SEM -3.2 ± 1.2 pA/pF/min, @ +100 mV mean ± SEM 5.4 ± 1.7 pA/pF/min; n = 6) and ZPT-treated cells (@ -100 mV mean ± SEM -38.9 ± 1.7 pA/pF/min @ +100 mV mean ± SEM 56.2 ± 7.9 pA/pF/min; n=6). Data was analyzed by Two-way ANOVA and Sidak's multiple comparisons test, *p<0.05, ***p<0.001, ****p<0.0001.

Table 1. The effect of 30 μM zinc pyrithione on rates of current activation for endogenously expressed VRACs in HEK293 and HCT116 cells

Values are means ± SEM (n). Swelling was induced 1 min after obtaining whole cell access by exchanging isotonic bath solution (300 mOsm) with specified hypotonic bath solution.

Cell Type	Hypo Bath Solution; Osmolarity	Rate of Activation @ -100 mV (pA/pF/min)	Rate pf Activation @ +100 mV (pA/pF/min)
HEK293	DMSO; 250 mOsm	-3.7 ± 1.6 (6)	6.0 ± 2.5 (6)
HEK293	30 μM ZPT; 250 mOsm	-44.3 ± 15.5 (6)	68.1 ± 25.0 (6)
HEK293	DMSO; 200 mOsm	-9.2 ± 4.1 (6)	16.6 ± 7.6 (6)
HEK293	30 μM ZPT; 200 mOsm	-77.6 ± 18.9 (5)	130 ± 33.4 (5)
HCT116	DMSO; 250 mOsm	-3.2 ± 1.2 (6)	5.4 ± 1.7 (6)
HCT116	30 μM ZPT; 250 mOsm	-38.9 ± 1.7 (6)	56.2 ± 7.9 (6)

Whole cell VRAC currents have been extensively characterized to be moderately outwardly rectifying with time-dependent inactivation at positive voltages [6]. To determine if the increase in rate of activation with ZPT treatment is VRAC-mediated, we compared steady-state swelling-activated whole cell currents of DMSO-treated and ZPT-treated cells using a voltage-clamp step protocol from -120 mV to +120 mV with +20 mV increments. Whole currents from ZPT-treated cells were virtually indistinguishable from DMSO-treated cells (Figure 13A), including the characteristic time-dependent inactivation at positive voltages. Aside from generally having larger currents, the ZPT-treated and DMSO-treated cells have the same I-V relationship with moderate outward rectification (Figure 13B).

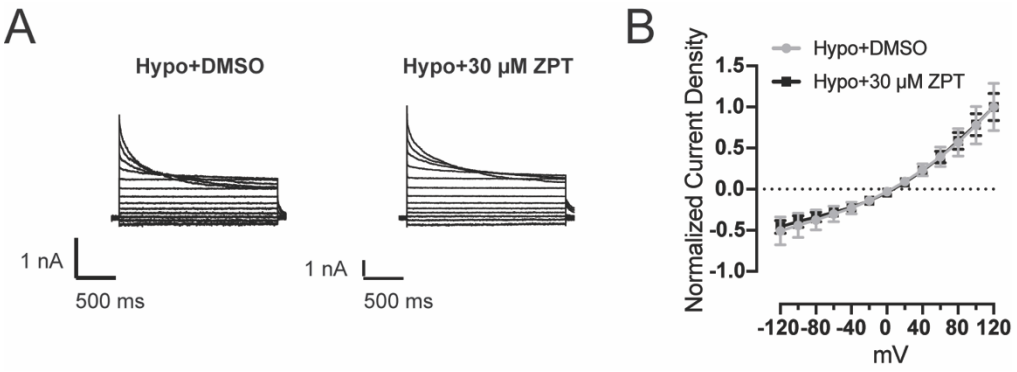

Figure 13. I-V relationship of swelling-activated currents in the presence of DMSO or ZPT

A) Whole-cell currents from HCT116 cells were measured using a step protocol from -120 mV to +120 mV, with 20 mV steps. Cells were exposed to hypotonic bath (250 mOsm) containing DMSO (vehicle) or 30 µM ZPT. B) I-V plot from currents recorded in A (n=4). Current density was normalized to currents at +120 mV.

In all of the experiments described thus far, ZPT was co-applied with hypotonic bath, raising the possibility that ZPT simply enhances the same regulatory process that activates VRAC during hypotonic cell swelling. As a first step toward determining if cell swelling and ZPT potentiate VRAC through the same or distinct processes, we tested if ZPT could potentiate VRAC currents that had already achieved a steady state during cell swelling. These experiments were performed in HCT116 cells using a 250 mOsm stimulus to activate VRAC. A representative experiment is shown in Figure 14A. After the VRAC current reached a steady state amplitude in the presence of vehicle control DMSO, bath application of 30 µM ZPT led to a striking potentiation of current amplitude at -100 mV and +100 mV. This was rapidly reversible following washout of ZPT from the bath. The results from four independent experiments showing significant potentiation ($P<0.05$) and washout ($P<0.05$) are summarized in Figure 14B.

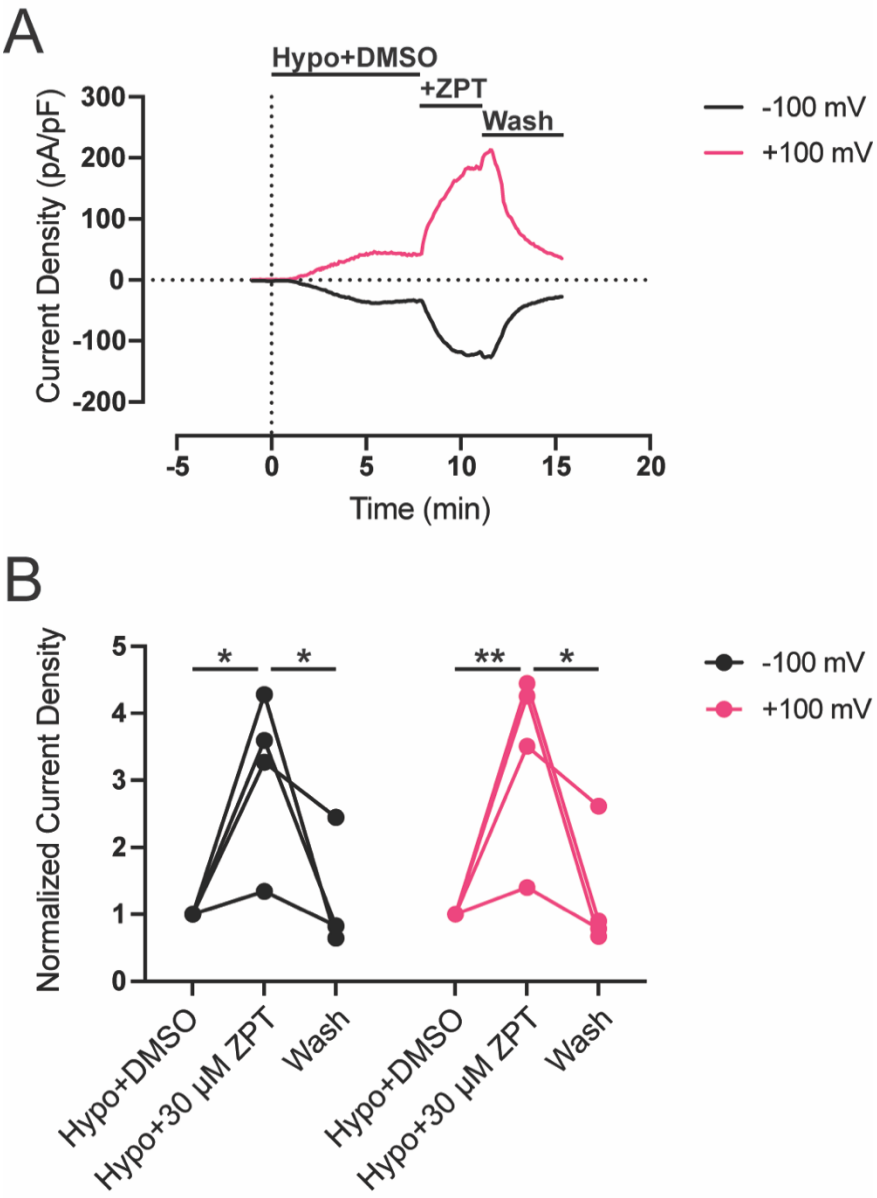

Figure 14. Zinc pyrithione further potentiates swelling-activated VRAC currents

A) Representative time course of swelling-activated whole-cell Cl- currents from HCT116 cells (n=4). Currents were measured using a ramp protocol from -100 mV to +100 mV. Cells were exposed to hypotonic bath (250 mOsm) containing DMSO at time = 0. Solution exchange with hypotonic bath containing 30 µM ZPT occurred once steady-state was reached (~time = 7 min). Solution exchange with hypotonic bath containing DMSO (wash) occurred once steady-state with ZPT was reach ~time = 12 min. B) Summary of steady state current density from A normalized to Hypo+DMSO. Data was analyzed by Two-way ANOVA and Sidak's multiple comparisons test, *p<0.05, **p<0.01.

ZPT potentiates VRAC in the absence of cell swelling

The experiments described in Figure 14 suggested that cell swelling and ZPT activate VRAC through independent mechanisms, raising the possibility that ZPT might also activate VRAC under isotonic conditions. Treating HCT116 cells with 30 μM ZPT (n=4) in isotonic (300 mOsm) bath activated significant ($P<0.0001$ @ -100 mV and @ +100 mV) Cl^- currents that reached steady-state within 3 minutes following solution exchange, whereas DMSO-treated cells (n=4) showed little to no current activation (Figure 15A-B). As Figure 15C-D shows, ZPT-induced currents are moderately outwardly rectifying and inactivate at positive voltages-characteristic of VRAC currents. Furthermore, the I-V relationship of ZPT-induced currents resembles the I-V relationship of swelling-activated currents (Figure 13B). Additionally, in support that ZPT activates VRAC, we show the best-in-class inhibitor of VRAC [173], DCPIB, inhibits these currents (Figure 15E-F). To ensure ZPT treatment did not cause cell swelling and subsequent VRAC activation, we measured cell volume and whole patch clamp recordings simultaneously (Figure 15G). We observed no significant difference in cell volume between DMSO-treated and ZPT-treated cells and interestingly, cell shrinkage was observed with some ZPT-treated cells (Figure 15G-H)

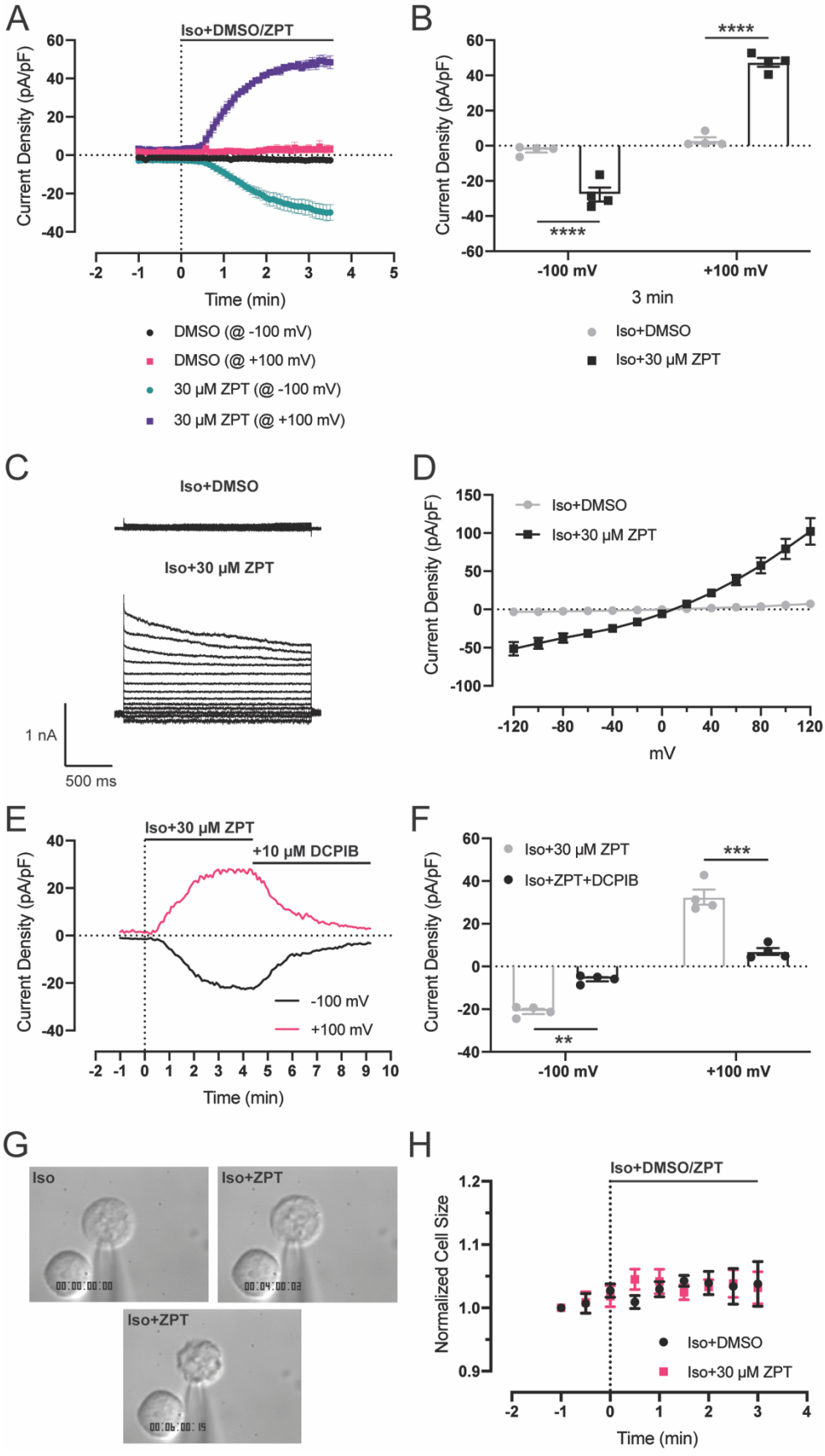
A
Iso+DMSO/ZPT
Current Density (pA/pF)
Time (min)
DMSO (@ -100 mV)
DMSO (@ +100 mV)
30 μM ZPT (@ -100 mV)
30 μM ZPT (@ +100 mV)
B
****
****
Current Density (pA/pF)
-100 mV
+100 mV
3 min
Iso+DMSO
Iso+30 μM ZPT
C
Iso+DMSO
Iso+30 μM ZPT
1 nA
500 ms
D
Iso+DMSO
Iso+30 μM ZPT
Current Density (pA/pF)
mV
E
Iso+30 μM ZPT
+10 μM DCPIB
Current Density (pA/pF)
-100 mV
+100 mV
Time (min)
F
Iso+30 μM ZPT
Iso+ZPT+DCPIB
***
**
Current Density (pA/pF)
-100 mV
+100 mV
G
Iso
Iso+ZPT
Iso+ZPT
H
Iso+DMSO/ZPT
Normalized Cell Size
Iso+DMSO
Iso+30 μM ZPT
Time (min)

Figure 15. Zinc pyrithione activates Cl^- currents under isotonic conditions

A) Time course of whole-cell Cl- currents from HCT116 cells. Currents were measured using a ramp protocol from -100 mV to +100 mV. Cells are exposed to an isotonic bath (300 mOsm) containing DMSO (vehicle) (n=4) or 30 μM ZPT (n=4) at time = 0 min. B) Summary of current density of DMSO-treated and ZPT-treated cells from -100 mV and +100 mV at time = 3 min. Data was analyzed by Two-way ANOVA and Sidak's multiple comparisons test, ****p<0.0001. C) Whole-cell currents from HCT116 cells were measured using a step protocol from -120 mV to +120 mV, with 20 mV steps. Cells were exposed to isotonic bath (300 mOsm) containing DMSO (vehicle) or 30 μM ZPT. D) I-V plot from currents recorded in C (DMSO (n=3); ZPT (n=5)). E) Representative time course of ZPT-activated and DCPIB-inhibitable whole-cell Cl- currents from HCT116 cells (n=4). Currents were measured using a ramp protocol from -100 mV to +100 mV. Cells were exposed to hypotonic bath (250 mOsm) containing 30 μM ZPT at time = 0. Solution exchange with hypotonic bath containing 30 μM ZPT and 10 μM DCPIB occurred once steady-state was reached (~time = 4 min). F) Summary of steady state current density from E. Data was analyzed by Two-way ANOVA and Sidak's multiple comparisons test, ***p<0.001, ****p<0.0001. G) Images from a ZPT-treated cell at Time = -1 min, +3 min, and +5 min. H) Time course of cell volume measurements from HCT116 cells. Cells were exposed to isotonic bath (300 mOsm) containing DMSO (n=3) or 30 μM ZPT (n=3) at Time = 0 min. Data was analyzed by Two-way ANOVA and Sidak's multiple comparisons test, not significant.

ZPT activates VRAC currents in a ROS-dependent manner

ZPT has anticancer properties by virtue of its ability to induce apoptotic cell death, in part by stimulating the production of reactive oxygen species (ROS) [236-239]. Another inducer of apoptosis, staurosporine (STS), has been shown to stimulate VRAC activation via ROS production [128, 130, 132]. These data raise the possibility that ZPT activates VRAC through a ROS-dependent mechanism. To test this hypothesis, we evaluated the effects of the broad-spectrum ROS scavenger N-acetyl cysteine (NAC) and the general NAD(P)H oxidase inhibitor, diphenyleneiodonium chloride (DPI) on ZPT-dependent activation of VRAC under isotonic conditions. Bath co-application of 10 mM NAC led to a complete abrogation of ZPT-induced VRAC activation (Figure 16A-B) but had no effect on swelling-induced channel activation (Figure 16C), indicating that NAC is not a general inhibitor of VRAC. Furthermore, bath co-application of DPI (10 μM) led to a partial but significant ($P<0.01$ at -100 mV and $P<0.0001$ at +100 mV) inhibition of ZPT-induced activation of VRAC (Figure 16A-B). The simplest interpretation of these data is that ZPT activates VRAC at least in part through a ROS-dependent mechanism.

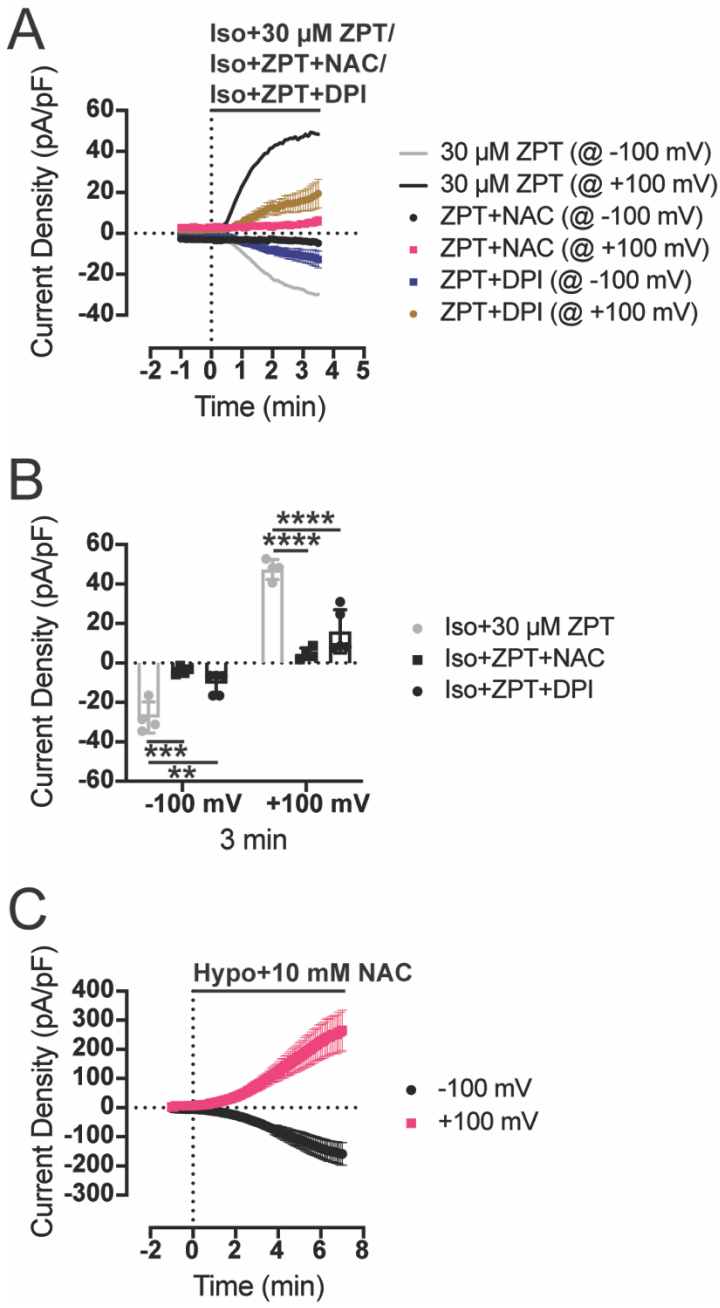

Figure 16. ZPT activates VRAC in a ROS-dependent manner

A) Time course of whole-cell Cl- currents from HCT116 cells. Currents were measured using a ramp protocol from -100 mV to +100 mV. Cells are exposed to an isotonic bath (300 mOsm) containing 30 μM ZPT (n=4), 30 μM ZPT+10 mM NAC (n=4), or 30 μM ZPT+20 μM DPI (n=5) at time = 0 min. Iso+ZPT data is originally shown in Figure 15. Average is depicted by solid lines. B) Summary of current density of ZPT-treated, ZPT+NAC-treated, and ZPT+DPI-treated cells from -100 mV and +100 mV at time = 3 min. C) Time course of whole-cell Cl- currents from HCT116 cells. Currents were measured using a ramp protocol from -100 mV to +100 mV. Cells are exposed to a hypotonic bath (250 mOsm) containing 10 mM NAC (n=4). Data was analyzed by Two-way ANOVA and Sidak's multiple comparisons test, **p<0.01, ***p<0.001, ****p<0.0001.

Discussion

Early cell physiological studies of VRAC currents largely depended on nonspecific VRAC inhibitors (e.g., DCPIB, tamoxifen, DIDS). We have recently shown that DCPIB, the best-in-class inhibitor of VRAC, also inhibits ATP production by disrupting mitochondrial function [188]. Since the discovery that *LRRC8* genes encode VRAC, laboratories have taken genetic approaches to verify previously postulated and discover new druggable physiological and pathophysiological roles of this channel. However, like the use of non-specific inhibitors of VRAC, genetic approaches to study the function of VRAC could lead to compensatory mechanisms and difficulty with interpretation of results [139, 140].

Furthermore, to date, there are no known direct activators of VRAC, which has been a barrier for understanding how these channels activate, a process that is still being debated today, as well as understanding the physiological and pathophysiological consequences of channel opening [6]. Several studies have identified various cellular factors that contribute to channel activation, including ATP, permissive Ca^{2+} levels, reactive oxygen species (ROS), and ionic strength [61, 107, 108, 112, 117, 118, 182]. Genetic approaches have found that attaching fluorescent proteins to the C-terminal end of LRRC8 proteins can activate heterologously-expressed heteromeric channels, eluding to importance of the C-terminal leucine-rich repeat region of LRRC8 proteins [103]. Studies using LRRC8 chimeras have generated swelling-activated homomeric channels by swapping EL1 and IL1 loops of LRRC8 proteins, identifying these protein regions as important for swelling-induced channel activation [102]. While these studies have provided insight into regions of the VRAC proteins that contribute to activation, these constructs do not exist in nature. Therefore, better tools for studying activation of endogenously expressed VRACs are needed and this was the motivation behind the present work.

We previously developed a molecular target-based HTS approach to identify new small-molecule modulators of VRAC [45]. The functional assay was modeled after fluorescence-based assays used to identify the genes that encode VRAC [51, 52]. From our previous screening efforts,

we identified Pranlukast as an inhibitor of VRAC by looking for compounds that attenuated I^- induced fluorescence quenching [45]. Through reanalysis of the existing data set, we set out to identify compounds that increased I^--induced fluorescence quenching in the window immediately following I^- addition (i.e., increased rate of fluorescence quenching). From this analysis we discovered zinc pyrithione reproducibly increased the rate of fluorescence quenching in the assay. Zinc pyrithione, or ZPT, is an FDA-approved compound commonly found in over-the-counter topical treatments such as antidandruff shampoos [240]. It is also used an antimicrobial agent and as an additive in antifouling paints or paints used to prevent marine organism from attaching to boat/ship hulls [241-243].

Here we report ZPT increases the rate of activation of swelling-activated VRAC currents, further potentiates steady-state VRAC currents, and can activate VRAC currents in the absence of a hypotonic stimulus. We showed that ZPT activates VRAC in two distinct cell lines suggesting that it acts through a shared mechanism. Interestingly, we show that ZPT inhibition is reversible, a characteristic of ion channel blockers. Further, ZPT-potentiated and -induced currents shared the biophysical properties of VRAC currents characterized in a myriad of different cell types [7]. It is conceivable that ZPT activates VRAC currents directly, however, we cannot rule out the possibility of an indirect effect on the channel itself.

Recent studies on ZPT have found it may also function as an anticancer agent by inducing apoptosis in various cancers such as acute myeloid leukemia, oral squamous cell carcinoma, and prostate cancer [236-239]. These studies show ZPT leads to mitochondrial-mediated apoptosis, with reports of increased ROS production and caspase activation [236-239]. Given VRAC's role in apoptotic volume decrease (AVD) and its regulation by intracellular oxidation, ZPT may be activating VRAC currents through a similar mechanism [128, 130, 132]. The Okada group showed pro-apoptotic drugs like staurosporine (STS) lead to VRAC activation in a ROS-dependent manner [132]. The ROS scavenger N-acetyl cysteine (NAC) was able to block STS-mediated VRAC activation [132]. Additionally, they show that the general inhibitor of NADP(H) oxidases,

diphenyleneiodonium chloride (DPI), also blocks STS-mediated VRAC activation [132]. Our interrogation of ZPT-mediated activation of VRAC also showed that these compounds either completely or partially blocked activation (Figure 16A-B). These data suggest that ZPT-activation of VRAC is mediated in a ROS-dependent manner.

An interesting question is whether ZPT activates all VRAC subtypes or only channels with certain subunit compositions. Studies in Xenopus oocytes have identified LRRC8E-containing heteromers were potentiated by intracellular oxidation [100]. Recently the Strange group published LRRC8-chimera constructs that can be singly expressed in LRRC8$^{-/-}$ cells and give rise to homomeric channels that are responsive to swelling-stimulus and recapitulates the biophysical properties of LRRC8A/LRRC8C/D/E heteromeric channels [102]. Future experiments are warranted testing the hypothesis that ZPT activates VRAC currents in a LRRC8E-dependent manner by using a LRRC8E-LRRC8A(IL1) chimera construct.

In conclusion, we have shown that HTS campaigns can identify molecules that lead to VRAC activation. Our HTS campaign using a saturating hypotonic stimulus yielded a 0.6% hit rate, a value on the upper end of typical HTS screens [244]. In efforts to increase the signal to noise ratio, we recommend using a sub-maximally activating hypotonic stimulus, as was used to generate a concentration-response curve in Figure 11D. We have also conducted HTS campaigns in solely isotonic conditions. These campaigns were unsuccessful in identifying activators. We believe this is due to the moderately outward rectification properties of VRAC leading to less activity at negative membrane voltage potentials compared to positive membrane voltage potentials, and therefore a low signal to noise ratio. Given VRAC's emerging roles in physiological processes such as insulin secretion and innate immunity, as well as the need for tools to better understand channel activation in general, there is a need to continue to identify and develop novel activators of VRAC.

Acknowledgements

This work was supported by National Institute of Diabetes and Digestive Kidney Disease grant 1F31DK120225-01 (to E. Figueroa) and institutional funds (to J. Denton).

CHATPER 4. CONCLUSIONS AND FUTURE DIRECTIONS

Summary

LRRC8-containing volume-regulated anion channels (VRACs) are ubiquitously expressed channels that are essential for cell volume-homeostasis in animal cells [6, 8, 53, 55, 57]. The recent cloning of the genes that encode the channel and the subsequent explosion of physiological and pathophysiological studies have established this channel as an emerging therapeutic target for diabetes, cancer, stroke, obesity, infertility, and most recently DNA viral infections that broadly implicate the innate immune response [10, 66, 98, 158-160, 165, 178, 179, 233]. The lack of specific and potent pharmacological tools has been barrier in testing the drugability of these important channels. The Denton lab has been a leader in ion channel drug discovery for over a decade with a primary focus on inward rectifying potassium channels [245-254]. We viewed the recent molecular identification of LRRC8 proteins as essential components of VRAC as an unprecedented opportunity to address the underdeveloped pharmacology this chloride channel. Through the use of patch clamp electrophysiology combined with fluorescence assays, we aimed to identify novel modulators of this channel that can be used to probe its physiological and pathophysiological roles, as well as study the structure-function related to channel closure and opening with inhibitors and activators, respectively.

In **CHAPTER 2** of this dissertation, we set out to develop an assay to use for high-throughput screening, a tried and true method for drug discovery [46]. Modeled after the fluorescence-based assay that was used to discover LRRC8A as the essential component of VRACs, we developed the Ozzy-fluorescence quenching assay as a reporter of VRAC function [51, 52]. Ozzy is a YFP mutant, containing a triple mutation (i.e., YFP F46L/H148Q/I152L), that makes the fluorescent protein brighter and more halide-sensitive [50]. Furthermore, we decided on screening against endogenously expressed VRACs rather than an overexpression model. Normally, overexpression of the channel typically leads to an increase in the signal-to-noise ratio

in the screening assay; however, the overexpression of the obligatory subunit LRRC8A led to a decrease in channel activity, and the complex stoichiometry of the channel might create unwanted variables [51, 52, 66]. Therefore, we settled on engineering HEK293 cells, which endogenously express VRACs, to express Ozzy.

We screened the FDA-approved drug library from SelleckChem containing approximately ~1200 compounds. A main benefit in screening this library is drug-repurposing. Drug repurposing or drug repositioning is the strategy of identifying new indications for existing drugs. Drugs undergo extensive development for beneficial pharmacokinetic, pharmacodynamic, and toxicity profiles; therefore, drug repurposing significantly de-risks the drug discovery process [255]. It also can expedite the process from "hit" identification to use in patients many-fold [255]. For our purposes, it would expedite the process of taking a "hit" from our screens and using the compound *in vivo*.

Our initial screening efforts identified Pranlukast as a novel VRAC inhibitor in the Ozzy-quenching assay. Pranlukast is a CysLT1 receptor antagonist used in the treatment of asthma [219, 220]. We characterized this compound in patch clamp electrophysiology and confirmed Pranlukast inhibited VRAC currents in a voltage-independent, reversible manner and modified voltage-dependent inactivation kinetics. Interestingly, the CysLT1 receptor had been implicated in positively modulating VRAC function. Therefore, we systematically tested if Pranlukast-dependent inhibition of VRAC was inhibiting VRAC directly or indirectly via the CysLT1 receptor. We found the CysLT1 receptor was not expressed in HEK293 cells, the parental cell line used in the HTS. This data coupled with electrophysiological evidence of Pranlukast inhibiting and altering biophysical properties, as well as the concentrations needed to inhibit VRAC vs the cognate receptor, led us to conclude Pranlukast inhibited VRAC independently of the receptor. Further, we show the structurally distinct CysLT1 receptor antagonist, Zafirlukast, also inhibits VRAC with higher efficacy, but lower potency.

In **CHAPTER 3** of this dissertation, we reanalyzed the existing data set from our initial screen that identified Pranlukast as a VRAC inhibitor with the purpose of identifying compounds that potentiated/activated VRAC. These efforts identified zinc pyrithione (ZPT) as a compound that potentiated VRAC activity in the Ozzy-quenching assay. ZPT is commonly found in over-the-counter formulations of antidandruff shampoo [240]. ZPT has also been shown to have antimicrobial, anticancer, and antifouling properties [236, 237, 239, 241-243]. We confirmed ZPT potentiated VRAC currents in HEK293 cells and HCT116 cells. ZPT increased the rate of activation of swelling-activated VRAC currents, potentiated state-state swelling-activated VRAC currents, and activated VRAC currents under isotonic conditions (i.e., non-swelling). All in all, these studies describe some of the first drug discovery efforts for these important channels and provide a framework for evaluating novel VRAC modulators.

Future Directions

LRRC8-containing volume-regulated anion channels

The studies in this dissertation describe some of the first drug discovery efforts for the LRRC8-containing volume-regulated anion channels (VRACs). We report proof-of-concept that YFP-fluorescence quenching assays can be utilized to identify novel inhibitors and activators of these important channels. Our inhibitor studies have identified two structurally distinct CysLT1 receptor antagonists, Pranlukast and Zafirlukast, as new inhibitors of VRAC. Pranlukast inhibited VRAC in the nanomolar range but had low efficacy. Zafirlukast was fully efficacious against VRAC with an IC_{50} of 17 μM [45]. These compounds may serve as novel scaffolds for structure-activity relationship studies to improve their properties towards the channel. Further studies on VRAC have consisted of investigating the binding site of Zafirlukast. I have interrogated R103 of the LRRC8A subunit as a potential residue involved in Zafirlukast binding. Recently, it was shown that LRRC8A R103 is important for binding ATP [69]. In electrophysiological studies, I found that there was no difference in Zafirlukast inhibition between WT LRRC8A and R103F LRRC8A

homomeric channels (Figure 17A). Next, I used various chimeras comprised primarily of one LRRC8 subunit (LRRC8A, LRRC8C, LRRC8D, or LRRC8E) to form homomeric channels. In patch clamp electrophysiology experiments I found there was no difference in Zafirlukast inhibition between the different chimeras (Figure 17B). This suggests that Zafirlukast may be binding to a conserved region among LRRC8 subunits or acting through other means such as a common regulatory protein shared by all subunits. Future experiments to determine the binding site of Zafirlukast are focused on determining the cryo-EM structure of one of the LRRC8 chimeras bound with Zafirlukast. This will provide structural information we can use to validate the binding site with directed-mutagenesis. Lastly, given our success on identifying novel inhibitors in a relatively small screen, a larger screen of >50,000 compounds is warranted.

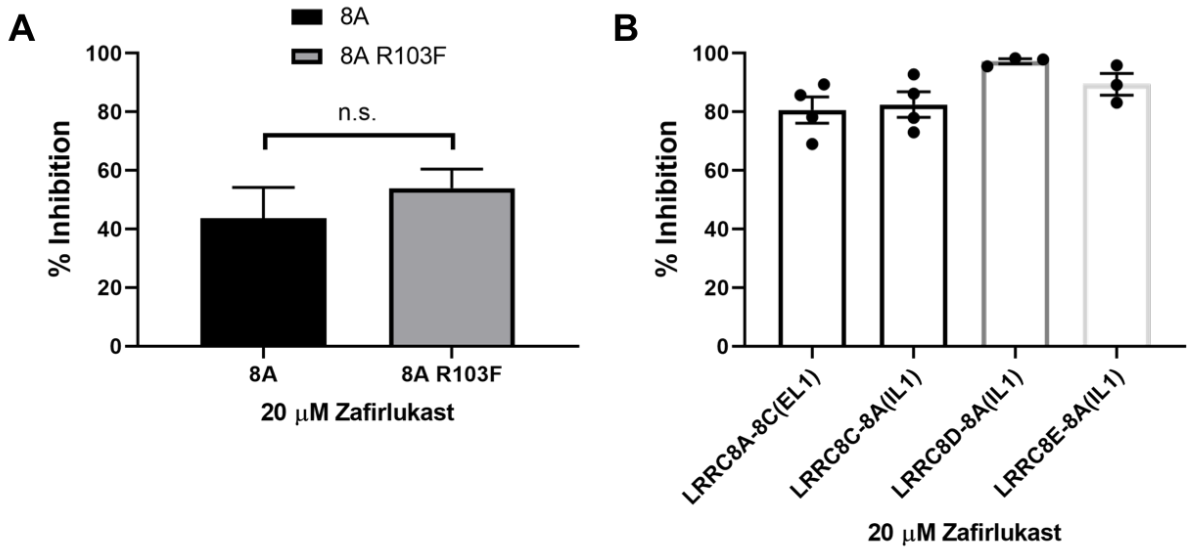

Figure 17. Structure/function analysis of Zafirlukast binding site

A) Zafirlukast inhibition of LRRC8A and LRRC8A R103F homomeric channels in whole-cell patch clamp electrophysiology. B) Zafirlukast inhibition of LRRC8 chimeras in whole-cell patch clamp electrophysiology.

Additionally, we were also able to identify novel activators of this channel, one of which, zinc pyrithione (ZPT), was extensively characterized in whole-cell patch clamp electrophysiology. ZPT potentiated swelling-activated VRAC currents, as well as activated VRAC in the absence of

the swelling stimulus. Further characterization must be performed to determine if ZPT is directly activating VRAC or indirectly through other means, such as ROS. Experiments determining if ZPT activates VRAC in the presence of a ROS-scavenger such as N-actyl cysteine are critical. If ROS is at play, subsequent experiments investigating VRAC subunit regulation is a logical next step. Previous studies show LRRC8E is potentiated by intracellular oxidation, whereas LRRC8C and LRRC8D were not [100]. Using LRRC8A/C/D/E chimeras that are already in our lab are great models to test this. If ZPT is not activating VRAC through ROS, it will be critical to test if pyrithione itself is activating VRAC. It has been reported Zn^{2+} and pyrithione dissociate from each other once in the cell [238, 239, 256] We know Zn^{2+} does not affect VRAC current, but pyrthione has yet to be investigated [257]. This can be tested by similar whole-cell patch clamp electrophysiology experiments used to characterize ZPT.

An emerging body of evidence indicates that VRACs containing different subunits are expressed in a cell type-specific manner and carry out unique physiological functions. For example, LRRC8D-containing VRACs favor transport of organic molecules such as taurine, myo-inositol, aspartate, and glutamate, whereas LRRC8C-containing channels preferentially conduct Cl- ions [98, 235]. Certain cancer tumors downregulate the LRRC8D subunit, which reduces the amount of platinum-based anticancer drugs (e.g., cisplatin/carboplatin) these tumor cells take up [98]. These data raise the possibility that it might be possible to develop sub-type specific inhibitors and activators of VRAC channels expressed in different cell types. Characterizing known VRAC inhibitors against molecularly defined VRACs comprised of different subunits using fluorescence-quenching assays and electrophysiology is a good first step toward testing this hypothesis. These studies will provide important new insights into the molecular pharmacology of VRACs and potentially identify new subtype-specific inhibitors that we and other investigators can use to probe the physiology of VRAC. We and others, [51, 258] have demonstrated that different VRAC subtypes can be functionally reconstituted in HCT116-LRRC8$^{-/-}$ cells. Therefore, we do not anticipate any technical barriers to the proposed study. Furthermore, HTS against molecularly

define VRAC subtypes is a logical next step and may be simplified by using LRRC8 chimeras comprised of homomeric channels.

APPENDIX A: DEVELOPING THE PHARMACOLOGY OF PROTON-ACTIVATED CHLORIDE CHANNELS

During the course of this thesis the gene for another understudied chloride channel, the proton-activated chloride channel (PAC), was identified. I subsequently started a side project developing the pharmacology of these under-studied chloride channels.

Introduction

Proton-activated ion channels have been shown to play important roles in human physiology as well as pathophysiology [259]. Since proton-activated currents were first described in 1980 [260, 261], it took nearly 20 years for the cloning of the cation-permissive ion channels [262], and nearly 40 years for the cloning of the anion-permissive ion channels [10, 11]. For the latter, two independent groups recently identified TMEM206 as the essential gene that encodes the proton-activated chloride channel (PAC) [10, 11].

PAC was initially described in 2003 in rat Sertoli cells [263] and has since been identified in a variety of cell types [264-268]. Several channels have been investigated as putative candidates for the proton-activated chloride current, such as, CLCs, VRAC, and TMEM16 channels, however, the molecular identity for PAC remained elusive. The biophysical properties of the channel have been studied extensively using patch clamp electrophysiology [10, 11, 263-268]. PAC channels have outwardly rectifying currents, are activated with a pH_{50} of approximately pH 5.1, and are permeable to various anions ($SCN^- > I^- > Br^- > Cl^-$ > gluconate) [264]. Further, several non-specific inhibitors have been shown to inhibit PAC channels [187, 264].

PACs have been shown to play a critical role in contributing to acidosis-induced necrotic cell death, a consequence of brain injury as observed in ischemic stroke [10, 11, 267]. Genetic knockout studies of PAC in mice suggest that PACs may be a novel therapeutic target for stroke [10]. However, the lack of specific and potent pharmacological tool compounds represents a

critical barrier to testing this hypothesis. Therefore, there is an unmet need to develop the pharmacology of PAC channels.

The recent cloning of PAC has created unprecedented opportunities to develop the molecular pharmacology of these channels. In the present study we develop a fluorescence-based assay for high-throughput screening (HTS) assay for discovering novel PAC inhibitors. Screening 10,000 compounds we found putative PAC inhibitors that show comparable inhibition to the best-in-class inhibitor of PAC, pregnenolone sulfate (PS) [269]. We also develop a random mutagenesis screen to identify key residues necessary for PS inhibition. The random mutagenesis screen identified a PAC mutant containing three mutations in the putative extracellular loop of channel that showed reduced PAC inhibition, as was confirmed using the patch clamp electrophysiology. The screen also revealed a PAC mutant that showed increased PAC function at a pH_{50}. Lastly, we also investigated a human PAC mutant reported in the DECIPHER database. We investigated this PAC mutant and found it had modest changes in its biophysical properties.

Materials and Methods

Chemicals

Pregnenolone sulfate was purchased from Tocris (Minneapolis, MN). All salts were purchased from Sigma-Aldrich and were of the highest grade available.

Molecular biology

The PACC1-pCMV6 plasmid was purchased from Origene Technologies. The YFP(F46L/H148Q/I152L) plasmid was generated as previously described (See Chapter 2 and [45]). PAC mut primers (Forward: 5'-CGGGAATTCGTCGACTGGAT-3'; Reverse: 5'-GCTGCCAGATCCTCTTCTGA-3') used for random mutagenesis flank PACC1 in pCMV6 plasmid.

Generation of PAC KO cell line

Using CRISPR/Cas9 technology, we generated monoclonal PAC KO cell lines. Guide RNA previously described [10] (5'-GGACCGAGAAGACGTTCTTC-3', negative strand) targeted the first putative TM of PAC. This guide RNA was subcloned into plasmid pSpCas9(BB)-2A-GFP (PX458) [270] that was a gift from Dr. Eric Delpire (Addgene plasmid #48138). HEK293 cells were transfected with this guide RNA plasmid using Lipofectamine LTX. 48 hrs post-transfection, cells were sorted using FACS into 96 well plates containing Dulbecco's Modified Eagle Medium (DMEM) supplemented with 20% Fetal Bovine Serum (FBS). Single colonies were isolated and expanded for genotyping analysis of frameshift mutations by target-site-specific PCR and subsequent Sanger sequencing. PAC KO cells were functionally confirmed using whole-cell patch clamp electrophysiology.

Cell culture and transient transfection

HEK293 and PAC KO cells were cultured in 75 cm2 flasks with Dulbecco's Modified Eagle Medium (DMEM) supplemented with 10% Fetal Bovine Serum (FBS) 1% Penicillin/Streptomycin (P/S). For patch clamp experiments, HEK293 or PAC KO cells were plated in 35-mm Nunclon dishes (Thermo Fisher Scientific, Rochester, NY). For high-throughput screening, stably transfected T-REX(HEK293)-PAC-Ozzy cells were cultured in 75 cm2 flasks with Dulbecco's Modified Eagle Medium (DMEM) supplemented with 10% Fetal Bovine Serum (FBS), 1% Penicillin/Streptomycin (P/S) and 700 µg/mL G418 Sulfate (Corning, Corning, NY). For random mutagenesis screening, PAC KO cells were transfected with PAC mutant library (described below) using lipofectamine LTX.

Patch clamp electrophysiology

The day of experiments, parental or transfected (see above) HEK293 cells were rinsed with divalent-free Hank's Balanced Salt Solution (HBSS), dissociated using 0.25% trypsin/1 mM EDTA for approximately 30-sec, diluted with complete medium, plated on poly-L-lysine-coated

round glass coverslips, and allowed to recover at 37ºC in a 5% CO2 incubator for at least 1 h before experiments. Patch pipettes were pulled from Clark Custom 8520 Patch Glass (1.5 o.d. × 1.16 i.d.) (Harvard Apparatus, Holliston, MA) using a P-1000 Flaming/Brown Microelectrode puller (Sutter Instruments) to a resistance of 2 – 4 MΩ when filled with the following solution (in mM): 135 CsCl, 2 $MgCl_2$, 2 $CaCl_2$, 10 HEPES, 5 EGTA, 2 Na2ATP, (pH 7.2 adjusted with CsOH, 280 mOsm). The pH 7.4 bath solution contained (in mM): 145 NaCl, 2 KCl, 2 $MgCl_2$, 1.5 $CaCl_2$, 10 HEPES, and 10 glucose (pH 7.4 adjusted with NaOH, 300 mOsm). pH 4.8 bath solution contained (in mM): 145 NaCl, 2 KCl, 2 $MgCl_2$, 1.5 $CaCl_2$, 5 Na_3-citrate and 10 glucose (pH 4.8 adjusted with citric acid, 300 mOsm). Macroscopic currents were recorded under voltage-clamp conditions using an Axopatch 200B amplifier (Molecular Devices, Sunnyvale, CA). Cells were voltage clamped at a holding potential of 0 mV and whole-cell currents were elicited by a voltage ramp or step protocol. For voltage ramps, membrane potential was first stepped to -40 mV for 15 msec and then ramped over 500 msec to +80 mV. This was followed by a step back to 0 mV for 4 sec before this protocol was repeated. Step changes in membrane voltage were induced by stepping membrane voltage to -80 mV to +80 mV for 1 sec, with 10 mV or 20 mV increments. Data were collected at 5 kHz and filtered at 1 kHz. Data acquisition and analysis were performed using pClamp 9.2 software suite (Molecular Devices). Percent inhibition of compounds was determined by normalizing data to currents inhibited by 30 μM PS.

Fluorescence reporter assay of PAC function

HEK293-PAC-Ozzy cells were dissociated using 0.25% trypsin/1 mM EDTA and plated at a density of 20,000 cells/well with 1 ug/mL tetracycline in clear bottomed, black-walled Corning PureCoat amine coated 384 well plates (Corning, Corning, NY) and cultured overnight at 37ºC in a 5% CO2 incubator. The following day cells were washed with a pH 7.4 wash buffer solution containing (in mM): 140 NaCl, 5 KCl, 1 $CaCl_2$, 1 $MgCl_2$, and 10 HEPES (pH 7.4 with NaOH). Compounds from the Vanderbilt Discovery Compound Collection library were dissolved in the pH 7.4 wash buffer solution and added simultaneously to all 384-wells at a final screening

concentration of 10 μM. After 5 min allowing for solution mixing, a PAC activating solution containing (in mM): 110 NaCl, 30 NaI, 5 KCl, 1 $CaCl_2$, 1 $MgCl_2$ (pH 3.0-6.0 adjusted with 5 mM total citric acid and Na_3-citrate) was added to all 384-wells simultaneously and Ozzy fluorescence was measured at 1Hz using a Panoptic kinetic imaging plate reader (WaveFront Bioscience, Franklin, TN, USA). Fluorescence values from each well were normalized to baseline readings (i.e. average of the first 5 readings before compound-containing solution is added). Percent fractional quenching was calculated by subtracting fluorescence readings obtained before and after PAC activating solution addition. Data were plotted with GraphPad Prism version 7.03 (GraphPad Software, San Diego, CA) to generate representative experiment traces and CRCs using a non-linear regression analysis.

Random mutagenesis

PAC mutants were generated using GenMorph II random mutagenesis kit (Agilent Technologies, Inc., Santa Clara, CA). PACC1-pCMV6 plasmid and PAC mut primers were used as reagents in the random mutagenesis kit. PAC mutants were subsequently subcloned into pCMV6. A library of 96 PAC mutants and Ozzy cDNA was then used for transient co-transfection into PAC KO cells. PAC mutant function was measured using the fluorescence-reporter assay described above.

Statistics

All data are presented as means ± SEM; n represents the number of cells in patch-clamp recordings, the number of plates in high throughput screens, or the number of wells in fluorescence-based assays. Statistical significance was determined by using Student's t test for unpaired means for two groups.

Results

Development of a PAC reporter assay for HTS

We developed a fluorescence-based assay for high-throughput screening (HTS) assay for discovering novel PAC inhibitors. Briefly, TREX-HEK-293 cells were engineered to overexpress PAC from a tetracycline-inducible promoter and constitutively express an iodide-sensitive YFP mutant (i.e. F46L, H148Q, I152L) termed Ozzy. The 384-well-based assay measures the quenching of intracellular Ozzy by iodide influx through PAC activated by acid treatment (Figure 18A-B). We show the overexpression of PAC can increase the signal intensity by >4 fold compared to endogenously expressed PAC (Figure 18C-D).

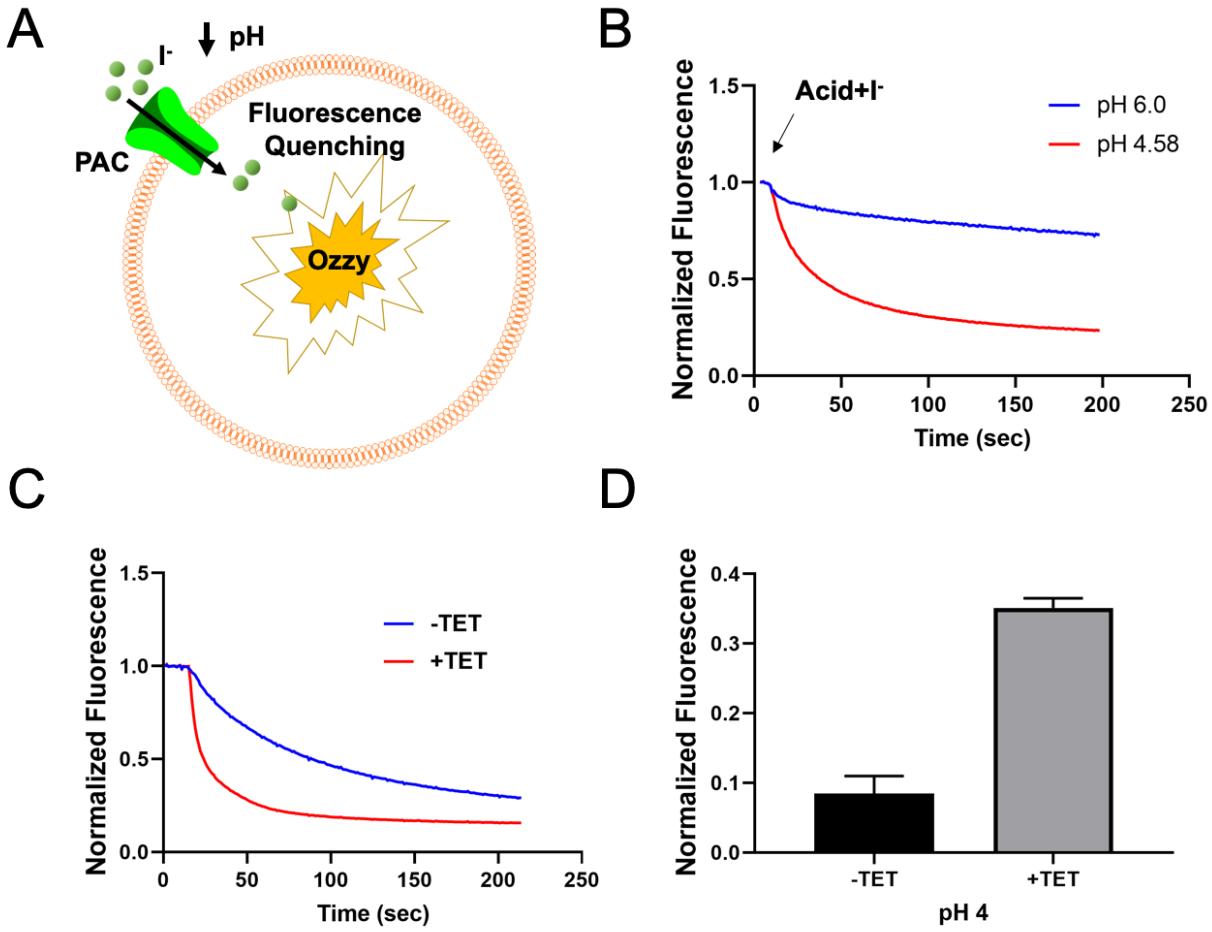

Figure 18. Application of Ozzy assay to measure PAC currents

A) Schematic of Ozzy fluorescence assay for PAC channels. B) Representative traces of Ozzy fluorescence assay. Cells are exposed to basic (pH 6.0) or acidic (pH 4.58) solutions containing iodide. C) Representative traces of cells treated with or without tetracycline >18hrs prior to conducting Ozzy fluorescence assay. D) Quantification of fluorescence at 30s shows a 4-fold increase in fluorescence quenching following iodide addition.

In order to test if the Ozzy fluorescence assay can report pharmacological inhibition of PAC, we used the known PAC inhibitor, pregnenolone sulfate (PS, Figure 19A) [269]. We found the fluorescence assay can report dose-dependent inhibition of PAC with PS (Figure 19B; IC_{50} of 6 μM). Further validation of the Ozzy fluorescence assay showed the range of 0.01-1% DMSO did not affect fluorescence and a preliminary Z-factor of 0.54 between DMSO and 100 μM PS treated wells (Figure 19C-D). To utilize the assay to identify both activators and inhibitors, we used an EC_{50} pH solution, pH 5.1, which enables me to identify compounds that activate PAC greater than 50% activity or inhibit PAC to less than 50% activity. I found these conditions produced a Z-factor of >0.5 in both the activator (mean ± SEM 0.59 ± 0.06) and inhibitor (mean ± SEM 0.6 ± 0.04) directions, hitting the standard for an "excellent" HTS assay (Z-factor > 0.5) [271].

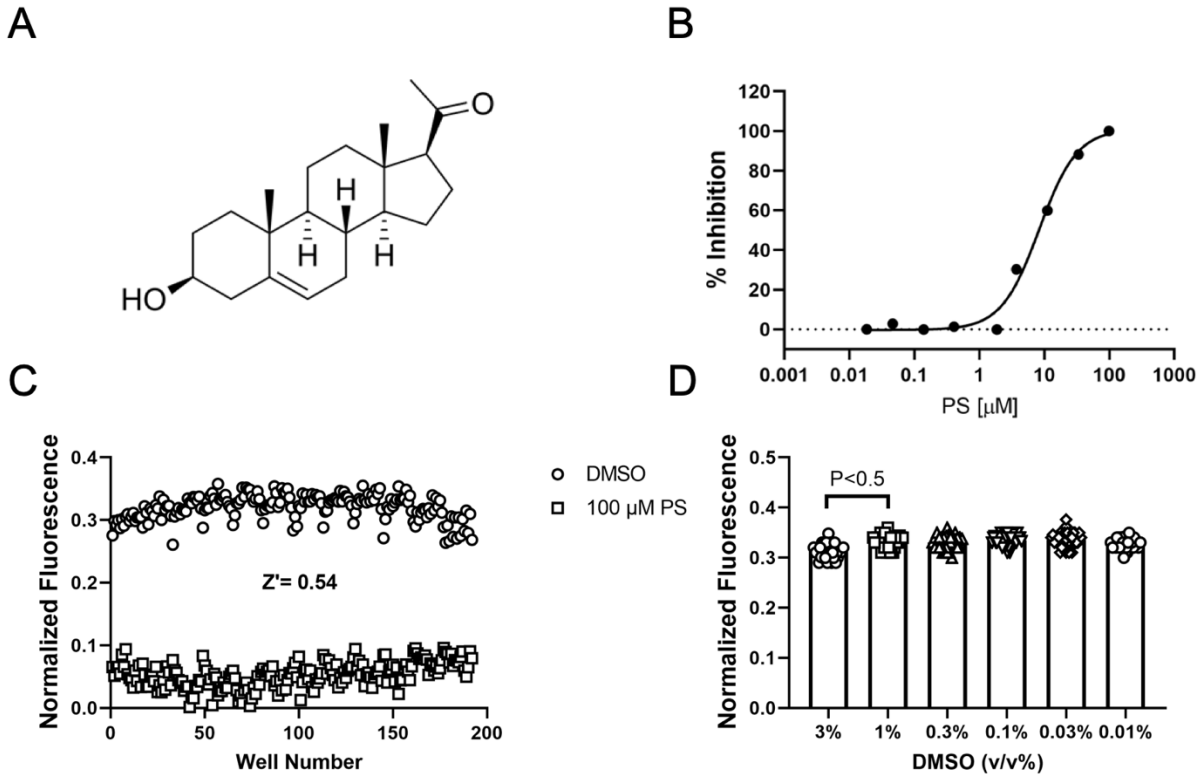

Figure 19. Optimization of Ozzy assay to detect inhibition of PAC by PS

A) Structure of pregnenolone sulfate (PS). B) Concentration-response curve of PS in pH 4.58 solution in the Ozzy fluorescence assay. C) Representative scatter plot for Ozzy fluorescence assay with cells treated with DMSO or 100 uM PS in pH 4.48 solution. D) The effect of DMSO on Ozzy fluorescence assay in pH 4.58 solution.

High-throughput screening for modulators of PAC

I performed two screens using this assay. One screen was against a small library of PS analogs to determine if there are any compounds with improved potency compared to PS. I found none of the PS analogs had improved potency and a majority were inactive (Figure 20). I also screened against 10,000 compounds selected for their diverse collection of compounds within Vanderbilt Discovery Compound Collection. I identified ten novel compounds that inhibited PAC in the screen (**TABLE 4**). Further characterization in whole-cell patch clamp electrophysiology is needed. Given the success of the 10,000 compound screen, a larger screen is warranted in efforts to increase the chances of identify novel modulators of PAC.

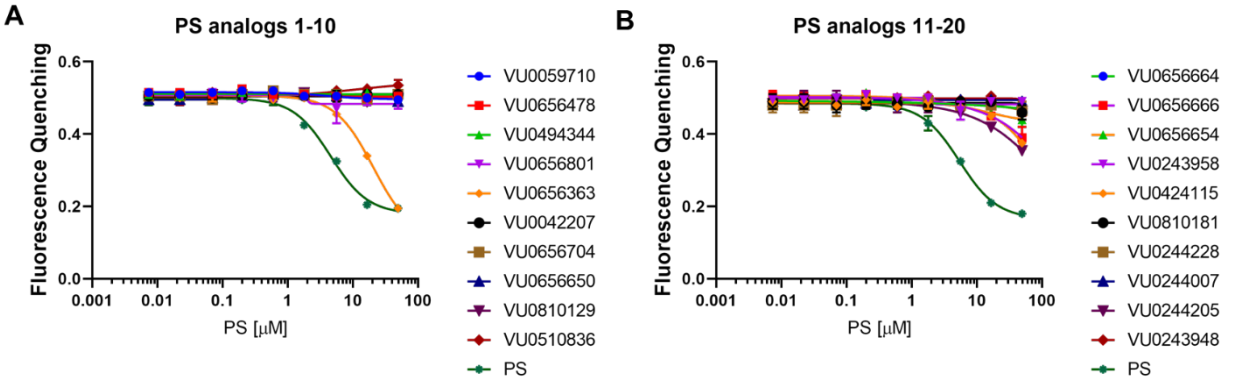

Figure 20. PS analogs in PAC Ozzy assay

Compounds were incubated at pH 7.4 assay buffer for 5 mins (-5 min) on cells prior to pH 5.1+100 mM iodide addition. Fluorescence quenching was determined 30 sec after pH 5.1 and iodide addition. Fluorescence was normalized to baseline (t= 0 sec).

Table 2. PAC inhibitor "HITS" from screen against Vanderbilt Discovery Compound Collection

Values are n=4. PAC is activated by pH 5.1 activating solution. Inhibition was calculated by normalizing fluorescence quenching to DMSO treated cells.

Compound	IC_{50} (μM)	Compound	IC_{50} (μM)
VU0496364	25.1	VU0613284	17.8
VU0497988	131.8	VU0637259	18.6
VU0498013	44.7	VU0637331	38.0
VU0523898	16.6	VU0637628	8.1
VU0523905	13.18	VU0628875	11.5
VU0548448	12.9	PS	16.5

Random mutagenesis screening identified PAC mutants with PS LOF and pH GOF

Pregnenolone sulfate or PS is the best in class inhibitor of PAC. It has an IC_{50} of ~2 μM in patch clamp electrophysiology and an IC50 of ~6 μM in the Ozzy assay. And it acutely and reversibly inhibits PAC with fast kinetics. However, there are several brain specific off-targets, including NMDA receptors, GABAA receptors, and TRPM3 channels, that make PS a poor compound to use to study the neurophysiology of the channel [272-274]. In an effort to improve the potency and selectivity of PAC, we set out to identify the binding site of PS. Knowing this structure-function information, we could make changes to the PS molecule in an informed manner to better bind and potentially increase potency and specificity towards PAC as well as learn more about its mechanism of action. Therefore, we performed random mutagenesis on PAC cDNA and utilized the fluorescence-based Ozzy assay to assess PAC mutants for PAC inhibition with PS as well as assess overall PAC function (Figure 21).

We identified several PAC mutants that showed loss PS inhibition or PAC GOF that were confirmed by Sanger sequencing. Two mutants were particularly interesting PAC

L168P/A278D/Q293K showed PS loss-of-function and PAC T90A showed PAC GOF (Figure 21C-D). These PAC mutants were confirmed in whole-cell patch clamp electrophysiology (Figure 22). Future studies for PAC L168P/A278D/Q293K will be to test each mutation individually to identify which residues are important for the PS loss-of-function. Future studies for PAC T90A will rely on testing PAC GOF function in acidosis-induced necrotic cell death functional assay.

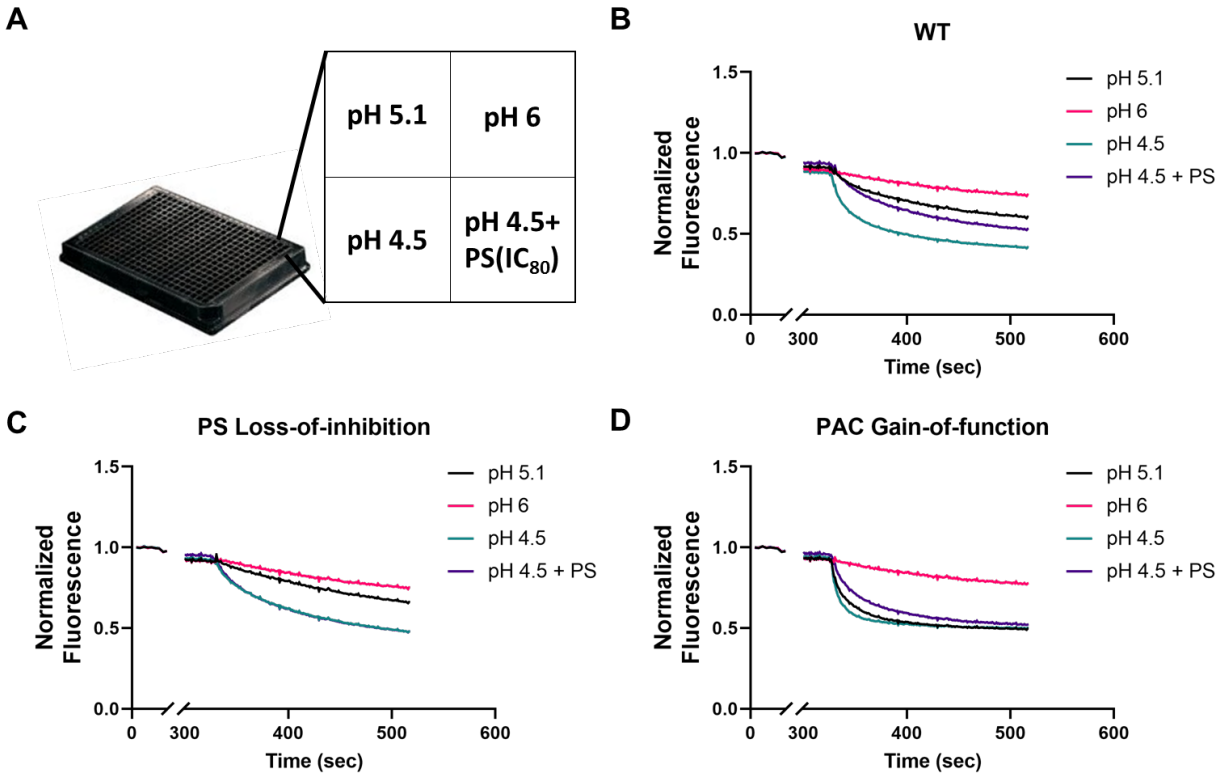

Figure 21. PAC random mutagenesis

A) Plating scheme of solutions added to cells. B) Representative Ozzy assay traces with WT PAC. C) Representative Ozzy assay traces with PAC L168P/A278D/Q293K mutant showing a PS loss-of-function. D) Representative Ozzy assay traces with PAC T90A showing a PAC gain-of-function. (Compounds were incubated at pH 7.4 assay buffer for 5 mins (-5 min) on cells prior to acid+100 mM iodide addition. Fluorescence was normalized to baseline (t= 0 sec)).

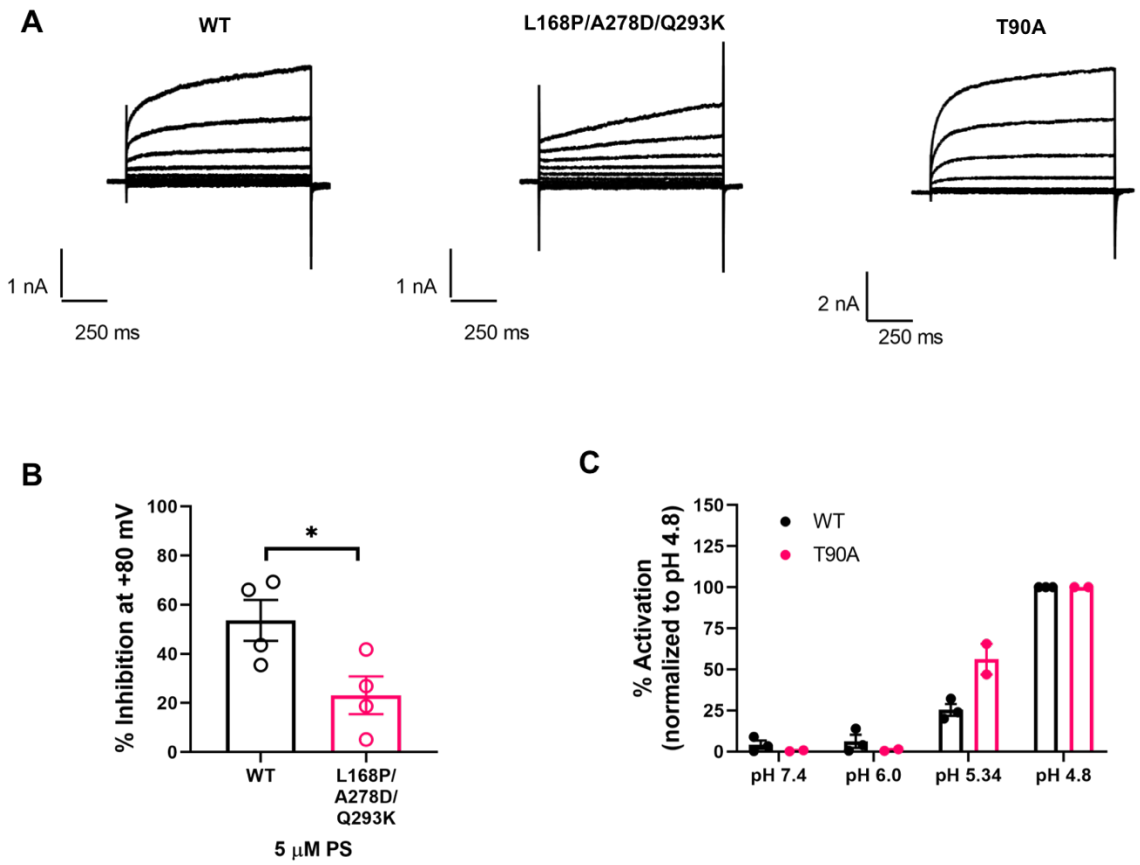

Figure 22 Electrophysiological characterization of PAC mutants

A) Representative whole-cell proton-activated chloride currents of WT and PAC mutants (pH 4.8). B) Percent inhibition with 5 μM PS. PAC KO cells were transfected with WT or PAC L168P/A278D/Q293K. PAC currents were elicited with pH 4.8 (n=4; *P<0.05; Analyzed with student's t-test). C) Percent activation of WT and PAC T90A at various pH values. Values are normalized to currents at pH 4.8 (n>2).

Characterization of human PAC mutant

We also characterized PAC R253W, a mutation identified in a patient with a neurodevelopmental disorder: We identified a patient with developmental disorder with a PAC mutation in the DECIPHER database (https://decipher.sanger.ac.uk/). The phenotype associated with the mutation was an "abnormality of the nervous system". This was interesting because PAC is primarily expressed in the brain (https://www.proteinatlas.org/). We made PAC R253W using site-directed mutagenesis and tested the mutant using patch clamp electrophysiology. We found that the mutant compared to WT PAC had larger currents overall, a reduction in the instantaneous

current and no significant difference in tail currents (Figure 23). Future characterization of this PAC mutant is warranted. While it may have modest changes biophysically, these changes may be sufficient to alter its physiological function. Therefore, studies assaying against acidosis-induced necrotic cell death is a good place to start.

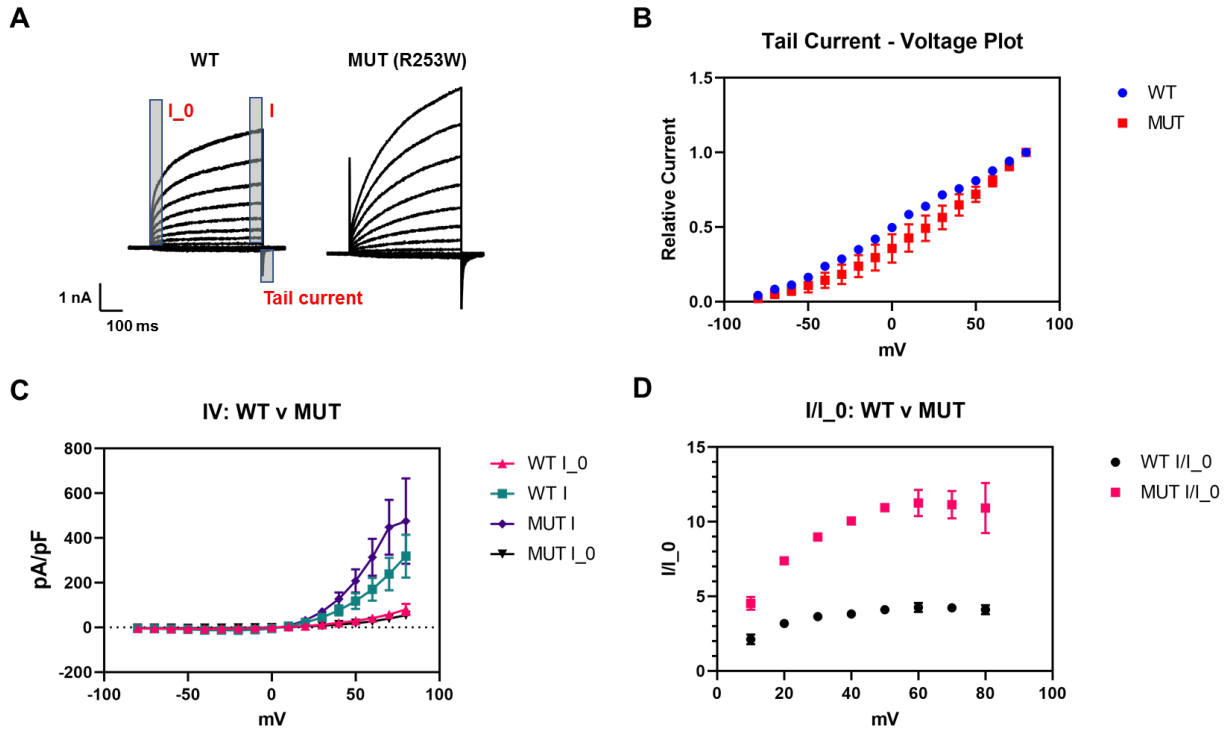

Figure 23. Electrophysiological characterization of PAC R253W

A) Representative current traces of PAC (WT) and PAC R253W (MUT). PAC KO cells were transfected with WT or (MUT) plasmid DNA and GFP. To activate the channel, cells were exposed to pH 4.8 bath solution. Step protocol from -80 mV to +80 mV with 10 mV step increments. 500 ms voltage pulse used. B) Tail current analysis of WT and MUT. Amplitude of tail current was plotted against voltage applied. C) Current density analysis of WT and MUT. Instantaneous current (I_0) or current at the end of the 500 ms voltage pulse (I) plotted against voltage. D) Analysis of I/I_0 for WT and MUT. I/I_0 plotted against voltage.

Discussion

PAC is one of the most recently cloned ion channels to date. Since its initial discovery, PACs have been shown to be pH-activated, temperature sensitive chloride channels that have been implicated in acidosis-induced necrotic cell death [263, 266, 267]. Genetic studies have

implicated the activation of PAC in contributing to the pathogenesis of stroke, positioning PAC as potential therapeutic target for ischemic stroke [10]. In addition to expression in the brain, PAC is ubiquitously expressed throughout the human body, suggesting PAC may also play physiological roles in other tissues that experience acidosis, such as the kidney [275]. The recent identification of the gene that encodes PAC, not only has created unprecedented opportunities to study the physiology of this channel, but to also to develop the molecular pharmacology and better understand the structure-function relationship. Our studies on PAC have focused on developing novel modulators of PAC to test the therapeutic potential of these channels, identifying the binding site for the best-in-class inhibitor of PAC, pregnenolone sulfate (PS), and characterizing PAC mutants we generated using random mutagenesis, as well as a PAC mutant found in a human patient.

PACC1 is the gene that encodes for PAC [10, 11]. We and others have found that we can increase PAC activity in cells by heterologously expressing *PACC1* alone (Figure 18; [10, 11]). This was evident in our Ozzy fluorescence assay, where we saw a 4-fold increase in PAC activity in heterologously expressed PAC over endogenously expressed PAC (Figure 18). We also confirmed this finding using whole-cell patch clamp electrophysiology (data not shown). This increase in channel activity is useful when developing high-throughput screening assays for identifying novel modulators of channels. From our screening efforts, we identified 11 compounds that had similar inhibition properties to our benchmark inhibitor, PS (Table 2). Subsequent studies will be focused on characterizing these inhibitors using whole-cell patch clamp electrophysiology the gold standard for measuring ion channel activity. In addition, given PAC's role in acidosis-induced necrotic cell death, these inhibitors will be tested for efficacy in acidosis cell death assays, which we hypothesize the most potent inhibitors of PAC will protect from cell death following acid treatment. We also screened a small library of PS analogs for improved efficacy and potency, however, none of the analogs showed improved properties (Figure 20).

Given the ability to measure PAC activity from heterologous expression, we developed a medium-throughput assay to generate PAC mutants and rapidly assess them using the Ozzy-fluorescence assay. The aim of the random mutagenesis approach was to rapidly identify key residues involved in PS inhibition as well as PAC function. We tested 96 putative PAC mutants against four test conditions, pH 4.5 (approximately max PAC activation), pH 5.1 (approximately pH_{50}), pH 4.5 + PS, and pH 6.0 (approximately no PAC activation). We identified mutants that showed reduced PS inhibition and PAC gain-of-function. One PAC mutant that had reduced PS inhibition had three mutations in the extracellular loop of PAC (L168P/A278D/Q293K) (Figure 21C). We further characterized this mutant in patch clamp electrophysiology and confirmed our finding (Figure 22A, 22B). Subsequent experiments will be focused on testing individual mutations. PAC A278D is of particular interest because the introduction of the negatively charged residue may repulse the negative sulfate group of pregnenolone sulfate, ultimately reducing PAC inhibition. One gain-of-function PAC mutant we identified, PAC T90A, showed increased PAC activity (Figure 21D). This finding was confirmed using patch clamp electrophysiology (Figure 22A, 22C). PAC T90A is found on the extracellular loop of PAC, near the transmembrane domain 1. We hypothesize this mutant is a gating mutant, however, further studies characterizing this mutation is needed.

We were also interested in determining if PAC mutations have been identified in humans and if they lead to disease. These studies could illuminate novel physiological roles for this channel. We searched publicly available databases for human mutations in the *PACC1* gene (previously known as *TMEM206*). We identified PAC R253W as a patient mutation in the DECIPHER database. The patient mutation was collected as a part of a smaller data set collected for the Deciphering Developmental Disorders study. In this study, patients with undiagnosed developmental disorders had their genome sequenced and made available through the DECIPHER database. The patient with PAC R253W was described to have an “abnormality of the nervous system”. PAC expression is high in the central nervous system, and has already been

implicated in another neurological disorder, therefore, we wanted to further characterize this mutation using patch clamp electrophysiology [10]. We found modest biophysical differences when compared to WT PAC, however, they may be sufficient to lead to disease. Further characterization in another functional assay, such as the cell death assay may be insightful.

In conclusion, our studies describe some early efforts in developing the molecular pharmacology and structure-function relationship of PAC channels. We show that YFP-based fluorescence assays are readily amendable to studying PAC activity and pharmacology in a high-throughput manner. Given the current state of PAC pharmacology there is a need to identify better tools to use for studying the physiology of PAC.

REFERENCES

1. Hille, B., *Ion channels of excitable membranes*. 3rd ed. 2001, Sunderland, Mass.: Sinauer. xviii, 814 p.

2. Guyton, A.C. and J.E. Hall, *Textbook of medical physiology*. 11th ed. 2006, Philadelphia: Elsevier Saunders. xxxv, 1116 p.

3. Duran, C., et al., *Chloride channels: often enigmatic, rarely predictable.* Annual Review of Physiology, 2010. **72**: p. 95-121.

4. Whitlock, J.M. and H.C. Hartzell, *Anoctamins/TMEM16 Proteins: Chloride Channels Flirting with Lipids and Extracellular Vesicles.* Annu Rev Physiol, 2017. **79**: p. 119-143.

5. Ye, W., et al., *Dynamic change of electrostatic field in TMEM16F permeation pathway shifts its ion selectivity.* Elife, 2019. **8**.

6. Strange, K., T. Yamada, and J.S. Denton, *A 30-year journey from volume-regulated anion currents to molecular structure of the LRRC8 channel.* J Gen Physiol, 2019. **151**(2): p. 100-117.

7. Pedersen, S.F., Y. Okada, and B. Nilius, *Biophysics and Physiology of the Volume-Regulated Anion Channel (VRAC)/Volume-Sensitive Outwardly Rectifying Anion Channel (VSOR).* Pflugers Arch, 2016. **468**(3): p. 371-83.

8. Jentsch, T.J., *VRACs and other ion channels and transporters in the regulation of cell volume and beyond.* Nat Rev Mol Cell Biol, 2016. **17**(5): p. 293-307.

9. Sabirov, R.Z., et al., *The organic anion transporter SLCO2A1 constitutes the core component of the Maxi-Cl channel.* EMBO J, 2017. **36**(22): p. 3309-3324.

10. Yang, J., et al., *PAC, an evolutionarily conserved membrane protein, is a proton-activated chloride channel.* Science, 2019. **364**(6438): p. 395-399.

11. Ullrich, F., et al., *Identification of TMEM206 proteins as pore of PAORAC/ASOR acid-sensitive chloride channels.* Elife, 2019. **8**.

12. Hille, B., *Ionic channels of excitable membranes*. 1984, Sunderland, Mass.: Sinauer Associates. 426 p.

13. Coombs, J.S., J.C. Eccles, and P. Fatt, *The specific ionic conductances and the ionic movements across the motoneuronal membrane that produce the inhibitory post-synaptic potential.* J Physiol, 1955. **130**(2): p. 326-74.

14. Lipicky, R.J., S.H. Bryant, and J.H. Salmon, *Cable parameters, sodium, potassium, chloride, and water content, and potassium efflux in isolated external intercostal muscle of normal volunteers and patients with myotonia congenita.* J Clin Invest, 1971. **50**(10): p. 2091-103.

15. Lipicky, R.J. and S.H. Bryant, *Sodium, potassium, and chloride fluxes in intercostal muscle from normal goats and goats with hereditary myotonia.* J Gen Physiol, 1966. **50**(1): p. 89-111.

16. Bryant, S.H., *Cable properties of external intercostal muscle fibres from myotonic and nonmyotonic goats.* J Physiol, 1969. **204**(3): p. 539-50.

17. Di Sant'Agnese, P.A., et al., *Abnormal electrolyte composition of sweat in cystic fibrosis of the pancreas; clinical significance and relationship to the disease.* Pediatrics, 1953. **12**(5): p. 549-63.

18. Quinton, P.M., *Chloride impermeability in cystic fibrosis.* Nature, 1983. **301**(5899): p. 421-2.

19. Jentsch, T.J., K. Steinmeyer, and G. Schwarz, *Primary structure of Torpedo marmorata chloride channel isolated by expression cloning in Xenopus oocytes.* Nature, 1990. **348**: p. 510-514.

20. Riordan, J.R., et al., *Identification of the cystic fibrosis gene: cloning and characterization of complementary DNA.* Science, 1989. **245**(4922): p. 1066-73.

21. Kerem, B., et al., *Identification of the cystic fibrosis gene: genetic analysis.* Science, 1989. **245**(4922): p. 1073-80.

22. Rommens, J.M., et al., *Identification of the cystic fibrosis gene: chromosome walking and jumping.* Science, 1989. **245**(4922): p. 1059-65.

23. Bear, C.E., et al., *Purification and functional reconstitution of the cystic fibrosis transmembrane conductance regulator (CFTR).* Cell, 1992. **68**(4): p. 809-18.

24. Gadsby, D.C., P. Vergani, and L. Csanady, *The ABC protein turned chloride channel whose failure causes cystic fibrosis.* Nature, 2006. **440**(7083): p. 477-83.

25. Cuthbert, A.W., *New horizons in the treatment of cystic fibrosis.* Br J Pharmacol, 2011. **163**(1): p. 173-83.

26. Koch, M.C., et al., *The skeletal muscle chloride channel in dominant and recessive human myotonia.* Science, 1992. **257**: p. 797-800.

27. Steinmeyer, K., et al., *Inactivation of muscle chloride channel by transposon insertion in myotonic mice.* Nature, 1991. **354**: p. 304-308.

28. Pusch, M., et al., *Mutations in dominant human myotonia congenita drastically alter the voltage dependence of the CIC-1 chloride channel.* Neuron, 1995. **15**(6): p. 1455-63.

29. Alvarez-Leefmans, F.J. and E. Delpire, *Physiology and Pathology of Chloride Transporters and Channels in the Nervous System From Molecules to Diseases Preface.* Physiology and Pathology of Chloride Transporters and Channels in the Nervous System: From Molecules to Diseases, 2009: p. Ix-X.

30. Duran, C., et al., *Chloride channels: often enigmatic, rarely predictable.* Annu Rev Physiol, 2010. **72**: p. 95-121.

31. Verkman, A.S. and L.J. Galietta, *Chloride channels as drug targets.* Nat Rev Drug Discov, 2009. **8**(2): p. 153-71.

32. Yu, H., et al., *Ivacaftor potentiation of multiple CFTR channels with gating mutations.* J Cyst Fibros, 2012. **11**(3): p. 237-45.

33. Van Goor, F., et al., *Correction of the F508del-CFTR protein processing defect in vitro by the investigational drug VX-809.* Proc Natl Acad Sci U S A, 2011. **108**(46): p. 18843-8.

34. Southern, K.W., et al., *Correctors (specific therapies for class II CFTR mutations) for cystic fibrosis.* Cochrane Database Syst Rev, 2018. **8**: p. CD010966.

35. Middleton, P.G., et al., *Elexacaftor-Tezacaftor-Ivacaftor for Cystic Fibrosis with a Single Phe508del Allele.* N Engl J Med, 2019. **381**(19): p. 1809-1819.

36. Keating, D., et al., *VX-445-Tezacaftor-Ivacaftor in Patients with Cystic Fibrosis and One or Two Phe508del Alleles.* N Engl J Med, 2018. **379**(17): p. 1612-1620.

37. Heijerman, H.G.M., et al., *Efficacy and safety of the elexacaftor plus tezacaftor plus ivacaftor combination regimen in people with cystic fibrosis homozygous for the F508del*

mutation: a double-blind, randomised, phase 3 trial. Lancet, 2019. **394**(10212): p. 1940-1948.

38. Santos, R., et al., *A comprehensive map of molecular drug targets.* Nat Rev Drug Discov, 2017. **16**(1): p. 19-34.

39. Neher, E. and B. Sakmann, *Single-channel currents recorded from membrane of denervated frog muscle fibres.* Nature, 1976. **260**(5554): p. 799-802.

40. Cole, K.S., *Dynamic Electrical Characteristics of the Squid Axon Membrane.* Archives Des Sciences Physiologiques, 1949. **3**(2): p. 253-258.

41. Hodgkin, A.L. and A.F. Huxley, *A quantitative description of membrane current and its application to conduction and excitation in nerve.* J Physiol, 1952. **117**(4): p. 500-44.

42. Meech, R.W. and N.B. Standen, *Potassium activation in Helix aspersa neurones under voltage clamp: a component mediated by calcium influx.* J Physiol, 1975. **249**(2): p. 211-39.

43. Wilson, W.A. and M.M. Goldner, *Voltage clamping with a single microelectrode.* J Neurobiol, 1975. **6**(4): p. 411-22.

44. Hamill, O.P., et al., *Improved patch-clamp techniques for high-resolution current recording from cells and cell-free membrane patches.* Pflugers Arch, 1981. **391**(2): p. 85-100.

45. Figueroa, E.E., et al., *CysLT1 receptor antagonists pranlukast and zafirlukast inhibit LRRC8-mediated volume regulated anion channels independently of the receptor.* Am J Physiol Cell Physiol, 2019. **317**(4): p. C857-C866.

46. Cox, B., M. Gosling, and Royal Society of Chemistry (Great Britain), *Ion channel drug discovery*. RSC drug discovery series,. 2015, Cambridge: Royal Society of Chemistry. xviii, 366 pages.

47. Wachter, R.M., et al., *Structural basis of spectral shifts in the yellow-emission variants of green fluorescent protein.* Structure, 1998. **6**(10): p. 1267-77.

48. Jayaraman, S., et al., *Mechanism and cellular applications of a green fluorescent protein-based halide sensor.* J Biol Chem, 2000. **275**(9): p. 6047-50.

49. Galietta, L.J., P.M. Haggie, and A.S. Verkman, *Green fluorescent protein-based halide indicators with improved chloride and iodide affinities.* FEBS Lett, 2001. **499**(3): p. 220-4.

50. Tertyshnikova, S., et al., *Cell-based assay for the quantitative high throughput screening of gamma-aminobutyric acid-induced halide transport*. 2006, Google Patents.

51. Voss, F.K., et al., *Identification of LRRC8 heteromers as an essential component of the volume-regulated anion channel VRAC.* Science, 2014. **344**(6184): p. 634-8.

52. Qiu, Z., et al., *SWELL1, a plasma membrane protein, is an essential component of volume-regulated anion channel.* Cell, 2014. **157**(2): p. 447-458.

53. Strange, K., F. Emma, and P.S. Jackson, *Cellular and molecular physiology of volume-sensitive anion channels.* Am.J.Physiol.(Cell Physiol.39), 1996. **270**: p. C711-C730.

54. Strange, K., *Cellular volume homeostasis.* Adv Physiol Educ, 2004. **28**(1-4): p. 155-9.

55. Hoffmann, E.K., I.H. Lambert, and S.F. Pedersen, *Physiology of cell volume regulation in vertebrates.* Physiol Rev, 2009. **89**(1): p. 193-277.

56. Lang, F., et al., *Functional significance of cell volume regulatory mechanisms.* Physiol.Rev., 1998. **78**(1): p. 247-306.

57. Wehner, F., et al., *Cell volume regulation: osmolytes, osmolyte transport, and signal transduction.* Rev Physiol Biochem Pharmacol, 2003. **148**: p. 1-80.

58. Evans, D.H., *Osmotic and ionic regulation : cells and animals*. 2009, Boca Raton: CRC Press. xvi, 590 p., 8 p. of plates.

59. Cahalan, M.D. and R.S. Lewis, *Role of potassium and chloride channels in volume regulation by T lymphocytes.* Soc Gen Physiol Ser, 1988. **43**: p. 281-301.

60. Hazama, A. and Y. Okada, *Ca 2+ sensitivity of volume-regulatory K + and Cl - channels in cultured human epithelial cells.* J Physiol, 1988. **402**: p. 687-702.

61. Nilius, B., et al., *Properties of volume-regulated anion channels in mammalian cells.* Progress in Biophysics and Molecular Biology, 1997. **68**(1): p. 69-119.

62. Wine, J.J. and D.B. Luckie, *P-glycoprotein - a cautionary tale.* Curr.Biol., 1996. **6**(11): p. 1410-1412.

63. Strange, K., *Molecular identity of the outwardly rectifying, swelling-activated anion channel: time to re-evaluate pICln.* Journal of General Physiology, 1998. **111**: p. 617-622.

64. Nilius, B. and G. Droogmans, *Amazing chloride channels: an overview.* Acta Physiol Scand, 2003. **177**(2): p. 119-47.

65. Abascal, F. and R. Zardoya, *LRRC8 proteins share a common ancestor with pannexins, and may form hexameric channels involved in cell-cell communication.* Bioessays, 2012. **34**(7): p. 551-60.

66. Nakamura, R., et al., *Cryo-EM structure of the volume-regulated anion channel LRRC8D isoform identifies features important for substrate permeation.* Commun Biol, 2020. **3**(1): p. 240.

67. Kern, D.M., et al., *Cryo-EM structures of the DCPIB-inhibited volume-regulated anion channel LRRC8A in lipid nanodiscs.* Elife, 2019. **8**.

68. Kasuya, G., et al., *Cryo-EM structures of the human volume-regulated anion channel LRRC8.* Nat Struct Mol Biol, 2018. **25**(9): p. 797-804.

69. Kefauver, J.M., et al., *Structure of the human volume regulated anion channel.* Elife, 2018. **7**.

70. Deneka, D., et al., *Structure of a volume-regulated anion channel of the LRRC8 family.* Nature, 2018. **558**(7709): p. 254-259.

71. Kubo, M. and Y. Okada, *Volume-regulatory Cl - channel currents in cultured human epithelial cells.* Journal of Physiology, 1992. **456**: p. 351-371.

72. Jackson, P.S. and K. Strange, *Volume-sensitive anion channels mediate swelling-activated inositol and taurine efflux.* Am.J.Physiol.(Cell Physiol.34), 1993. **265**: p. C1489-C1500.

73. Lewis, R.S., P.E. Ross, and M.D. Cahalan, *Chloride channels activated by osmotic stress in T lymphocytes.* Journal of General Physiology, 1993. **101**: p. 801-826.

74. Akita, T. and Y. Okada, *Characteristics and roles of the volume-sensitive outwardly rectifying (VSOR) anion channel in the central nervous system.* Neuroscience, 2014. **275**: p. 211-31.

75. Emma, F., M. McManus, and K. Strange, *Intracellular electrolytes regulate the volume set point of the organic osmolyte/anion channel VSOAC.* Am J Physiol (Cell Physiol), 1997. **272**: p. C1766-C1775.

76. Jackson, P.S., et al., *Swelling-activated anion conductance in skate hepatocytes: regulation by cell Cl - and ATP.* Am.J.Physiol.(Cell Physiol.39), 1996. **270**: p. C57-C66.

77. Boese, S.H., F. Wehner, and R.H.K. Kinne, *Taurine permeation through the swelling-activated anion conductance in rat IMCD cells in primary culture.* American Journal of Physiology (Renal, Fluid and Electrolyte Physiology 40), 1996. **271**: p. F498-F507.

78. Manolopoulos, V.G., et al., *Swelling-activated efflux of taurine and other organic osmolytes in endothelial cells.* American Journal of Physiology: Cell Physiology, 1997. **273**(1): p. C214-C222.

79. Lambert, I.H., et al., *Physiological role of taurine - from organism to organelle.* Acta Physiologica, 2015. **213**(1): p. 191-212.

80. Ternovsky, V.I., Y. Okada, and R.Z. Sabirov, *Sizing the pore of the volume-sensitive anion channel by differential polymer partitioning.* FEBS Lett, 2004. **576**(3): p. 433-6.

81. Nilius, B., *Is the volume-regulated anion channel VRAC a "water-permeable" channel?* Neurochem Res, 2004. **29**(1): p. 3-8.

82. Nilius, B., J. Prenen, and G. Droogmans, *Modulation of volume-regulated anion channels by extra- and intracellular pH.* Pflugers Archiv - European Journal of Physiology, 1998. **436**: p. 742-748.

83. Blum, A.E., B.C. Walsh, and G.R. Dubyak, *Extracellular osmolarity modulates G protein-coupled receptor-dependent ATP release from 1321N1 astrocytoma cells.* Am J Physiol Cell Physiol, 2010. **298**(2): p. C386-96.

84. Jackson, P.S. and K. Strange, *Characterization of the voltage-dependent properties of a volume-sensitive anion conductance.* Journal of General Physiology, 1995. **105**: p. 661-676.

85. Voets, T., G. Droogmans, and B. Nilius, *Modulation of voltage-dependent properties of a swelling-activated Cl - current.* Journal of General Physiology, 1997. **110**(3): p. 313-325.

86. Anderson, J.W., J.D. Jirsch, and D. Fedida, *Cation regulation of anion current activated by cell swelling in two types of human epithelial cancer cells.* Journal of Physiology, 1995. **483**(3): p. 549-557.

87. Braun, A.P. and H. Schulman, *Distinct voltage-dependent gating behaviours of a swelling-activated chloride current in human epithelial cells.* Journal of Physiology, 1996. **495 Suppl. 3**: p. 743-753.

88. Gosling, M., J.W. Smith, and D.R. Poyner, *Characterization of a volume-sensitive chloride current in rat osteoblast-like (ROS 17/2.8) cells.* J Physiol, 1995. **485**(3): p. 671-682.

89. Meyer, K. and C. Korbmacher, *Cell swelling activates ATP-dependent voltage-gated Cl - channels in M-1 mouse cortical collecting duct cells.* Journal of General Physiology, 1996. **108**: p. 177-193.

90. Tsumura, T., et al., *Sensitivity of volume-sensitive Cl - conductance in human epithelial cells to extracellular nucleotides.* Am.J.Physiol.(Cell Physiol.40), 1996. **271**(6): p. C1872-C1878.

91. Okada, Y., *Volume expansion-sensing outward-rectifier Cl - channel: fresh start to the molecular identity and volume sensor.* Am.J.Physiol.(Cell Physiol.42), 1997. **273**(3): p. C755-C789.

92. Doroshenko, P. and E. Neher, *Volume-sensitive chloride conductance in bovine chromaffin cell membrane.* Journal of Physiology, 1992. **449**: p. 197-218.

93. Stoddard, J.S., J.H. Steinbach, and L. Simchowitz, *Whole cell Cl - currents in human neutrophils induced by cell swelling.* Am.J.Physiol.(Cell Physiol.34), 1993. **265**: p. C156-C165.

94. Nilius, B., et al., *Activation of a Cl - current by hypotonic volume increase in human endothelial cells.* Journal of General Physiology, 1994. **103**: p. 787-805.

95. Jackson, P.S. and K. Strange, *Single channel properties of a swelling-activated anion conductance. Current activation occurs by abrupt switching of closed channels to an open state.* Journal of General Physiology, 1995. **105**: p. 643-660.

96. Okada, Y., et al., *Osmotic swelling activates intermediate-conductance Cl - channels in human intestinal epithelial cells.* Japanese Journal of Physiology, 1994. **44**: p. 403-409.

97. Inoue, H., et al., *Volume-sensitive chloride channels in mouse cortical neurons: characterization and role in volume regulation.* Eur J Neurosci, 2005. **21**(6): p. 1648-58.

98. Planells-Cases, R., et al., *Subunit composition of VRAC channels determines substrate specificity and cellular resistance to Pt-based anti-cancer drugs.* EMBO J, 2015. **34**(24): p. 2993-3008.

99. Lutter, D., et al., *Selective transport of neurotransmitters and modulators by distinct volume-regulated LRRC8 anion channels.* J Cell Sci, 2017. **130**(6): p. 1122-1133.

100. Gradogna, A., et al., *Subunit-dependent oxidative stress sensitivity of LRRC8 volume-regulated anion channels.* J Physiol, 2017. **595**(21): p. 6719-6733.

101. Ghosh, A., et al., *Leucine-rich repeat-containing 8B protein is associated with the endoplasmic reticulum Ca(2+) leak in HEK293 cells.* J Cell Sci, 2017. **130**(22): p. 3818-3828.

102. Yamada, T. and K. Strange, *Intracellular and extracellular loops of LRRC8 are essential for volume-regulated anion channel function.* J Gen Physiol, 2018. **150**(7): p. 1003-1015.

103. Gaitan-Penas, H., et al., *Investigation of LRRC8-Mediated Volume-Regulated Anion Currents in Xenopus Oocytes.* Biophys J, 2016. **111**(7): p. 1429-1443.

104. Syeda, R., et al., *LRRC8 Proteins Form Volume-Regulated Anion Channels that Sense Ionic Strength.* Cell, 2016. **164**(3): p. 499-511.

105. Zhou, P., M.M. Polovitskaya, and T.J. Jentsch, *LRRC8 N termini influence pore properties and gating of volume-regulated anion channels (VRACs).* J Biol Chem, 2018. **293**(35): p. 13440-13451.

106. Ullrich, F., et al., *Inactivation and Anion Selectivity of Volume-regulated Anion Channels (VRACs) Depend on C-terminal Residues of the First Extracellular Loop.* J Biol Chem, 2016. **291**(33): p. 17040-8.

107. Cannon, C.L., S. Basavappa, and K. Strange, *Intracellular ionic strength regulates the volume sensitivity of a swelling-activated anion channel.* Am J Physiol (Cell Physiol), 1998. **275**: p. C416-C422.

108. Nilius, B., et al., *Activation of volume-regulated chloride currents by reduction of intracellular ionic strength in bovine endothelial cells.* J Physiol, 1998. **506 Suppl. 2**: p. 353-361.

109. Voets, T., et al., *Reduced intracellular ionic strength as the initial trigger for activation of endothelial volume-regulated anion channels.* Proc Natl Acad Sci USA, 1999. **96**: p. 5298-5303.

110. Sabirov, R.Z., et al., *Reduction of ionic strength activates single volume-regulated anion channels (VRAC) in endothelial cells.* Pflugers Arch, 2000. **439**(3): p. 315-20.

111. Bond, T., et al., *ATP dependence of the ICl, swell channel varies with rate of cell swelling: evidence for two modes of channel activation.* J Gen Physiol, 1999. **113**: p. 441-456.

112. Jackson, P.S., R. Morrison, and K. Strange, *The volume-sensitive organic osmolyte-anion channel VSOAC is regulated by nonhydrolytic ATP binding.* Am.J.Physiol.(Cell Physiol.36), 1994. **267**: p. C1203-C1209.

113. Oiki, S., M. Kubo, and Y. Okada, *Mg 2+ and ATP-dependence of volume-sensitive Cl - channels in human epithelial cells.* Japanese Journal of Physiology, 1994. **44**: p. S77-S79.

114. Carpenter, E. and C. Peers, *Swelling- and cAMP-activated Cl - currents in isolated rat carotid body type I cells.* J Physiol, 1997. **503**(3): p. 497-511.

115. Bryan-Sisneros, A., et al., *Dual role of ATP in supporting volume-regulated chloride channels in mouse fibroblasts.* Biochim Biophys Acta, 2000. **1468**(1-2): p. 63-72.

116. Wang, Y., et al., *Autocrine signaling through ATP release represents a novel mechanism for cell volume regulation.* Proc.Natl.Acad.Sci.U.S.A., 1996. **93**(21): p. 12020-12025.

117. Akita, T., S.V. Fedorovich, and Y. Okada, *Ca2+ nanodomain-mediated component of swelling-induced volume-sensitive outwardly rectifying anion current triggered by autocrine action of ATP in mouse astrocytes.* Cell Physiol Biochem, 2011. **28**(6): p. 1181-90.

118. Akita, T. and Y. Okada, *Regulation of bradykinin-induced activation of volume-sensitive outwardly rectifying anion channels by Ca2+ nanodomains in mouse astrocytes.* J Physiol, 2011. **589**(Pt 16): p. 3909-27.

119. Fisher, S.K., et al., *Volume-dependent osmolyte efflux from neural tissues: regulation by G-protein-coupled receptors.* J Neurochem, 2008. **106**(5): p. 1998-2014.

120. Franco, R., M.I. Panayiotidis, and L.D. de la Paz, *Autocrine signaling involved in cell volume regulation: the role of released transmitters and plasma membrane receptors.* J Cell Physiol, 2008. **216**(1): p. 14-28.

121. Barakat, A.I., et al., *A flow-activated chloride-selective membrane current in vascular endothelial cells.* Circ.Res, 1999. **85**: p. 820-828.

122. Nakao, M., et al., *Mechanical stress-induced Ca2+ entry and Cl- current in cultured human aortic endothelial cells.* Am J Physiol, 1999. **276**(1): p. C238-49.

123. Hagiwara, N., et al., *Stretch-activated anion currents of rabbit cardiac myocytes.* J Physiol, 1992. **456**: p. 285-302.

124. Zhang, J.J. and T.J.C. Jacob, *Three different Cl - channels in the bovine ciliary epithelium activated by hypotonic stress.* Journal of Physiology, 1997. **499 Supp. 2**: p. 379-389.

125. Nilius, B., et al., *Annexin II modulates volume-activated chloride currents in vascular endothelial cells.* J Biol Chem, 1996. **271**: p. 30631-30636.

126. Trouet, D., et al., *Caveolin-1 modulates the activity of the volume-regulated chloride channel [In Process Citation].* J Physiol (Lond.), 1999. **520 Pt 1**: p. 113-119.

127. Trouet, D., et al., *Inhibition of volume-regulated anion channels by dominant-negative caveolin-1.* Biochem Biophys Res Commun, 2001. **284**(2): p. 461-5.

128. Okada, Y., et al., *Roles of volume-regulatory anion channels, VSOR and Maxi-Cl, in apoptosis, cisplatin resistance, necrosis, ischemic cell death, stroke and myocardial infarction.* Curr Top Membr, 2019. **83**: p. 205-283.

129. Coca-Prados, M., et al., *PKC-sensitive Cl - channels associated with ciliary epithelial homologue of pI Cln.* American Journal of Physiology: Cell Physiology, 1995. **268**: p. C572-C579.

130. Okada, Y., et al., *Volume-sensitive chloride channels involved in apoptotic volume decrease and cell death.* J Membr Biol, 2006. **209**(1): p. 21-9.

131. d'Anglemont de Tassigny, A., et al., *Volume-sensitive chloride channels (ICl,vol) mediate doxorubicin-induced apoptosis through apoptotic volume decrease in cardiomyocytes.* Fundam Clin Pharmacol, 2004. **18**(5): p. 531-8.

132. Shimizu, T., T. Numata, and Y. Okada, *A role of reactive oxygen species in apoptotic activation of volume-sensitive Cl(-) channel.* Proc Natl Acad Sci U S A, 2004. **101**(17): p. 6770-3.

133. Choi, H., et al., *LRRC8A channels support TNFalpha-induced superoxide production by Nox1 which is required for receptor endocytosis.* Free Radic Biol Med, 2016. **101**: p. 413-423.

134. Gill, D.R., et al., *Separation of drug transport and chloride channel functions of the human multidrug resistance P-glycoprotein.* Cell, 1992. **71**(1): p. 23-32.

135. Valverde, M.A., M. Diaz, and F.V. Sepulveda, *Volume-regulated chloride channels associated with the human multidrug-resistance P-glycoprotein.* Nature, 1992. **355**: p. 830-833.

136. Paulmichl, M., et al., *New mammalian chloride channel identified by expression cloning.* Nature, 1992. **356**: p. 238-241.

137. Krapivinsky, G.B., et al., *Molecular characterization of a swelling-induced chloride conductance regulatory protein, pI Cln.* Cell, 1994. **76**: p. 439-448.

138. Duan, D., et al., *Molecular identification of a volume-regulated chloride channel.* Nature, 1997. **390**(6658): p. 417-421.

139. Schalkwyk, L.C., et al., *Interpretation of knockout experiments: the congenic footprint.* Genes Brain Behav, 2007. **6**(3): p. 299-303.

140. Eisener-Dorman, A.F., D.A. Lawrence, and V.J. Bolivar, *Cautionary insights on knockout mouse studies: the gene or not the gene?* Brain Behav Immun, 2009. **23**(3): p. 318-24.

141. Sawada, A., et al., *A congenital mutation of the novel gene LRRC8 causes agammaglobulinemia in humans.* J Clin Invest, 2003. **112**(11): p. 1707-13.

142. Kumar, L., et al., *Leucine-rich repeat containing 8A (LRRC8A) is essential for T lymphocyte development and function.* J Exp Med, 2014. **211**(5): p. 929-42.

143. Platt, C.D., et al., *Leucine-rich repeat containing 8A (LRRC8A)-dependent volume-regulated anion channel activity is dispensable for T-cell development and function.* J Allergy Clin Immunol, 2017. **140**(6): p. 1651-1659 e1.

144. Zhou, C., et al., *Transfer of cGAMP into Bystander Cells via LRRC8 Volume-Regulated Anion Channels Augments STING-Mediated Interferon Responses and Anti-viral Immunity.* Immunity, 2020. **52**(5): p. 767-781 e6.

145. Lahey, L.J., et al., *The LRRC8A:C Heteromeric Channel Is a cGAMP Transporter and the Dominant cGAMP Importer in Human Vasculature Cells.* bioRxiv, 2020: p. 2020.02.13.948273.

146. Shen, M.R., et al., *Differential expression of volume-regulated anion channels during cell cycle progression of human cervical cancer cells.* J Physiol, 2000. **529 Pt 2**: p. 385-94.

147. Chen, L., et al., *Cell cycle-dependent expression of volume-activated chloride currents in nasopharyngeal carcinoma cells.* Am J Physiol Cell Physiol, 2002. **283**(4): p. C1313-23.

148. Rubino, S., et al., *Downregulation of Leucine-Rich Repeat-Containing 8A Limits Proliferation and Increases Sensitivity of Glioblastoma to Temozolomide and Carmustine.* Front Oncol, 2018. **8**: p. 142.

149. Maertens, C., et al., *Inhibition of volume-regulated anion channels in cultured endothelial cells by the anti-oestrogens clomiphene and nafoxidine.* Br J Pharmacol, 2001. **132**(1): p. 135-42.

150. Xue, Y., et al., *Natural and synthetic flavonoids, novel blockers of the volume-regulated anion channels, inhibit endothelial cell proliferation.* Pflugers Arch, 2018. **470**(10): p. 1473-1483.

151. Wondergem, R., et al., *Blocking swelling-activated chloride current inhibits mouse liver cell proliferation.* J Physiol., 2001. **532**: p. 661-672.

152. Rouzaire-Dubois, B., et al., *Control of cell proliferation by cell volume alterations in rat C6 glioma cells.* Pflugers Arch, 2000. **440**(6): p. 881-8.

153. Liang, W., et al., *Swelling-activated Cl- currents and intracellular CLC-3 are involved in proliferation of human pulmonary artery smooth muscle cells.* J Hypertens, 2014. **32**(2): p. 318-30.

154. Lee, C.C., et al., *The protein synthesis inhibitor blasticidin s enters mammalian cells via leucine-rich repeat-containing protein 8D.* J Biol Chem, 2014. **289**(24): p. 17124-31.

155. Best, L., et al., *Electrical activity in pancreatic islet cells: The VRAC hypothesis.* Islets, 2010. **2**(2): p. 59-64.

156. Ashcroft, F.M. and P. Rorsman, *K(ATP) channels and islet hormone secretion: new insights and controversies.* Nat Rev Endocrinol, 2013. **9**(11): p. 660-9.

157. Best, L., *Glucose-induced electrical activity in rat pancreatic beta-cells: dependence on intracellular chloride concentration.* J Physiol, 2005. **568**(Pt 1): p. 137-44.

158. Kang, C., et al., *SWELL1 is a glucose sensor regulating beta-cell excitability and systemic glycaemia.* Nat Commun, 2018. **9**(1): p. 367.

159. Stuhlmann, T., R. Planells-Cases, and T.J. Jentsch, *LRRC8/VRAC anion channels enhance beta-cell glucose sensing and insulin secretion.* Nat Commun, 2018. **9**(1): p. 1974.

160. Zhang, Y., et al., *SWELL1 is a regulator of adipocyte size, insulin signalling and glucose homeostasis.* Nat Cell Biol, 2017. **19**(5): p. 504-517.

161. Alghanem, A.F., et al., *The SWELL1-LRRC8 complex regulates endothelial AKT-eNOS-mTOR signaling and vascular function.* bioRxiv, 2020: p. 2020.08.04.236182.

162. Chen, L., et al., *The LRRC8/VRAC anion channel facilitates myogenic differentiation of murine myoblasts by promoting membrane hyperpolarization.* J Biol Chem, 2019. **294**(39): p. 14279-14288.

163. Mongin, A.A., *Volume-regulated anion channel--a frenemy within the brain.* Pflugers Arch, 2016. **468**(3): p. 421-41.

164. Hyzinski-Garcia, M.C., A. Rudkouskaya, and A.A. Mongin, *LRRC8A protein is indispensable for swelling-activated and ATP-induced release of excitatory amino acids in rat astrocytes.* J Physiol, 2014. **592**(22): p. 4855-62.

165. Yang, J., et al., *Glutamate-Releasing SWELL1 Channel in Astrocytes Modulates Synaptic Transmission and Promotes Brain Damage in Stroke.* Neuron, 2019. **102**(4): p. 813-827 e6.

166. Kimelberg, H.K., et al., *Acute treatment with tamoxifen reduces ischemic damage following middle cerebral artery occlusion.* Neuroreport, 2000. **11**(12): p. 2675-9.

167. Kimelberg, H.K., et al., *Neuroprotective activity of tamoxifen in permanent focal ischemia.* J Neurosurg, 2003. **99**(1): p. 138-42.

168. Boulos, A.S., et al., *Tamoxifen as an effective neuroprotectant in an endovascular canine model of stroke.* J Neurosurg, 2011. **114**(4): p. 1117-26.

169. Feustel, P.J., Y. Jin, and H.K. Kimelberg, *Volume-regulated anion channels are the predominant contributors to release of excitatory amino acids in the ischemic cortical penumbra.* Stroke, 2004. **35**(5): p. 1164-8.

170. Phillis, J.W., D. Song, and M.H. O'Regan, *Tamoxifen, a chloride channel blocker, reduces glutamate and aspartate release from the ischemic cerebral cortex.* Brain Res, 1998. **780**(2): p. 352-5.

171. Phillis, J.W., D. Song, and M.H. O'Regan, *Inhibition by anion channel blockers of ischemia-evoked release of excitotoxic and other amino acids from rat cerebral cortex.* Brain Res, 1997. **758**(1-2): p. 9-16.

172. Zhang, Y., et al., *DCPIB, a specific inhibitor of volume regulated anion channels (VRACs), reduces infarct size in MCAo and the release of glutamate in the ischemic cortical penumbra.* Exp Neurol, 2008. **210**(2): p. 514-20.

173. Decher, N., et al., *DCPIB is a novel selective blocker of I(Cl,swell) and prevents swelling-induced shortening of guinea-pig atrial action potential duration.* Br J Pharmacol, 2001. **134**(7): p. 1467-79.

174. Friard, J., et al., *Comparative Effects of Chloride Channel Inhibitors on LRRC8/VRAC-Mediated Chloride Conductance.* Front Pharmacol, 2017. **8**: p. 328.

175. Deng, W., et al., *The ICl,swell inhibitor DCPIB blocks Kir channels that possess weak affinity for PIP2.* Pflugers Arch, 2016. **468**(5): p. 817-24.

176. Bowens, N.H., et al., *DCPIB, the proposed selective blocker of volume-regulated anion channels, inhibits several glutamate transport pathways in glial cells.* Mol Pharmacol, 2013. **83**(1): p. 22-32.

177. Fujii, T., et al., *Inhibition of gastric H+,K+-ATPase by 4-(2-butyl-6,7-dichloro-2-cyclopentylindan-1-on-5-yl)oxybutyric acid (DCPIB), an inhibitor of volume-regulated anion channel.* Eur J Pharmacol, 2015. **765**: p. 34-41.

178. Luck, J.C., et al., *LRRC8/VRAC anion channels are required for late stages of spermatid development in mice.* J Biol Chem, 2018. **293**(30): p. 11796-11808.

179. Bao, J., et al., *Deficient LRRC8A-dependent volume-regulated anion channel activity is associated with male infertility in mice.* JCI Insight, 2018. **3**(16).

180. Abdullaev, I.F., et al., *Pharmacological comparison of swelling-activated excitatory amino acid release and Cl- currents in cultured rat astrocytes.* J Physiol, 2006. **572**(Pt 3): p. 677-89.

181. Harrigan, T.J., et al., *Activation of microglia with zymosan promotes excitatory amino acid release via volume-regulated anion channels: the role of NADPH oxidases.* J Neurochem, 2008. **106**(6): p. 2449-62.

182. Liu, H.T., et al., *Bradykinin-induced astrocyte-neuron signalling: glutamate release is mediated by ROS-activated volume-sensitive outwardly rectifying anion channels.* J Physiol, 2009. **587**(Pt 10): p. 2197-209.

183. Schlichter, L.C., T. Mertens, and B. Liu, *Swelling activated Cl- channels in microglia: Biophysics, pharmacology and role in glutamate release.* Channels (Austin), 2011. **5**(2): p. 128-37.

184. Stott, J.B., et al., *Functional and pharmacological characterization of volume-regulated anion channels in human normal and cystic fibrosis bronchial and nasal epithelial cells.* Eur J Pharmacol, 2014. **740**: p. 183-91.

185. Sabirov, R.Z. and Y. Okada, *ATP release via anion channels.* Purinergic Signal, 2005. **1**(4): p. 311-28.

186. Sabirov, R.Z., et al., *The properties, functions, and pathophysiology of maxi-anion channels.* Pflugers Arch, 2016. **468**(3): p. 405-20.

187. Sato-Numata, K., et al., *Distinct pharmacological and molecular properties of the acid-sensitive outwardly rectifying (ASOR) anion channel from those of the volume-sensitive outwardly rectifying (VSOR) anion channel.* Pflugers Arch, 2016. **468**(5): p. 795-803.

188. Afzal, A., et al., *The LRRC8 volume-regulated anion channel inhibitor, DCPIB, inhibits mitochondrial respiration independently of the channel.* Physiol Rep, 2019. **7**(23): p. e14303.

189. Minieri, L., et al., *The inhibitor of volume-regulated anion channels DCPIB activates TREK potassium channels in cultured astrocytes.* Br J Pharmacol, 2013. **168**(5): p. 1240-54.

190. Kurbannazarova, R.S., et al., *Swelling-activated anion channels are essential for volume regulation of mouse thymocytes.* Int J Mol Sci, 2011. **12**(12): p. 9125-37.

191. Klausen, T.K., et al., *Cell cycle-dependent activity of the volume- and Ca2+-activated anion currents in Ehrlich lettre ascites cells.* J Cell Physiol, 2007. **210**(3): p. 831-42.

192. Helix, N., et al., *Inhibition of the endogenous volume-regulated anion channel (VRAC) in HEK293 cells by acidic di-aryl-ureas.* J Membr Biol, 2003. **196**(2): p. 83-94.

193. Fan, H.T., et al., *Phloretin differentially inhibits volume-sensitive and cyclic AMP-activated, but not Ca-activated, Cl(-) channels.* Br J Pharmacol, 2001. **133**(7): p. 1096-106.

194. Zhang, J.J., et al., *Tamoxifen blocks chloride channels. A possible mechanism for cataract formation.* Journal of Clinical Investigation, 1994. **94**: p. 1690-1697.

195. Tominaga, M., et al., *Volume-sensitive chloride channel activity does not depend on endogenous P-glycoprotein.* Journal of Biological Chemistry, 1995. **270**(46): p. 27887-27893.

196. Yang, X., et al., *Cisplatin activates volume-sensitive like chloride channels via purinergic receptor pathways in nasopharyngeal carcinoma cells.* J Membr Biol, 2015. **248**(1): p. 19-29.

197. Dick, G.M., I.D. Kong, and K.M. Sanders, *Effects of anion channel antagonists in canine colonic myocytes: comparative pharmacology of Cl-, Ca2+ and K+ currents.* Br J Pharmacol, 1999. **127**(8): p. 1819-31.

198. Leaney, J.L., S.J. Marsh, and D.A. Brown, *A swelling-activated chloride current in rat sympathetic neurones.* J Physiol, 1997. **501.3**: p. 555-564.

199. Zhang, H., et al., *Volume regulated anion channel currents of rat hippocampal neurons and their contribution to oxygen-and-glucose deprivation induced neuronal death.* PLoS One, 2011. **6**(2): p. e16803.

200. Benfenati, V., et al., *Carbenoxolone inhibits volume-regulated anion conductance in cultured rat cortical astroglia.* Channels (Austin), 2009. **3**(5): p. 323-36.

201. Kubo, M. and Y. Okada, *Volume-regulatory Cl- channel currents in cultured human epithelial cells.* J Physiol, 1992. **456**: p. 351-71.

202. Boese, S.H., R.H.K. Kinne, and F. Wehner, *Single-channel properties of swelling-activated anion conductance in rat inner medullary collecting duct cells.* Am J Physiol (Renal Fluid Electrolyte Physiol.40), 1996. **271**: p. F1224-F1233.

203. Bakhramov, A., C. Fenech, and T.B. Bolton, *Chloride current activated by hypotonicity in cultured human astrocytoma cells.* Exp Physiol, 1995. **80**(3): p. 373-89.

204. Shen, M.R., S.N. Wu, and C.Y. Chou, *Volume-sensitive chloride channels in the primary culture cells of human cervical carcinoma.* Biochim Biophys Acta, 1996. **1315**(2): p. 138-44.

205. Okada, Y., K. Sato, and T. Numata, *Pathophysiology and puzzles of the volume-sensitive outwardly rectifying anion channel.* J Physiol, 2009. **587**(Pt 10): p. 2141-9.

206. Nilius, B., J. Sehrer, and G. Droogmans, *Permeation properties and modulation of volume-activated Cl - -currents in human endothelial cells.* British Journal of Pharmacology, 1994. **112**: p. 1049-1056.

207. Hazama, A. and Y. Okada, *Ca2+ sensitivity of volume-regulatory K+ and Cl- channels in cultured human epithelial cells.* J Physiol, 1988. **402**: p. 687-702.

208. Voets, T., et al., *Blockers of volume-activated Cl - currents inhibit endothelial cell proliferation.* Pflugers Archiv European Journal of Physiology, 1995. **431**(1): p. 132-134.

209. Doroshenko, P., V. Sabanov, and N. Doroshenko, *Cell cycle-related changes in regulatory volume decrease and volume-sensitive chloride conductance in mouse fibroblasts.* J Cell Physiol, 2001. **187**(1): p. 65-72.

210. Mao, J., et al., *Blockage of volume-activated chloride channels inhibits migration of nasopharyngeal carcinoma cells.* Cell Physiol Biochem, 2007. **19**(5-6): p. 249-58.

211. Ransom, C.B., J.T. O'Neal, and H. Sontheimer, *Volume-activated chloride currents contribute to the resting conductance and invasive migration of human glioma cells.* J Neurosci, 2001. **21**(19): p. 7674-83.

212. Nilius, B. and G. Droogmans, *Ion channels and their functional role in vascular endothelium.* Physiol Rev, 2001. **81**(4): p. 1415-59.

213. Basarsky, T.A., D. Feighan, and B.A. MacVicar, *Glutamate release through volume-activated channels during spreading depression.* J Neurosci, 1999. **19**: p. 6439-6445.

214. Best, L., E.A. Sheader, and P.D. Brown, *A volume activated anion conductance in insulin-secreting cells.* Pflugers Archiv European Journal of Physiology, 1996. **431**(3): p. 363-370.

215. Kinard, T.A. and L.S. Satin, *An ATP-sensitive Cl - channel current that is activated by cell swelling, cAMP, and glyburide in insulin-secreting cells.* Diabetes, 1995. **44**: p. 1461-1466.

216. Holm, J.B., R. Grygorczyk, and I.H. Lambert, *Volume-sensitive release of organic osmolytes in the human lung epithelial cell line A549: role of the 5-lipoxygenase.* Am J Physiol Cell Physiol, 2013. **305**(1): p. C48-60.

217. Wang, R., et al., *The volume-regulated anion channel (LRRC8) in nodose neurons is sensitive to acidic pH.* JCI Insight, 2017. **2**(5): p. e90632.

218. Ye, Z.C., et al., *Pharmacological "cross-inhibition" of connexin hemichannels and swelling activated anion channels.* Glia, 2009. **57**(3): p. 258-69.

219. Yamaguchi, T., et al., *A novel leukotriene antagonist, ONO-1078, inhibits and reverses human bronchial contraction induced by leukotrienes C4 and D4 and antigen in vitro.* Am Rev Respir Dis, 1992. **146**(4): p. 923-9.

220. Yamaguchi, T., et al., *[Preventive effect of a novel leukotrienes antagonist ONO-1078 on leukotriene C4- and D4-induced human bronchial smooth muscle contraction].* Arerugi, 1990. **39**(11): p. 1477-83.

221. Hoshino, M., T. Izumi, and T. Shimizu, *Leukotriene D4 activates mitogen-activated protein kinase through a protein kinase Calpha-Raf-1-dependent pathway in human monocytic leukemia THP-1 cells.* J Biol Chem, 1998. **273**(9): p. 4878-82.

222. Duroudier, N.P., et al., *Functional polymorphism and differential regulation of CYSLTR1 transcription in human airway smooth muscle and monocytes.* Cell Biochem Biophys, 2007. **47**(1): p. 119-30.

223. Sasaki, F. and T. Yokomizo, *The leukotriene receptors as therapeutic targets of inflammatory diseases.* Int Immunol, 2019.

224. Pedersen, S., et al., *Leukotriene D4-induced Ca2+ mobilization in Ehrlich ascites tumor cells.* J Membr Biol, 1997. **155**(1): p. 61-73.

225. Jorgensen, N.K., I.H. Lambert, and E.K. Hoffmann, *Role of LTD4 in the regulatory volume decrease response in Ehrlich ascites tumor cells.* J Membr Biol, 1996. **151**(2): p. 159-73.

226. Hougaard, C., et al., *K+ currents activated by leukotriene D4 or osmotic swelling in Ehrlich ascites tumour cells.* Pflugers Arch, 2000. **440**(2): p. 283-94.

227. Atwood, B.K., et al., *Expression of G protein-coupled receptors and related proteins in HEK293, AtT20, BV2, and N18 cell lines as revealed by microarray analysis.* BMC Genomics, 2011. **12**: p. 14.

228. Lambert, I.H., E.K. Hoffmann, and P. Christensen, *Role of prostaglandins and leukotrienes in volume regulation by Ehrlich ascites tumor cells.* J.Membr.Biol., 1987. **98**: p. 247-256.

229. Lynch, K.R., et al., *Characterization of the human cysteinyl leukotriene CysLT1 receptor.* Nature, 1999. **399**(6738): p. 789-93.

230. Kahnt, A.S., et al., *Cysteinyl leukotriene-receptor-1 antagonists interfere with PGE2 synthesis by inhibiting mPGES-1 activity.* Biochem Pharmacol, 2013. **86**(2): p. 286-96.

231. Brocks, D.R., et al., *The single and multiple dose pharmacokinetics of pranlukast in healthy volunteers.* Eur J Clin Pharmacol, 1996. **51**(3-4): p. 303-8.

232. Dekhuijzen, P.N. and P.P. Koopmans, *Pharmacokinetic profile of zafirlukast.* Clin Pharmacokinet, 2002. **41**(2): p. 105-14.

233. Xie, L., et al., *Induction of adipose and hepatic SWELL1 expression is required for maintaining systemic insulin-sensitivity in obesity.* Channels (Austin), 2017. **11**(6): p. 673-677.

234. Osei-Owusu, J., et al., *Molecular Biology and Physiology of Volume-Regulated Anion Channel (VRAC).* Curr Top Membr, 2018. **81**: p. 177-203.

235. Jentsch, T.J., et al., *VRAC: molecular identification as LRRC8 heteromers with differential functions.* Pflugers Arch, 2016. **468**(3): p. 385-93.

236. Tailler, M., et al., *Antineoplastic activity of ouabain and pyrithione zinc in acute myeloid leukemia.* Oncogene, 2012. **31**(30): p. 3536-46.

237. Srivastava, G., et al., *Anticancer activity of pyrithione zinc in oral cancer cells identified in small molecule screens and xenograft model: Implications for oral cancer therapy.* Mol Oncol, 2015. **9**(8): p. 1720-35.

238. Mo, J., et al., *Apoptosis in HepG2 cells induced by zinc pyrithione via mitochondrial dysfunction pathway: Involvement of zinc accumulation and oxidative stress.* Ecotoxicol Environ Saf, 2018. **161**: p. 515-525.

239. Carraway, R.E. and P.R. Dobner, *Zinc pyrithione induces ERK- and PKC-dependent necrosis distinct from TPEN-induced apoptosis in prostate cancer cells.* Biochim Biophys Acta, 2012. **1823**(2): p. 544-57.

240. Baran, R. and H.I. Maibach, *Textbook of cosmetic dermatology*. Fifth edition. ed. 2017, Boca Raton: CRC Press/Taylor & Francis Group. xii, 594 pages.

241. Blanchard, C., et al., *Zinc Pyrithione Improves the Antibacterial Activity of Silver Sulfadiazine Ointment.* mSphere, 2016. **1**(5).

242. Van Cutsem, J., et al., *The in vitro antifungal activity of ketoconazole, zinc pyrithione, and selenium sulfide against Pityrosporum and their efficacy as a shampoo in the treatment of experimental pityrosporosis in guinea pigs.* J Am Acad Dermatol, 1990. **22**(6 Pt 1): p. 993-8.

243. Sousa, A.P. and B. Nunes, *Standard and biochemical toxicological effects of zinc pyrithione in Daphnia magna and Daphnia longispina.* Environ Toxicol Pharmacol, 2020. **80**: p. 103402.

244. Zhu, T., et al., *Hit identification and optimization in virtual screening: practical recommendations based on a critical literature analysis.* J Med Chem, 2013. **56**(17): p. 6560-72.

245. Kharade, S., et al., *Pore polarity and charge determine differential block of Kir1.1 and Kir7.1 potassium channels by the small-molecule inhibitor VU590.* Mol Pharmacol, 2017.

246. Swale, D.R., et al., *An insecticide resistance-breaking mosquitocide targeting inward rectifier potassium channels in vectors of Zika virus and malaria.* Sci Rep, 2016. **6**: p. 36954.

247. Swale, D.R., et al., *ML418: The First Selective, Sub-Micromolar Pore Blocker of Kir7.1 Potassium Channels.* ACS Chem Neurosci, 2016. **7**(7): p. 1013-23.

248. Swale, D.R., et al., *Computational and Functional Analyses of a Small-Molecule Binding Site in ROMK.* Biophys J, 2015. **108**(5): p. 1094-103.

249. Rouhier, M.F., et al., *Pharmacological Validation of an Inward-Rectifier Potassium (Kir) Channel as an Insecticide Target in the Yellow Fever Mosquito Aedes aegypti.* PLoS One, 2014. **9**(6): p. e100700.

250. Raphemot, R., et al., *Direct Activation of beta-cell KATP Channels with a Novel Xanthine Derivative.* Mol Pharmacol, 2014.

251. Raphemot, R., et al., *Discovery and Characterization of a Potent and Selective Inhibitor of Aedes aegypti Inward Rectifier Potassium Channels.* PLoS One, 2014. **9**(11): p. e110772.

252. Bhave, G., et al., *Development of a selective small-molecule inhibitor of Kir1.1, the renal outer medullary potassium channel.* Mol Pharmacol, 2011. **79**(1): p. 42-50.

253. Raphemot, R., et al., *Discovery, characterization, and structure-activity relationships of an inhibitor of inward rectifier potassium (Kir) channels with preference for kir2.3, kir3.x, and kir7.1.* Front Pharmacol, 2011. **2**: p. 75.

254. Lewis, L.M., et al., *High-throughput screening reveals a small-molecule inhibitor of the renal outer medullary potassium channel and Kir7.1.* Mol Pharmacol, 2009. **76**(5): p. 1094-103.

255. Pushpakom, S., et al., *Drug repurposing: progress, challenges and recommendations.* Nat Rev Drug Discov, 2019. **18**(1): p. 41-58.

256. Rudolf, E. and M. Cervinka, *Zinc pyrithione induces cellular stress signaling and apoptosis in Hep-2 cervical tumor cells: the role of mitochondria and lysosomes.* Biometals, 2010. **23**(2): p. 339-54.

257. Okada, Y., et al., *Cell Volume-Activated and Volume-Correlated Anion Channels in Mammalian Cells: Their Biophysical, Molecular, and Pharmacological Properties.* Pharmacol Rev, 2019. **71**(1): p. 49-88.

258. Yamada, T., et al., *Leucine-rich repeat containing protein LRRC8A is essential for swelling-activated Cl- currents and embryonic development in zebrafish.* Physiol Rep, 2016. **4**(19).

259. Wemmie, J.A., R.J. Taugher, and C.J. Kreple, *Acid-sensing ion channels in pain and disease.* Nat Rev Neurosci, 2013. **14**(7): p. 461-71.

260. Gruol, D.L., et al., *Hydrogen ions have multiple effects on the excitability of cultured mammalian neurons.* Brain Res, 1980. **183**(1): p. 247-52.

261. Krishtal, O.A. and V.I. Pidoplichko, *A receptor for protons in the nerve cell membrane.* Neuroscience, 1980. **5**(12): p. 2325-7.

262. Waldmann, R., et al., *A proton-gated cation channel involved in acid-sensing.* Nature, 1997. **386**(6621): p. 173-7.

263. Auzanneau, C., et al., *A Novel voltage-dependent chloride current activated by extracellular acidic pH in cultured rat Sertoli cells.* J Biol Chem, 2003. **278**(21): p. 19230-6.

264. Capurro, V., et al., *Functional analysis of acid-activated Cl(-) channels: properties and mechanisms of regulation.* Biochim Biophys Acta, 2015. **1848**(1 Pt A): p. 105-14.

265. Lambert, S. and J. Oberwinkler, *Characterization of a proton-activated, outwardly rectifying anion channel.* J Physiol, 2005. **567**(Pt 1): p. 191-213.

266. Sato-Numata, K., et al., *Acid-sensitive outwardly rectifying (ASOR) anion channels in human epithelial cells are highly sensitive to temperature and independent of ClC-3.* Pflugers Arch, 2013. **465**(11): p. 1535-43.

267. Wang, H.Y., et al., *Role of acid-sensitive outwardly rectifying anion channels in acidosis-induced cell death in human epithelial cells.* Pflugers Arch, 2007. **454**(2): p. 223-33.

268. Ma, Z.Y., et al., *A proton-activated, outwardly rectifying chloride channel in human umbilical vein endothelial cells.* Biochem Biophys Res Commun, 2008. **371**(3): p. 437-40.

269. Drews, A., et al., *Structural requirements of steroidal agonists of transient receptor potential melastatin 3 (TRPM3) cation channels.* Br J Pharmacol, 2014. **171**(4): p. 1019-32.

270. Ran, F.A., et al., *Genome engineering using the CRISPR-Cas9 system.* Nat Protoc, 2013. **8**(11): p. 2281-2308.

271. Zhang, J.H., T.D. Chung, and K.R. Oldenburg, *A Simple Statistical Parameter for Use in Evaluation and Validation of High Throughput Screening Assays.* J Biomol Screen, 1999. **4**(2): p. 67-73.

272. Majeed, Y., et al., *Cis-isomerism and other chemical requirements of steroidal agonists and partial agonists acting at TRPM3 channels.* Br J Pharmacol, 2010. **161**(2): p. 430-41.

273. Seljeset, S., et al., *Probing GABAA receptors with inhibitory neurosteroids.* Neuropharmacology, 2018. **136**(Pt A): p. 23-36.

274. Wu, F.S., T.T. Gibbs, and D.H. Farb, *Pregnenolone sulfate: a positive allosteric modulator at the N-methyl-D-aspartate receptor.* Mol Pharmacol, 1991. **40**(3): p. 333-6.

275. Kraut, J.A. and N.E. Madias, *Metabolic acidosis: pathophysiology, diagnosis and management.* Nat Rev Nephrol, 2010. **6**(5): p. 274-85.